STARS

Cholesteric Liquid Crystal Photonic Crystal Lasers And Photonic Devices

Ying Zhou
University of Central Florida

University of Central Florida

STARS
Showcase of Text, Archives, Research & Scholarship

www.manaraa.com

CHOLESTERIC LIQUID CRYSTAL PHOTONIC CRYSTAL LASERS AND PHOTONIC DEVICES

By

YING ZHOU
BS in Optical Engineering Department, Zhejiang University, P. R. China, 2000
MS in Optical Engineering Department, Zhejiang University, P. R. China, 2003
MS in College of Optics and Photonics, University of Central Florida, US, 2005

A dissertation submitted in partial fulfillment of the requirements
for the degree of Doctor of Philosophy
in the College of Optics and Photonics
at University of Central Florida
Orlando, Florida

Spring Term
2008

Major Professor: Shin-Tson Wu

© 2008 Ying Zhou

ABSTRACT

This dissertation discusses cholesteric liquid crystals (CLCs) and polymers based photonic devices including one-dimensional (1D) photonic crystal lasers and broadband circular polarizers. CLCs showing unique self-organized chiral structures have been widely used in bistable displays, flexible displays, and reflectors. However, the photonic band gap they exhibit opens a new way for generating laser light at the photonic band edge (PBE) or inside the band gap. When doped with an emissive laser dye, cholesteric liquid crystals provide distributed feedback so that mirrorless lasing is hence possible. Due to the limited surface anchoring, the thickness of gain medium and feedback length is tens of micrometers. Therefore lasing efficiency is quite limited and laser beam is highly divergent. To meet the challenges, we demonstrated several new methods to enhance the laser emission while reducing the beam divergence from a cholesteric liquid crystal laser.

Enhanced laser emission is demonstrated by incorporating a single external CLC reflector as a polarization conserved reflector. Because the distributed feedback from the active layer is polarization selective, a CLC reflector preserves the original polarization of the reflected light and a further stimulated amplification ensues. As a result of virtually doubled feedback length, the output is dramatically enhanced in the same circular polarization state. Meanwhile, the laser beam divergence is dramatically reduced due to the increased cavity length from micrometer to millimeter scale.

Enhanced laser emission is also demonstrated by the in-cell metallic reflector because the active layer is pumped twice. Unlike a CLC reflector, the output from a mirror-reflected

CLC laser is linearly polarized as a result of coherent superposition of two orthogonal circular polarization states. The output linear polarization direction can be well controlled and fine tuned by varying the operating temperature and cell gap.

Enhanced laser emission is further demonstrated in a hybrid *photonic band edge - Fabry-Perot* (FP) type structure by sandwiching the CLC active layer within a circular polarized resonator consisting of two CLC reflectors. The resonator generates multiple FP modes while preserving the PBE mode from the active layer. More importantly this band edge mode can be greatly enhanced by the external resonator under some conditions. Theoretical analysis is conducted based on 4×4 transfer matrix and scattering matrix and the results are consistent with our experimental observations.

To make the CLC laser more compact and miniaturized, we have developed a flexible polymer laser using dye-doped cholesteric polymeric films. By stacking the mirror reflecting layer, the active layer and the CLC reflecting layer, enhanced laser emission was observed in opposite-handed circular polarization state, because of the light recycling effect.

On the other hand, we use the stacked cholesteric liquid crystal films, or the cholesteric liquid crystals and polymer composite films to demonstrate the single film broadband circular polarizers, which are helpful for converting a randomly polarized light into linear polarization. New fabrication methods are proposed and the circular polarizers cover ~280 nm in the visible spectral range. Both theoretical simulation and experimental results are presented with a good match.

To my Parents, Zicheng Zhou and Linsheng Guo
To my Sister, Lillian Zhou

ACKNOWLEDGMENTS

I would like to express my deepest gratitude to my advisor, Prof. Shin-Tson Wu, for his patient guidance, encouragements, and support throughout my Ph.D. degree pursuit at College of Optics and Photonics, University of Central Florida. I greatly appreciate his technical insights and his dedication in working with me on every progress of my research work. What I have learned is not only technical skills but more importantly the way of how to do the research creatively and independently. Moreover, I would like to thank him for giving me enough flexibility to look into the new area and make a discovery, which was the starting point of my dissertation. The training I have obtained under his supervision will definitely benefit both my future professional career and my personal life.

I would also like to take this opportunity to thank my dissertation committee members: Prof. David H. Hagan, Prof. Patrick L. LiKamWa, and Prof. Thomas X. Wu, who have been taking time to evaluate my thesis work over the years. Besides, Prof. Hagan gave me great support in my society award applications. Prof. LiKamWa and Prof. Thomas Wu made lots of valuable suggestions to my research and had stimulating discussions with me.

More appreciation goes to all LCD group members, who have assisted me in one way or another during my dissertation course. Special thanks go to Dr. Yuhua Huang, Dr. Xinyu Zhu, and Dr. Hongwen Ren for their great help in experiments, discussions, and inspirations. Also thank Dr. Zhibing Ge, Dr. Qi Hong, Dr. Xiangyi Nie, Dr. Yi-Hsin Lin and Dr. Yung-Hsun Wu for their help in simulations and measurements.

Last but not least, I am greatly indebted to my parents and my elder sister for their

understanding, patience, and support during the entire period of my study. No matter where I am, they are always the ones who give me the most love and understanding, which makes all my achievements possible.

TABLE OF CONTENTS

LIST OF FIGURES

LIST OF TABLES

LIST OF ACRONYMS / ABBREVIATIONS

LC   Liquid crystal

LCD   Liquid crystal display

CLC   Cholesteric liquid crystal

PBG   Photonic band gap

PBE   Photonic band edge

DFB   Distributed feedback

DBR   Distributed Bragg reflector

HTP   Helical twisting power

RCP   Right-handed circularly polarized light

LCP   Left-handed circularly polarized light

LP   Linearly polarized light

CR   Contrast ratio

FWHM   Full width of half maximum

VIS   Visible spectral range

DOS   Density of state

ASE   Amplified spontaneous emission

ITO   Indium-tin-oxide

Nd:YAG   Neodymium-doped yttrium aluminium garnet

CHAPTER 1   INTRODUCTION

1.1   Motivations

Nowadays, liquid crystal (LC) has been extensively used in both display and photonic devices. In our daily life, liquid crystal displays (LCDs) have been widely used in cell phones, car navigations, laptop computers, desktop monitors, projectors, and TVs, etc. While for photonic applications, due to its unique optical properties LC plays an important role in tunable filters, tunable laser cavities, tunable focus lens, spatial light modulators, and diffraction gratings for various applications such as laser beam steering, adaptive optics, lasers and optical communications [1-4].

It is only in recent years that liquid crystals are utilized to generate a laser light other than to control and manipulate a light. Typically a liquid crystal laser involves laser dye as emissive medium and liquid crystal as feedback cavity. Liquid crystals arranged in a helical structure, or a regular and periodic dielectric structure can be used to generate a coherent laser light. Such materials could be cholesteric liquid crystals, ferroelectric liquid crystals, blue phase liquid crystals, or liquid crystal polymers [5-8]. The soft matter nature of these materials and their response to external stimuli lead to tuning feasibilities from near ultraviolet through visible to near infrared. The broad wavelength tuning range of LC lasers, coupled with their microscopic size, narrow linewidth (< 0.1 nm) and high optical efficiency as compared with more conventional solid-state lasers, could open up new possibilities for labs-on-a-chip, medical diagnostics, dermatology, spectrum analysis, laser arrays, and holography [9].

1

In order to elevate liquid crystal lasers to a more practical stage, high lasing efficiency, low threshold, high output power, good beam quality, portability, large tuning range are highly desired. Usually the thickness of a CLC laser is limited to tens of micrometers and thus the feedback length is not sufficient. As a result, lasing efficiency is restricted and laser beam is highly divergent. In reality, the lasing efficiency is very much related to the order of the materials as well as the laser cavities. Although our research scope is focused on cholesteric liquid crystals, the concepts prove to be general for different liquid crystal materials.

On the other hand, our research on cholesteric liquid crystals extends to other photonic devices as broadband circular polarizers, which are of great importance to display applications. Details will be discussed in Chapter 6.

1.2   Thesis Overview

The research endeavor in this dissertation mainly covers two parts: 1) CLC lasers and cholesteric polymer lasers; 2) CLC and polymer-based broadband circular polarizers. For CLC lasers, our goal is to develop novel CLC laser structures from a device viewpoint in order to achieve higher lasing efficiency, smaller beam divergence and flexible control of output polarization states. For CLC broadband circular polarizers, our goal is to develop a single-film circular polarizer with a broad bandwidth and good reflectivity.

The thesis is organized as follows:

Chapter 2 reviews the fundamentals of liquid crystals, especially cholesteric liquid crystals including their basic optical and photonic properties.

Chapter 3 discusses the single reflector enhancement approaches which include the CLC external passive reflector, the in-cell metallic mirror reflector, and the external metallic mirror reflector. Prior arts on CLC lasers are briefly reviewed. Then the experimental results as far as lasing output power, beam divergence, output polarization states are given for different reflector scenarios and the corresponding mechanism is analyzed in details. Moreover, the rotation of the linearly polarized laser direction from an in-cell mirror reflector is demonstrated using temperature and cell gap dependent tuning strategies.

In Chapter 4, we put the CLC laser within a circular polarized resonator consisting of two CLC reflectors and demonstrate the emission enhanced CLC photonic band edge laser with the support from Fabry-Perot cavity. The potential longitudinal mode, together with the laser amplification from an active device is theoretically analyzed using 4×4 transfer matrix and scattering matrix. The theoretical calculation confirms our experimental results and the responsible mechanisms are explained.

Chapter 5 discusses the cholesteric liquid crystalline polymer-based CLC lasers. We not only demonstrated a free-standing and flexible CLC polymer film laser but also developed the enhanced CLC polymer film laser in opposite-handed circular polarization state with high purity based on light recycling effect.

In Chapter 6, two methods for developing broadband circular polarizers are demonstrated using stacked CLC polymers or CLC/CLC polymer composite films.

Finally in Chapter 7, we summarize the achievements and highlight the newness of our research work.

3

1.3 References

1. G. D. Love, "Wave-front correction and production of Zernike modes with a liquid-crystal spatial light modulator," Appl. Opt. 36, 1517(1997).

2. A. Linnenberger, S. Serati, and J. Stockley, "Advances in optical phased array technology," Proc. SPIE. 6304, 63040T (2006).

3. H. Ren, D. Fox, B. Wu, and S. T. Wu, " Liquid crystal lens with large focal length tunability and low operating voltage," Opt. Express, 15, 11328 (2007).

4. Y. Q. Lu, F. Du, Y. H. Lin, and S. T. Wu "Variable optical attenuator based on polymer-stabilized twisted nematic liquid crystal," Opt. Express 12, 1221 (2004).

5. V. I. Kopp, B. Fan, H. K. M. Vithana, and A. Z. Genack, "Low-threshold lasing at the edge of a photonic stop band in cholesteric liquid crystals," Opt. Lett. 23, 1707(1998).

6. M. Ozaki, M. Kasano, D. Ganzke, W. Haase, and K. Yoshino, "Mirrorless lasing in a dye-doped ferroelectric liquid crystal," Adv. Mater. 14, 306 (2002).

7. W. Y. Cao, A. Munoz, P. Palffy-Muhoray, and B. Taheri, "Lasing in a three-dimensional photonic crystal of the liquid crystal blue phase," Nat. Mater. 1, 111 (2002).

8. T. Matsui, R. Ozaki, K. Funamoto, M. Ozaki, and K. Yoshino, "Flexible mirrorless laser based on a free-standing film of photo polymerized cholesteric liquid crystal," Appl. Phys. Lett. 81, 3741 (2002).

9. A. D. Ford, S. M. Morris, and H. J. Coles, "Photonics and lasing in liquid crystals," Materials Today, 9, 7 (2006).

CHAPTER 2 OPTICAL AND PHOTONIC PROPERTIES OF LIQUID CRYSTALS

2.1 Liquid crystals

Liquid crystal (LC) is an intermediate state of matter between isotropic fluids and crystal solids [1]. They are fluid-like, yet the arrangement of molecules within them exhibit structural orders. The first LC material was discovered by an Austrian botanist Friedrich Reinitzer in 1888, when he found the substance melted to a cloudy liquid and then became clear liquid as the temperature increased [2]. Three types of liquid crystals have been discovered so far: (i) thermotropic, (ii) lyotropic, and (iii) polymeric. Among them, thermotropic liquid crystals have been extensively studied and their applications reached a mature stage. Polymer LCs are potential candidates for low weight, flexible electronic devices and ultra-high-strength materials.

Nematic **Smectic A** **Cholesteric**
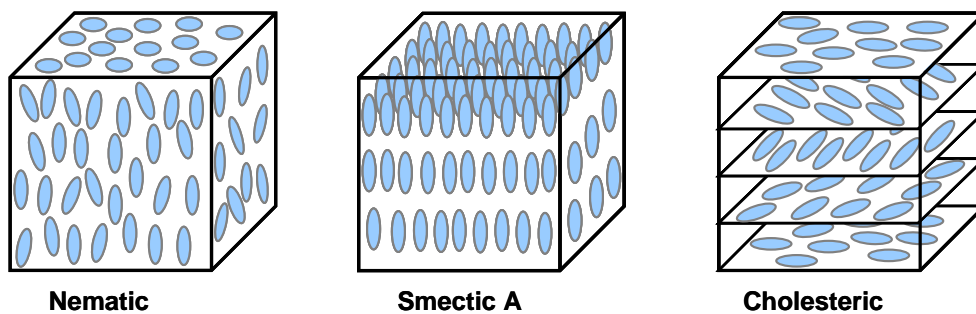
Fig. 2.1 Illustration of three thermotropic liquid crystals: nematic, smectic A and cholesteric phase.

As the temperature increases, the thermotropic liquid crystals go through a series of phase transitions: from solid to liquid crystal, to isotropic liquid, and finally to vapor phase. At each stage, the refractive indices, dielectric constants, elastic constants, and viscosities are

5

different depending on the temperature. There are three phases of thermotropic liquid crystals: nematic phase, smectic phase, and cholesteric phase, as Fig. 2.1 indicates.

In nematic phase the LC molecules possess a general orientational order but no positional long range order [1]. The aligned nematic LC molecules, on the average, are characterized by one symmetry axis, called the director **n**. The director can be reoriented by an external field, such as electric field, magnetic field or optical field when the field strength exceeds the Freedericksz transition threshold. Since liquid crystals are birefringent, the field-induced director axis reorientation imparts a large phase change on an optical field traversing the film. The phase change can be a pure phase modulation (without changing the polarization state of the incident light), a phase retardation, or a polarization rotation depending on the molecular alignment of the LC directors.

Smectic phase, unlike nematic phase, are characterized by additional degrees of positional order. Generally, the molecules are arranged in layers in these mesophases, which can be considered as one-dimensional density waves. In each layer the molecules are positionally random, but directionally ordered with their long axis normal to the plane of the layer. The order parameter of smectic phase is usually higher then that of a nematic phase.

Cholesteric liquid crystal is the phase that we will focus in this dissertation. Therefore, we will introduce what cholesteric liquid crystal is and its properties, especially its photonic properties in Sec. 2.3.

2.2   Optical and dielectric anisotropy

The optical properties of a LC are highly dependent on the molecular distribution.

When parallel aligned (homogeneously aligned) between two substrates with surface treatment, nematic LC functions as a uniaxial layer and exhibits optical and dielectric anisotropies. Birefringence ($\Delta n = n_e - n_o$) is defined as the difference between the refractive indices of the extraordinary ray (n_e) and the ordinary ray (n_o) [3, 4]. Birefringence of a LC is mainly determined by the molecular conjugation, differential oscillator strength, and order parameter. A more linearly conjugated rod-like LC would exhibit a larger optical anisotropy. Almost all the light modulation mechanisms, except guest-host displays, utilize a voltage-induced LC refractive index changed caused by molecular reorientation.

The dielectric anisotropy is defined as $\Delta\varepsilon = \varepsilon_{//} - \varepsilon_{\perp}$, where $\varepsilon_{//}$ and $\varepsilon_{\perp}$ denote the dielectric permittivity parallel and perpendicular to the LC director, respectively [3, 4]. The origin of the dielectric anisotropy is the anisotropic distribution of the molecular dipoles in liquid crystal phase. Therefore, nematic phase formed by elongated molecules carrying longitudinal and transverse dipoles have respectively positive and negative dielectric anisotropy, whose magnitude increases with that of the molecular dipoles and with the degree of ordering. Dielectric anisotropy determines the behavior of LC reorientation under the applied voltage. For the LC material with a positive $\Delta\varepsilon$, the LC director follows the electric field while those with negative $\Delta\varepsilon$, the directors tend to be reoriented perpendicular to the electric field.

2.3   Cholesteric liquid crystals and their photonic properties

Cholesteric (or chiral nematic) liquid crystal resembles nematic liquid crystal in all physical properties except that the molecules tend to align themselves into a helical structure

7

with the helical axis perpendicular to the director, as depicted in Fig. 2.2. The helical structure leads to a selective reflection in wavelength and circular polarization [4]. The length over which the LC directors rotate by 2π is defined as helical pitch, which indicates the extent of twist of LC molecules.
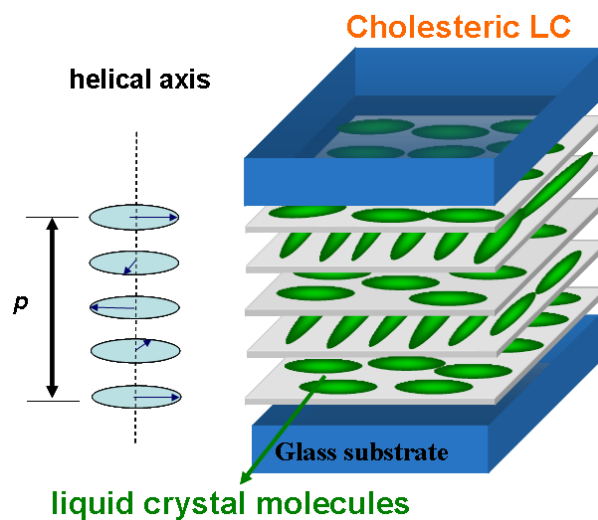
Fig. 2.2 Cholesteric liquid crystal planar structure with helical axis perpendicular to substrates;

The polarization states of the reflected and transmitted waves highly depend on the pitch length of the cholesteric [1]:

(i) If the helical pitch is much larger than the incident light wavelength, both reflected and transmitted waves are plane-polarized and periodically modulated by the pitch of the liquid crystal structure.

(ii) If the helical pitch is much smaller than the wavelength, there are two circularly polarized waves in the medium.

(iii) If the incident wavelength is comparable to the helical pitch, the reflected light is strongly circularly polarized. One circular component is almost totally reflected while the

8

other passes through practically unchanged. The reflected wave preserves its sense of circular polarization.

The selected reflection for circular polarization is determined by simple relationships through Eqs. (2-1)- (2-2):

$$\lambda_0 = <n> p \qquad (2-1)$$

$$\Delta\lambda = \Delta n \cdot p \qquad (2-2)$$

where $\lambda_0, \Delta\lambda, <n>, \Delta n$, and p represent the central wavelength of the reflection band, bandwidth of the reflection band, average refractive index, birefringence of the LC mixture and the pitch length. Pitch length is related to helical twist power (HTP) of the chiral dopant and the concentration (c wt%) by Eq.(2-3):

$$p = \frac{1}{HTP \cdot c\%} \qquad (2-3)$$

Usually cholesteric liquid crystals will go through three stages in response to the increasing external voltage (V) [4]. At V=0, the LC directors are planar aligned and Bragg reflection is established so that it shows selective reflection band. As the voltage increases, the LC directors turn into a focal conic texture which is a strong scattering mode, where the chiral structure is strongly disturbed into a random distribution due to the competition of electric force and anchoring force. Under high voltage driven, the electric force dominates so that it becomes homeotropic texture. Figure 2.3 depicts the LC distribution in different textures.
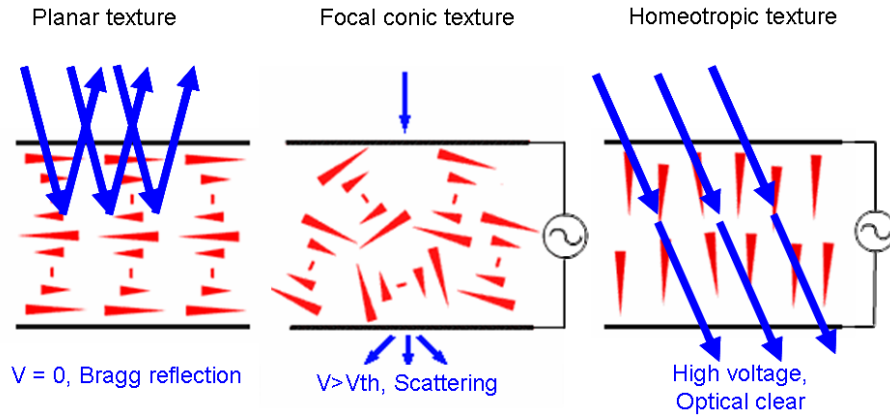
Fig. 2.3 Cholesteric liquid crystal under voltage driving at planar texture (V=0), focal conic texture (V>V_{th}) and homeotropic texture (high V).

In recent years, cholesteric liquid crystals are discovered to be a promising photonic band gap material [5]. Photonic crystals (PCs) – the bulk materials with 1D, 2D, or 3D periodic refractive index change exhibit the photonic band gap (PBG) for photons where the photons within a certain frequency range are forbidden to propagate through. They are particularly useful in shaping the density of states (DOS), localizing photons, and guiding the waves [6, 7].

From a photonic viewpoint, the self-organized helical structure and alternating refractive index change, i.e. n_e-n_o-n_e…in CLC lead to the formation of a band gap due to Bragg reflection. It resembles the energy gap in semiconductors so as to be regarded 1D photonic crystal. Dowling et al predicted that low threshold lasing should occur at the edge of a photonic stop band of a 1D periodic structure because the group velocity ($v_g = \dfrac{d\omega}{dk}$) near the band edge is substantially reduced [8]. Correspondingly, the photon dwell time τ ($\tau \propto^{-1} v_g$) and DOS ($DOS \propto^{-1} v_g$) are dramatically enhanced. In contrast, within the band gap, the wave is evanescent and decays exponentially, so that the circular polarized wave

10

vanishes in large structures and spontaneous emission is suppressed. This is known as the photonic band edge mode. Lasing action at the band edge and a suppressed DOS of waves propagating in the directions of the periodic modulation can be readily observed in dye-doped cholesteric liquid crystals [9].

The lifetime of the excited state can be modified not only at the band edge but within the band gap as well [6]. If a single defect is introduced into an otherwise perfect PC, a localized defect mode (or a group of defect modes) may appear at the frequency inside the band gap. Such cavity modes formed from a single defect can be utilized to produce low-threshold lasing. The vertical cavity surface-emitting laser (VCSEL), in which an optical mode is sharply peaked near a defect layer between two sets of distributed Bragg reflectors, is a direct demonstration of this [10].

Accordingly, chiral photonic band structure works as a distributed feedback (DFB) cavity for band-edge resonance or distributed Bragg reflector (DBR) for localized defect mode resonance. As an emerging class of low-threshold and mirrorless laser, stimulated emission based on chiral liquid crystals attracted tremendous interests in the past few years. Furthermore, the concept has also been extended to micro-cavity lasers and polymer lasers. This is also the research focus of this dissertation.

2.4   References

1. I. C. Khoo and S. T. Wu, *Optics and Nonlinear Optics of Liquid Crystals* (World Scientific, Singapore, 1993).

2. http://nobelprize.org/educational_games/physics/liquid_crystals/history/index.html

3. P. Yeh and C. Gu, *Optics of Liquid Crystal Displays* (John Wiley & Sons, New York, 1999).

4. S. T. Wu and D. K. Yang, *Reflective Liquid Crystal Displays* (John Wiley & Sons, New York, 2001).

5. V. I. Kopp, Z. Q. Zhang and A. Z. Genack, "Lasing in chiral photonic structures," Prog. Quantum Electron. 27, 369 (2003).

6. E. Yabolonovitch, "Inhibited spontaneous emission in solid-state physics and electronics," Phys. Rev. Lett. 58, 2059 (1987).

7. J. D. Joannopoulos, R. D. Meade, and J. N. Winn, *Photonic Crystals: Modeling the Flow of Light* (Princeton University Press, Princeton, NJ, 1995).

8. J. P. Dowling, M. Scalora, M. J. Bloemer, and C. M. Bowden, "The photonic band edge laser: A new approach to gain enhancement," J. Appl. Phys. 75, 1896 (1994).

9. V. I. Kopp, B. Fan, H. K. M. Vithana, and A. Z. Genack, "Low-threshold lasing at the edge of a photonic stop band in cholesteric liquid crystals," Opt. Lett. 23, 1707 (1998).

10. H. Yokoyama and K. Ujihara, (Eds.), *Spontaneous Emission and Laser Oscillation in Microcavities* (CRC Press, Boca Raton, FL, 1995).

CHAPTER 3   EMISSION ENHANCEMENT OF CHOLESTERIC LIQUID CRYSTAL LASERS USING AN EXTERNAL REFLECTOR

3.1   Introduction

3.1.1   Prior art

The earliest work on cholesteric liquid crystal based DFB laser stems from 1978 when N.V. Kukhtarev successfully demonstrated a dye-doped CLC laser [1] and 1980 when I. P. Chishin demonstrated temperature tuning of dye-doped CLC laser [2]. About 15 years later when photonic crystal and liquid crystal technologies grow to a more mature level, CLC laser is refreshed from photonic crystal viewpoint and again attracts much research interests. After the theoretical prediction of photonic band edge lasing by Dowling et al. in 1994 [3], low threshold PBE lasing action from cholesteric liquid crystal was experimentally observed [4-8]. With the similar chiral structure, PBE lasing can also be achieved in dye-doped ferroelectric liquid crystals [9, 10], blue phase (3D photonic crystal) [11, 12], CLC elastomer [13], CLC glasses [14] and polymer network [15, 16]. It is also interesting to note that by using cholesteric liquid crystalline polymers, flexible standing film can be obtained for lasing [17-20]. The micro-laser array was realized by the dye-doped helical liquid crystal embedded in the periodic, polymeric micro-channels using optical holography [21]. Because of the elongated length, the cavity shows a higher quality factor and ultra-low threshold.

Photonic defect mode lasing has also been observed when a twist discontinuity is introduced into the 1D periodic structure, corresponding to the additional resonant mode

inside the band gap. For CLCs, defect may be introduced by replacing a thin layer of CLC by isotropic materials [22], anisotropic material [23], or by introducing a phase jump in the cholesteric helix [24-25]. More defect mode lasing methods are mentioned in Sec. 4.1. As far as phase jump defect is concerned, it cannot be accomplished by a low molar mass CLC, so polymeric CLC film should be applied.

One of the advantages for CLC lasers is the tuning flexibility. Chiral liquid crystals show the photonic reflection band where the chiral pitch is determined by the chiral dopant concentration. The change of pitch, and therefore the lasing tunability can be controlled by changing the chiral dopant concentration. Lasing wavelength can also be adjusted by the control of chiral concentration [26], external electric field [27, 28], mechanical stress [13], temperature [29], and photochemical effect [30-34]. In order to broaden the tuning range, two different laser dyes were mixed together to achieve a much broader fluorescence band [35].

On the other hand, there have also been some efforts addressing the optical efficiency improvement. From a material point of view, there are many factors which contribute to the final laser output, e.g., LC birefringence (determines the index modulation contrast), average refractive index, dye concentration, absorption and emission order parameters of laser dye, surface alignment, solubility, etc. Although no general rules for comparing different materials, order parameter is proven to play an important role. Morris et al have demonstrated the pumping efficiency (~17%) by choosing a suitable LC host and dye with high order parameter [36-38]. Araoka applied polymeric dye which improved S_T (transition dipole moment order parameter of dye) to 0.49 in order for better lasing efficiency (25-30%) [39].

In this chapter, we incorporate different types of reflectors, including a passive external CLC reflector, an in-cell metallic mirror or an external metallic mirror to the CLC laser in order to get higher lasing efficiency. Amemiya et al [40] applied a similar idea using a spin-coated CLC film and evaporated aluminum layer inside LC cells where only enhanced emission was reported with no detailed discussion on the polarization states and beam qualities.

3.1.2 Amplified spontaneous emission

In this dissertation, the laser dye we used is DCM (4-(dicyanomethylene)-2-methyl-6-(4-dimethlyaminostryl)-4H-pran, from Exiton). The molecular structure is shown in Fig. 3.1.
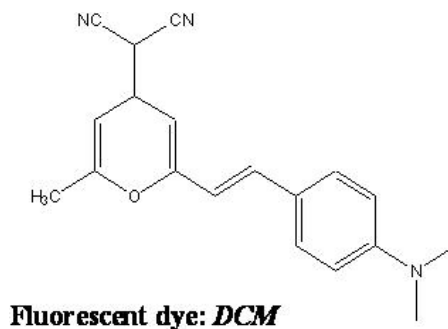
Fig. 3.1 Molecular structure of fluorescent dye DCM.

Figure 3.2 shows the absorption and fluorescence spectra of DCM. The absorption peak is around 470 nm and fluorescence peak is around 590-615 nm. In the experiment, we may observe the band edge lasing from cholesteric liquid crystals up to 660 nm which is far from the fluorescence peak.
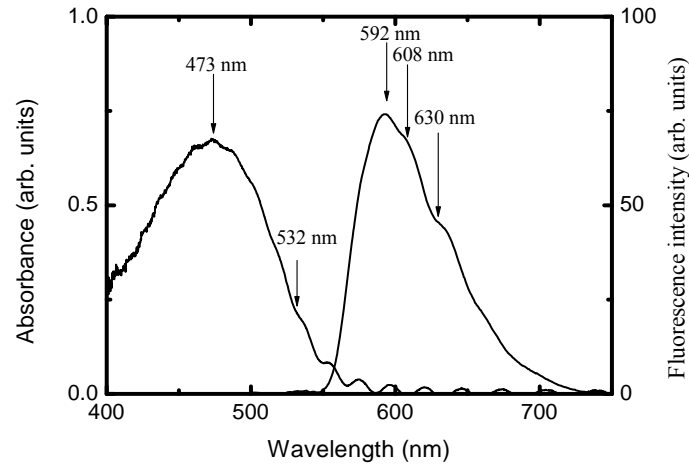
Fig. 3.2 Absorption and fluorescence spectrum of laser dye DCM (Courtesy of Prof. Harry J. Coles, University of Cambridge, UK)

DCM exhibits dichroism so that it absorbs light more strongly along one axis than the other. As a positive dye whose major component of the transition moment is along the long molecular axis, it absorbs more light polarized along the long molecular axis than the perpendicular one. We measured the dye absorption transition dipole moment (order parameter S) for different dye concentrations from 0.2-2 wt % in nematic LC host (BL006) without chiral dopant. Results are shown in Fig. 3.3, where the order parameter S decreases as dye concentration increases. These data were collected by measuring the normalized transmittance (by eliminating the effect of Fresnel reflection and absorption) parallel ($T_{//}$) and perpendicular ($T_{\perp}$) to the linearly polarized incident light at λ=532 nm through Eqs. (3-1) and (3-2):

$$\text{Dichroic Ratio (DR)} = \frac{\log(T_{//})}{\log(T_{\perp})} \tag{3-1}$$

$$S = \frac{DR - 1}{2DR + 2} \tag{3-2}$$

16
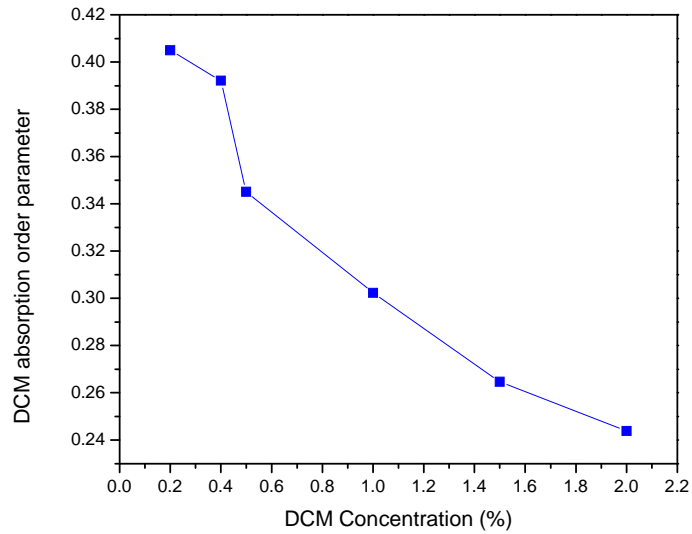
Fig. 3.3 Concentration-dependent absorption order parameter of DCM in BL006 LC host.

The organic laser dye is a highly emissive material so that the small surface reflection (~4% at each surface) from two glass substrates provides a feedback for the spontaneous emission. As the result, amplified spontaneous emission (ASE) was observed in DCM doped BL006 mixture in a 15 μm homogeneous cell, as shown in Fig. 3.5. The pumping source is frequency-doubled Nd:YAG pulsed laser operated at λ=532 nm, 4 ns pulse width, 1 Hz repetition rate and 0.3 mJ /pulse. The set up is shown in Fig. 3.4 where the pump beam is focused into the dye-doped nematic LC cell. Laser emission is filtered and collected by a focusing lens into fiber-based spectrometer (HR2000, Ocean Optics).
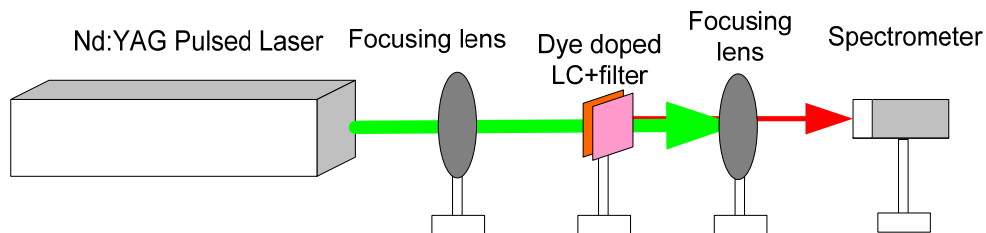
Fig. 3.4 Experimental setup of amplified spontaneous emission of dye doped liquid crystal.
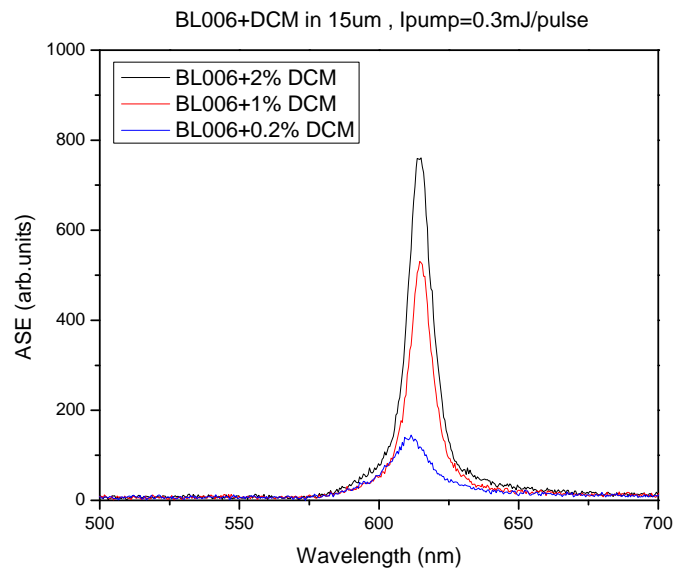
Fig. 3.5 Amplified spontaneous emission from DCM doped BL006 at different dye concentrations. Pump intensity is 0.3 mJ/pulse; Cell gap is 15 μm.

Compared to dye-doped CLC laser, much higher pump energy is needed for light emission. No threshold is observed so we believe this is ASE but not a stimulated emission. Samples with dye concentration at 0.2%, 1% and 2% were measured. Considering the small absorption spectrum tail overlapped with the fluorescence peak, ASE peak wavelength of the DCM doped BL006 is around λ=615 nm. The full width of half maxima (FWHM) is around 10~13 nm. The best concentration for achieving strong laser output is 1% - 2%.

3.2   Emission enhancement by a single cholesteric liquid crystal reflector

3.2.1 Introduction

Lasing efficiency and beam divergence are the two major concerns when designing a laser. They are mainly determined by two factors: the gain medium and the laser cavity structure. Higher lasing efficiency can be obtained by using an optical gain medium with

higher emission efficiency. With the same optical gain medium, more efficient feedback from the laser cavity is needed to achieve a higher lasing efficiency. For a CLC laser, a thicker LC layer can provide a longer DFB, i.e. more efficient feedback which, in turn, increases the lasing efficiency and reduces the beam divergence. However without a special fabrication process, the thickness of a defect-free CLC is typically limited to ~10 μm due to insufficient surface anchoring force in the bulk area. As a result, the lasing efficiency of a CLC laser is highly restricted and such a short cavity length gives rise to a highly divergent laser beam. Here, we focus our attention on the novel structure of laser cavity, capable of providing more efficient feedback for emitted photons. In this section, we incorporate a passive CLC reflector to the dye-doped CLC active cell (master lasing cell) to serve as a polarization conserved reflector. Because of this CLC reflector, the effective laser cavity length is significantly increased. Consequently, the lasing efficiency is enhanced dramatically and the beam divergence is reduced significantly. Another advantage of this polarization conserved reflector is that it enables a higher lasing performance from a thinner active CLC layer. A thinner CLC cell is easier to obtain a defect-free morphology than a thicker layer due to stronger surface anchoring energy. To validate this hypothesis, we investigate the cell gap effects of the active CLC cell. An optimal cell gap for our dye-doped CLC laser system is about 10 μm. The corresponding physical mechanisms are explained.

3.2.2 Sample preparation and experiments

To fabricate an active CLC cell, we first prepared a right-handed CLC host mixture by

mixing nematic liquid crystal BL006 ($n_e = 1.826, \Delta n = 0.286$ at λ=589 nm and T=20 ^{o}C, from Merck) with 27.3% right-handed chiral agent MLC-6248 (HTP=11.3 μm^{-1}, from Merck). Afterwards, we doped 1.5 wt% of fluorescent dye DCM to the CLC mixture. The whole mixture was thoroughly mixed before it was capillary-filled into the empty LC cell in an isotropic state. The inner surfaces of the glass substrates were first coated with a thin indium-tin-oxide (ITO) layer and then over coated with a thin (~80 nm) polyimide layer. The substrates were subsequently rubbed in anti-parallel directions to produce ~2-3° pretilt angle. A slow cooling process was necessary to obtain defect-free single domain morphology. To study the cell gap effects, we fabricated three active CLC cells with 8 μm, 10 μm, and 15 μm cell gaps. In a short pitch CLC layer, the strong chiral turn competes with the surface anchoring force so that multi-domain cholesteric defects cannot be completely eliminated, especially for the cell gap larger than 10 μm. Hence, light scattering is introduced which increases the loss in the laser cavity. To prepare a right-handed passive CLC reflector, we mixed ~25 wt% MLC-6248 into BL006. The passive CLC reflector has a 5 μm cell gap, whose reflection band covers the lasing wavelength of the active CLC laser. In the lasing experiment, the passive CLC cell is in proximity contact with the active CLC cell to avoid any air gap and interface reflections.

Figure 3.6 sketches the experimental setup used to characterize the CLC laser output and beam divergence. The pump source is a frequency-doubled Nd:YAG pulsed laser (Minilite II, Continuum) operated at wavelength λ=532 nm, 4 ns pulse width, and 1 Hz repetition rate. The reason we chose such a low repetition rate is to reduce the thermal

accumulation inside the active CLC cell. The local temperature increase at pumping area is estimated ~10°C, which does not affect the local cholesteric planar structure noticeably because the mixture's clearing point is above 100 ^{o}C. The pumping beam was separated into two channels by the beam splitter: one was sent to an energy meter (Laserstar, Ophir) for monitoring the input energy and the other was focused onto the CLC cell. Because the absorption dichroism of the dye molecules is distributed in a helical manner, the CLC laser does not exhibit any polarization preference for the pumping beam [41]. However, we chose the left-handed circularly polarized (LCP) light to pump the right-handed CLC cell in order to reduce Bragg reflection even if the reflection band overlaps with the pumping wavelength [42]. Since the reflection band of the passive CLC layer covers the lasing wavelength but transmits the pumping wavelength, the configuration in normal incident pump will reduce the surface reflection to its maximum. The emitted laser light is collected into a fiber-based spectrometer (Ocean Optics, HR2000, resolution = 1.0 nm) along the direction exactly perpendicular to the glass substrates where the periodic refractive index modulation lies.
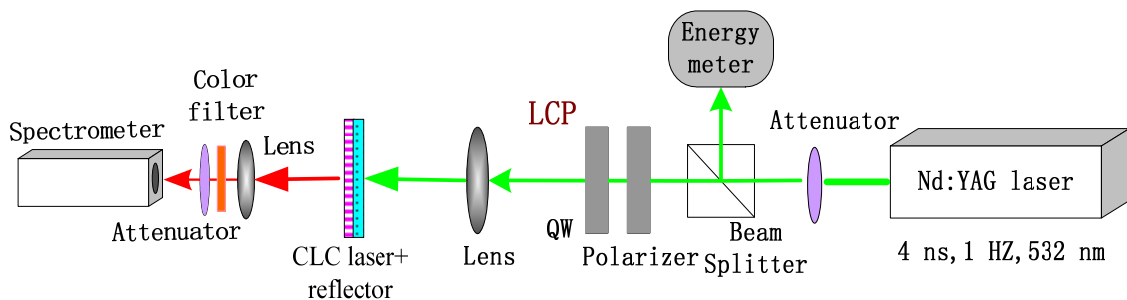
Fig. 3.6 Experimental setup at normal incidence. LCP: left-handed circularly polarized light; QW: quarter wave plate.

3.2.3 Microscopic morphology of CLC cells

The morphologies of our three CLC active cells (8 μm, 10 μm, and 15 μm) and the 5 μm passive CLC reflector were investigated using a polarizing optical microscope (Objective 10, Olympus). Results are shown in Figs. 3.7(a)-(d), respectively. As the cell gap increases from 5 μm to 15 μm, the single domain of cholesteric planar structure gradually deteriorates and defect lines begin to aggregate, which results in a higher scattering loss in a thicker cell, e.g., the 15 μm cell.

The color difference in Fig. 3.7(d) originates from the different chiral concentration of the passive CLC reflector. From Eq. (2-3), a larger chiral concentration leads to a shorter pitch length and hence a shorter reflection wavelength (green).
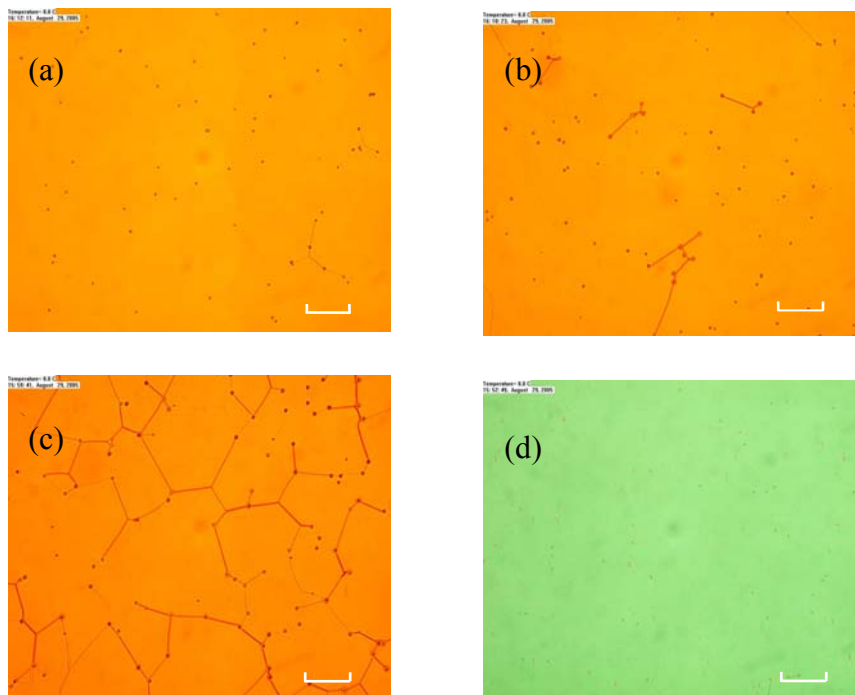
Fig. 3.7 Microscopy images of cholesteric liquid crystal morphologies: (a) 8 μm DCM-doped CLC cell, (b) 10 μm DCM-doped CLC cell, (c) 15 μm DCM-doped CLC cell, and (d) 5 μm CLC cell. The white bar in each figure shows a scale of 100 μm.

3.2.4 CLC laser output power

Figure 3.8 shows the wavelength dependent normalized transmittance of the three active CLC cells at 8 μm, 10 μm, and 15 μm gaps and the passive CLC cell at 5 μm gap. The lasing spectrum using a single 8 μm active CLC cell pumped at 30 μJ/pulse is also included in the figure as an example. It is seen that the reflection band of the passive cell covers the photonic band edge (long wavelength edge) of the active cell where lasing takes place. The short wavelength edges of the active CLC cells are obscured by the DCM absorption. The full width of half maximum (FWHM) of the lasing spectrum was measured to be 0.8-1.0 nm. The lasing wavelength for the single 8 μm, 10 μm, and 15 μm cell is located at around λ=603 nm.
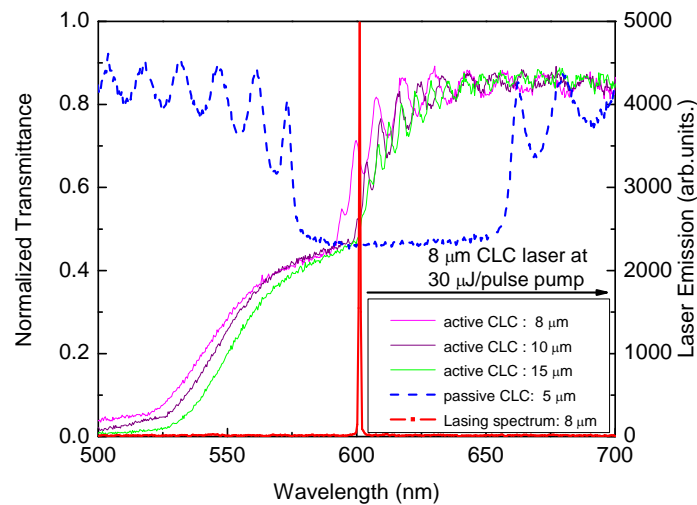
Fig. 3.8 Wavelength dependent normalized transmittance of three active CLC cells (8, 10, and 15 μm) and a passive CLC cell (5 μm). The red line is the lasing spectrum of the 8 μm active CLC cell at 30 μJ/pulse pump.

To demonstrate how the CLC reflector improves the lasing efficiency and reduces beam divergence, we have conducted experiments using an active CLC cell with/without the CLC reflector. Figures 3.9-3.11 plot the pumping energy dependent lasing performance using

23

a 5 μm passive CLC cell combined with the 8, 10, and 15 μm active cells respectively and compare the performance to those without the passive CLC cell. The passive CLC reflector is kept at 5 μm for two reasons: 1) it provides enough reflectivity at the lasing wavelength, and 2) the thin layer is defect-free. In Figs. 3.9-3.11, the red and magenta curves represent the total laser output power and its corresponding left-handed circularly polarized (LCP) component for the active-passive layered CLC laser, respectively. Similarly, blue and green curves are for the single layer CLC lasers. The lasing threshold for the single 8, 10, and 15 μm active cells was measured to be 1.8, 1.0, and 0.5 μJ /pulse, respectively. Laser action was observed at the long wavelength band-edge but at a slightly different wavelength (603, 604, and 604 nm). With the passive CLC reflector, the lasing threshold does not drop noticeably because the laser output intensity is unstable near the threshold. As a result, the threshold change could be easily obscured by the intensity fluctuation of the pumping pulse. A remarkable threshold drop (from 22-10 μJ/pulse) was observed when using a 5 μm-thick active cell and the same passive reflector. However, the 5-μm CLC double-cell assembly has a much lower lasing efficiency so that its data are not included here for comparison. The fluctuations observed in the curves result from the fluctuation of the pumping Nd: YAG laser and different reflection point on the passive cell each time a pulse is captured.
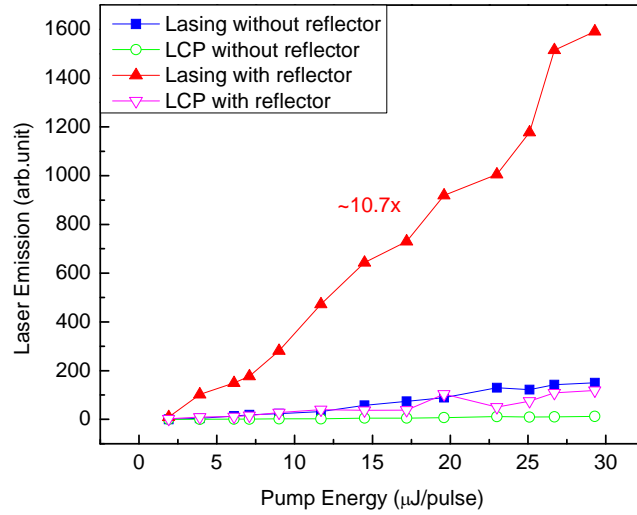
Fig. 3.9 Pumping energy dependent laser output power of the 8-µm active CLC cell with a 5 µm passive CLC reflector. Threshold ~1.8 µJ/pulse at λ=532 nm. The average enhancement ratio is ~10.7X.
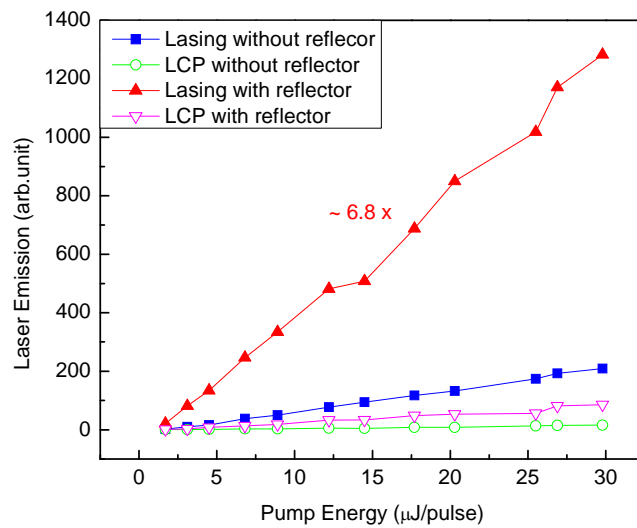
Fig. 3.10 Pumping energy dependent laser output power of the 10-µm active CLC cell with a 5 µm passive CLC reflector. Threshold ~1.0 µJ/pulse at λ=532 nm. The average enhancement ratio is ~6. 8X.
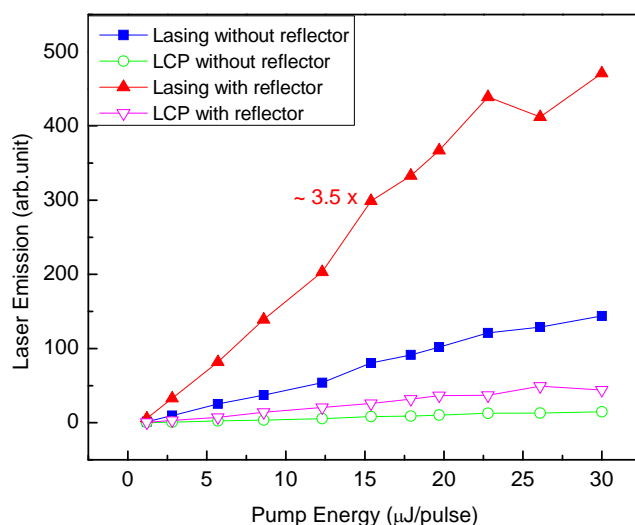
Fig. 3.11 Pumping energy dependent laser output power of the 15-μm active CLC cell with a 5 μm passive CLC reflector. Threshold ~0.5 μJ/pulse at λ=532 nm. The average enhancement ratio is ~3.5X.

From Figs. 3.9-3.11, the single active CLC laser generates a circularly polarized light in the same handedness as the cholesteric helix (RCP light in our case). As a consequence of CLC-based polarization selective DFB, only circularly polarized light in the same handedness experiences high reflectivity inside the cavity. Yet a small part (<10%) of the opposite circularly polarized light (LCP) exists due to the imperfection of CLC's periodic structure and the surface reflection from the glass substrates.

In a double-cell CLC structure, laser output power is enhanced by more than twice (actually 3.5-10.7X) in all the three lasers studied despite of their different active layer thickness. Besides, RCP component still dominates the total output. That means the reflected light from the CLC reflector gets further amplified by the gain medium. In the same helical handedness as the master CLC lasing cell, the passive CLC reflector well preserves the

original polarization state of the reflected beam without introducing π phase change. As a result, the reflected beam is still at band edge wavelength and more importantly, in the same polarization state as can be facilitated by DFB cavity for a band edge mode resonance. Under this circumstance the passive cell functions equivalently as a "polarization conserved reflector" for the polarization selective cavity and the effective length of the amplifier is therefore doubled.

However, the lasing enhancement ratio due to the passive CLC reflector is different for the three lasing samples. Figures 3.9-3.11 show that the enhancement ratio decreases as the master CLC cell gap increases. Usually, a thicker CLC cell provides a longer DFB length, i.e., a larger optical gain which leads to a higher lasing efficiency. Nevertheless another two factors contributes to the enhancement as well: 1) the increase of net gain (the difference between gain and loss in the cavity) due to passive CLC reflector, and 2) how much light can be reflected back into the original cavity. With a virtually length-doubled amplifier and feedback, both gain and loss are simultaneously doubled. One can benefit from a doubled net gain caused by a length doubled amplifier if the single path net gain is positive. As long as the total length is below the saturation length (the length corresponding to the saturation output intensity), the output power grows exponentially with the increase of gain length, leading to the dramatic enhancement we observed. On the other hand, the overlap of the original laser beam and the reflected laser beam creates the possibility of further amplification. For a single layer CLC laser, a thicker cell has smaller beam divergence but also a smaller acceptance angle for the reflected beam. Because the passive "polarization

conserved CLC mirror" is not curved, it further diverges the beam upon reflection. Thus the smaller acceptance angle in a thicker cell restricts the output enhancement more heavily. According to our experimental results, the acceptance angle is the killing factor which determines the enhancement ratio.

3.2.5 CLC laser beam divergence and beam profile

In addition to the dramatic enhancement of the output laser power, the polarization conserved CLC reflector also reduces the beam divergence significantly. Using a high speed CCD camera (ST-2000XM, SBIG), we captured the CLC laser beam spot at a gradually increased distance from the lasing cell. For comparison, the far field patterns of the CLC lasers with and without a passive CLC reflector for the 8 μm, 10 μm, and 15 μm active cells were measured. Results are compared in Figs. 3.12-3.14.

From Figs. 3.12-3.14, we find that as the observation plane moving further away the beam spot size increases quickly. Here, we mainly refer to the center spot since the outer fringes are caused by diffraction. For the single layer active CLC laser, half divergence angle was measured to be 4.43^o, 4.65^o, and 4.77^o for the 8, 10, and 15 μm cell gaps, respectively. A thinner cell seems to have a slightly less divergence than a thicker cell but the difference is quite insignificant considering the measurement error. The large divergence angle of CLC laser originates from the short gain medium length (in μm scale) and the small cross-section area of the emission (~150 μm in diameter). Usually the longer cavity length the smaller divergence angle it is. The reason why the 15 μm laser does not show an obvious advantage

in beam divergence is owing to the strong light scattering from the defect lines.
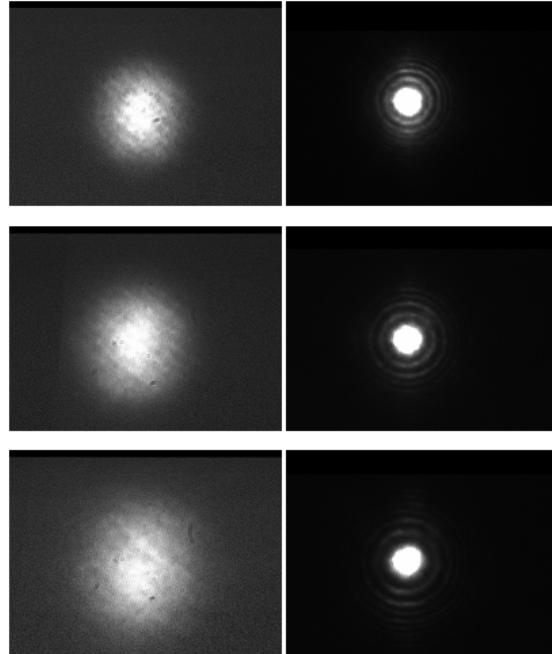
Fig. 3.12 Far field laser patterns of the 8-μm CLC laser at 3.2 cm (top), 4.3 cm (middle), 5.3 cm (bottom) away from the lasing cell. Pumping laser energy is 38 μJ/pulse and λ =532 nm. Left column: single active layer CLC lasers; Right column: active-passive layered CLC lasers.
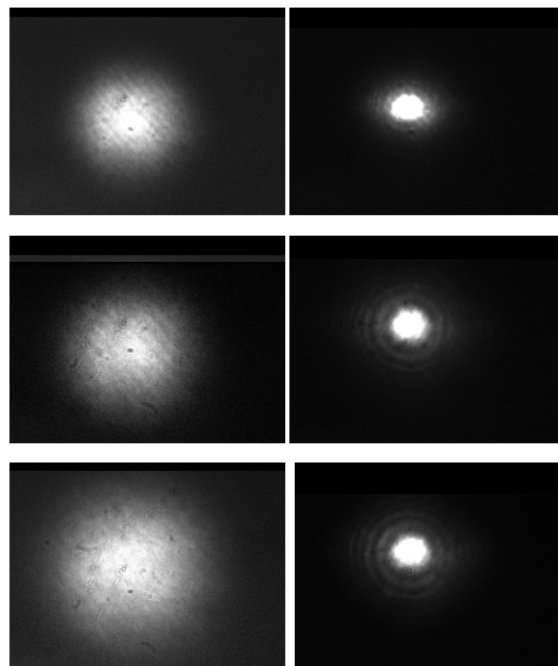
Fig. 3.13 Far field laser patterns of the 10-μm CLC laser at 3 cm (top), 4 cm (middle), and 5 cm (bottom) away from the lasing cell. Pumping laser energy is 38 μJ/pulse and λ =532 nm.

المنارة للاستشارات

www.manaraa.com
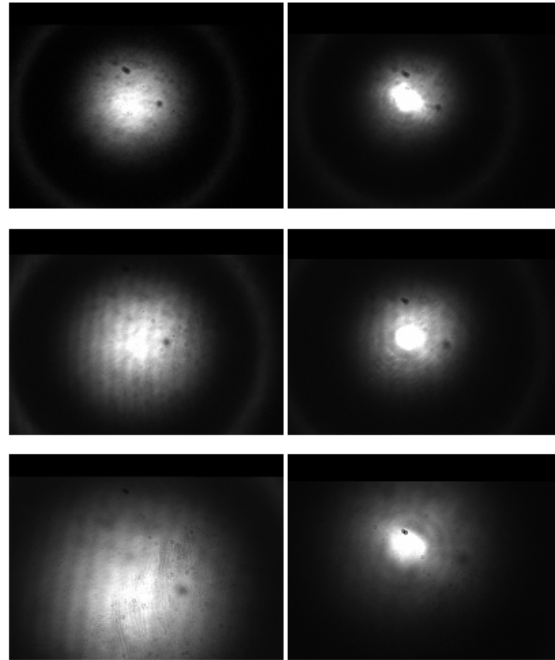
Fig. 3.14 Far field laser beam spot of 15-μm CLC laser at 2.5 cm (top), 3.3 cm (middle), 5.0 cm (bottom) away from lasing cell. Pumping laser energy is 38 μJ/pulse and λ =532 nm. Left column: single active layer CLC lasers; Right column: active-passive layered CLC lasers.

By incorporating a passive CLC reflector to the master lasing cell, the laser spot dramatically shrinks with clearer diffraction fringes. Laser emission energy also becomes much more concentrated within the central spot and the peak intensity remarkably increases. The half divergence angles for the active-passive layered CLC lasers decrease to 0.69°, 0.69°, and 0.37° for the 8, 10, and 15 μm cell gaps, respectively, considering the bright center spot only. No distinct increase in spot size is observed except the appearance of a halation circle around the central spot for the 15 μm double-layered laser whose divergence angle is $\sim3^\circ$.

This evident improvement of beam divergence from the active/passive CLC lasers is due to the effectively increased cavity length. By adding a passive CLC cell which is a "plane

mirror", we introduce two glass substrates (totally 2.2 mm thick) of the LC cells into the cavity so that the cavity length, as a whole, is increased from μm scale to mm scale. Though a virtually doubled gain length also contributes to the decrease of divergence angle, the insert of glass substrate plays a dominant role. In the 15-μm double-layered laser, multi-domain scattering not only limits the output power but also causes degradation of long-range periodic structure within the cell gap. This is why we observed the extra halation around the main spot.

Correspondingly, we extracted the 2D beam profile from the CCD pictures in Figs. 3.12-3.14 as Figs. 3.15-3.17, respectively. The beam shape is neither Gaussian nor Lorentzian, which implies higher order transverse modes should be present, leading to the increased divergence. In Fig. 3.15-3.17, the left column and the right column shows the 2D beam profile without and with a CLC reflector. The vertical axis is the laser intensity in arbitrary units.

31
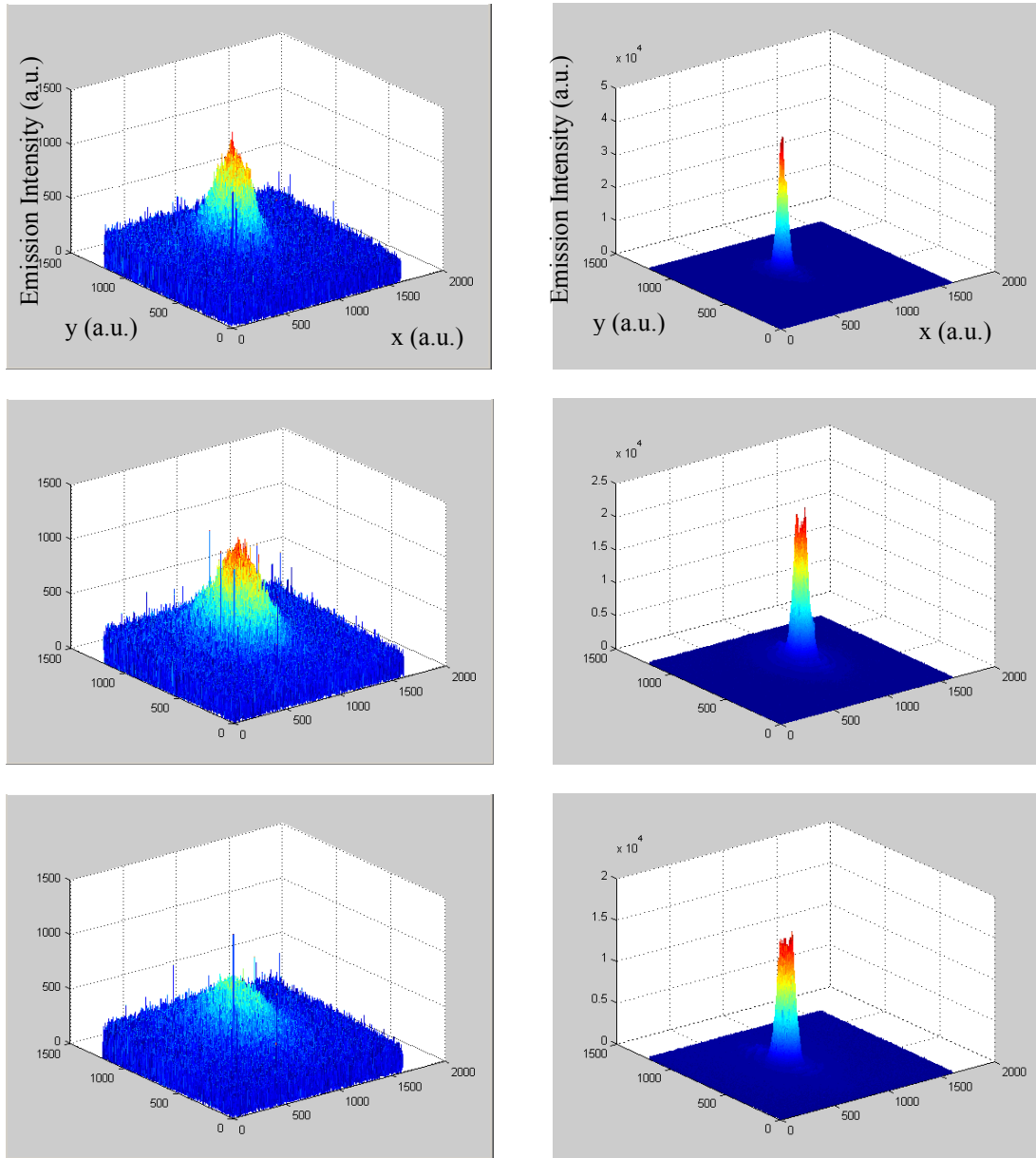
Fig. 3.15 2D laser beam profile of the 8-μm CLC laser at 3.2 cm (top), 4.3 cm (middle), 5.3 cm (bottom) away from the lasing cell. Pumping laser energy is 38 μJ/pulse and λ =532 nm. Left column: single active layer CLC lasers; Right column: active-passive layered CLC lasers.
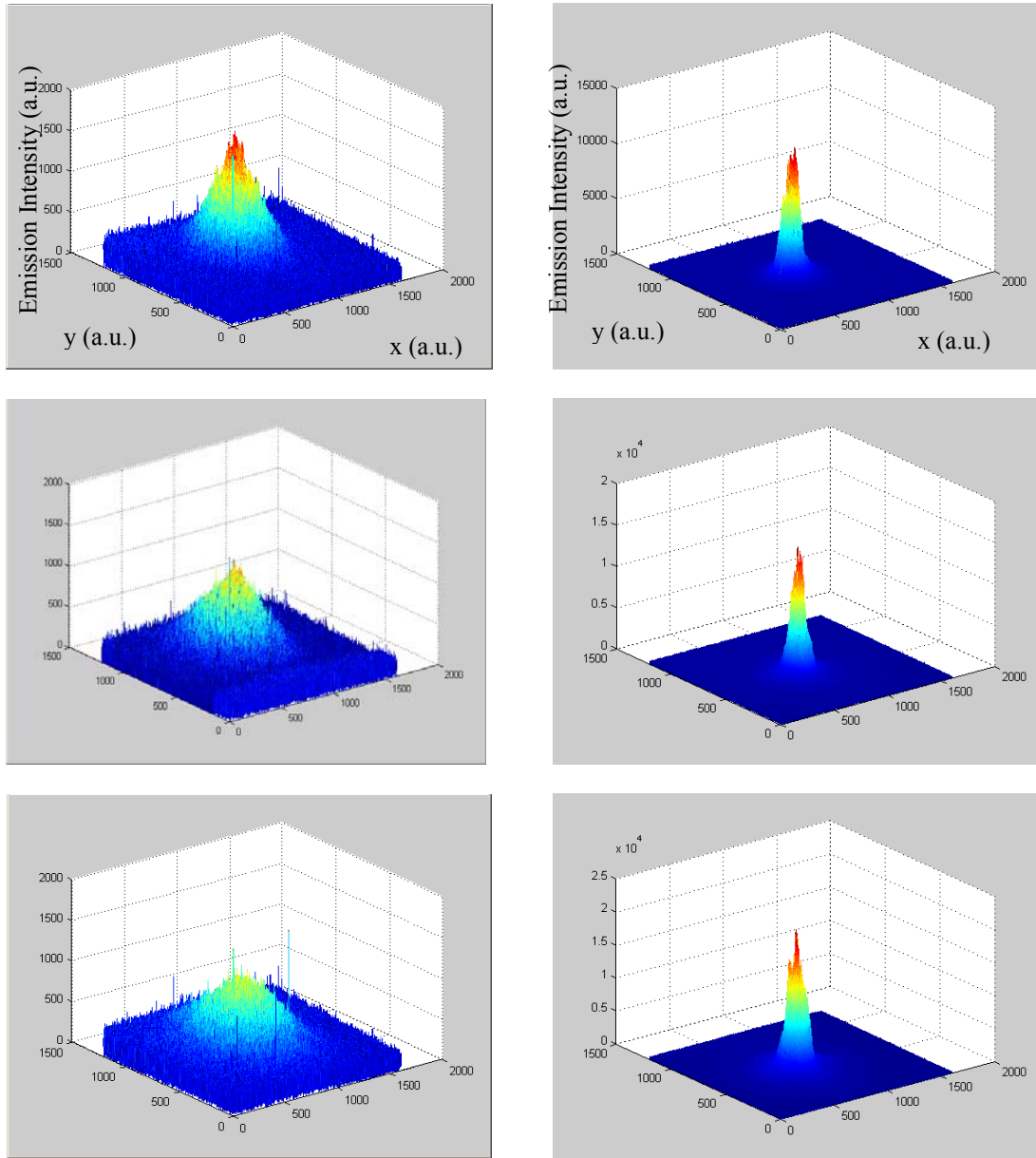
Fig. 3.16 2D laser beam profile of the 10-μm CLC laser at 3 cm (top), 4 cm (middle), and 5 cm (bottom) away from the lasing cell. Pumping laser energy is 38 μJ/pulse and λ =532 nm. Left column: single active layer CLC lasers; Right column: active-passive layered CLC lasers.
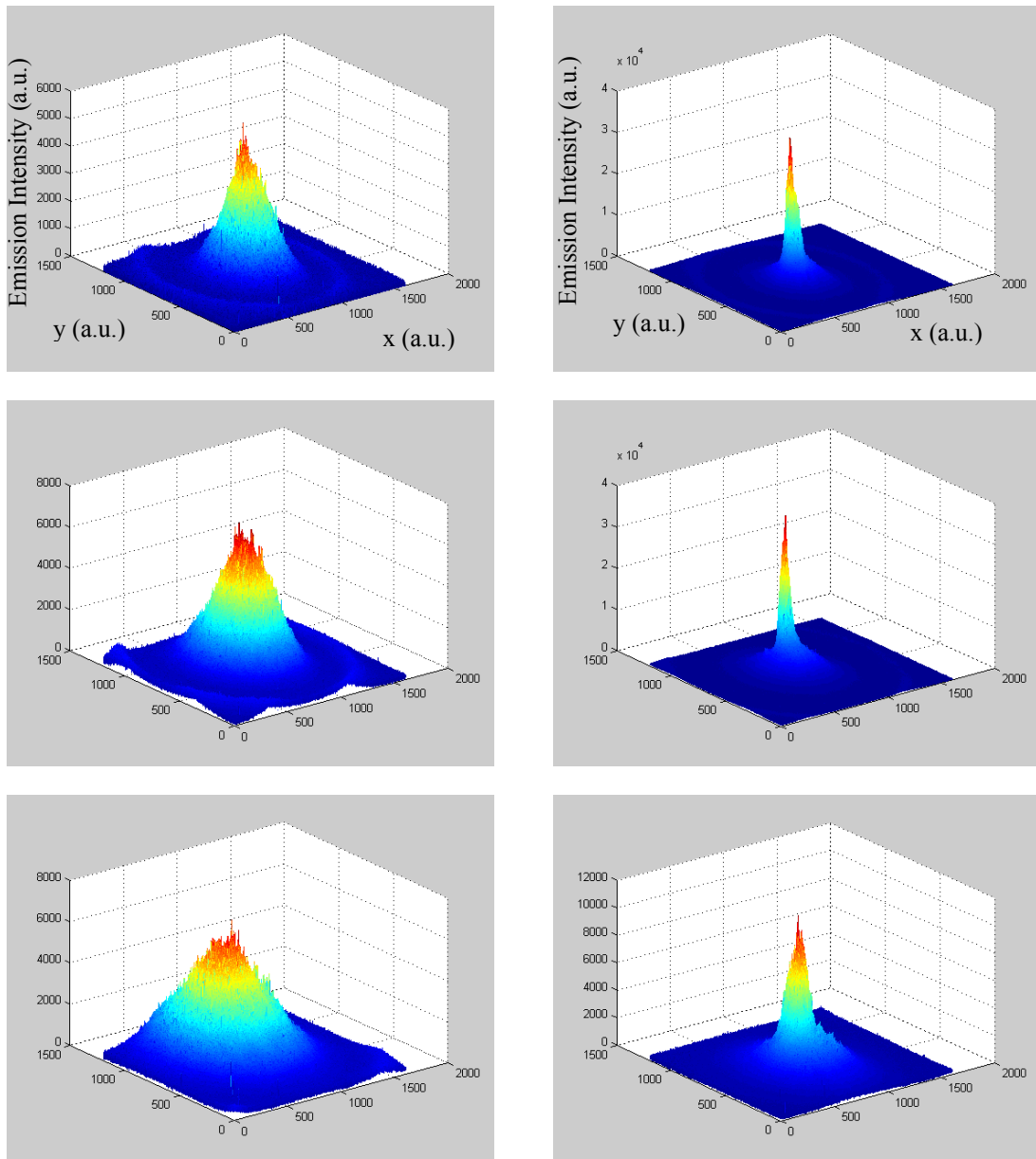
Fig. 3.17 2D laser beam profile of 15-μm CLC laser at 2.5 cm (top), 3.3 cm (middle), 5.0 cm (bottom) away from lasing cell. Pumping laser energy is 38 μJ/pulse and λ =532 nm. Left column: single active layer CLC lasers; Right column: active-passive layered CLC lasers.

3.3 Emission enhancement by an in-cell metallic mirror

3.3.1 Introduction

Because of the chiral structure, laser emission generated from dye-doped CLCs is intrinsically *circularly* polarized in the same sense as the cholesteric helix. The symmetric structure leads to double-sided emission in both forward and backward directions, which is not considered very practical. From Sec.3.2, we know that a passive CLC reflector will enhance the emission and the right-handed polarized emission still dominates the output. On the other hand, an external metallic mirror only doubles the emission because the output from one side is redirected to another based on incoherent superposition. The coherent superposition only takes place when the phase retardation of the two components is smaller than the coherent length of the laser. Accordingly, unlike the external metallic mirror, an in-cell metallic mirror reflector will preserve the coherence of the beam towards two sides.

We use Aluminum (Al) coated homogeneous cell to demonstrate a single-sided CLC laser with the emission dramatically enhanced due to double pumping effect. More importantly, the immediate contact between the active layer and the reflection layer enables coherent superposition of two orthogonal circular polarization states, which produces a *linearly* polarized laser beam with high linearity. Such a method not only enhances the laser emission but also opens a way for flexible manipulation and control on the polarization state as well. Direction tunable linearly polarized laser devices would be useful for various photonic applications.

3.3.2 Sample preparation and experiments

The linearly polarized direction can be fine-tuned within 360° range. We will discuss the tuning strategies in details in Sec. 3.3.5. In order to demonstrate the rotation period of linearly polarized laser, we made two different CLC mixtures with different birefringence. Mixture 1 is composed of BL006 ($\Delta n=0.286$) and 27.3 wt% of MLC6248. Mixture 2 is composed of ZLI-1694 ($\Delta n=0.13$) and 22.9 wt% of MLC6248. Besides, 1-1.5 wt% of laser dye DCM was doped into the CLC mixtures as the active medium. The whole mixture was thoroughly mixed before it was capillary-filled into the homogeneous LC cell in an isotropic state. One of the inner surfaces was coated with aluminum as a mirror reflector and the other was coated with a thin indium-tin-oxide (ITO) transparent electrode. Polyimide layers were spun-coated on both sides and then rubbed in anti-parallel direction to produce 2-3° pretilt angle. After a slow cooling process, a defect-free single-domain cholesteric planar structure was formed.

For experimental setup, we used a reflective configuration at 30° oblique incidence, as Fig. 3.18 shows. The pump source is a frequency-doubled Nd:YAG pulsed laser (Minilite II, Continuum) with pumping wavelength $\lambda=532$ nm, 4 ns pulse width, and 1 Hz repetition rate. The pump beam is separated into two paths with one of them monitored by the energy meter (Laserstar, Ophir) and the other focused on the CLC cell. Again, the circularly polarized pump in counter handedness with respect to the cholesteric helix is employed in order to reduce the CLC Bragg reflection. Then the emitted laser light is collected into fiber-based spectrometer (Ocean Optics, HR2000, resolution=1.0 nm) along the direction exactly

www.manaraa.com

perpendicular to the glass substrates where lies the periodic refractive index modulation.
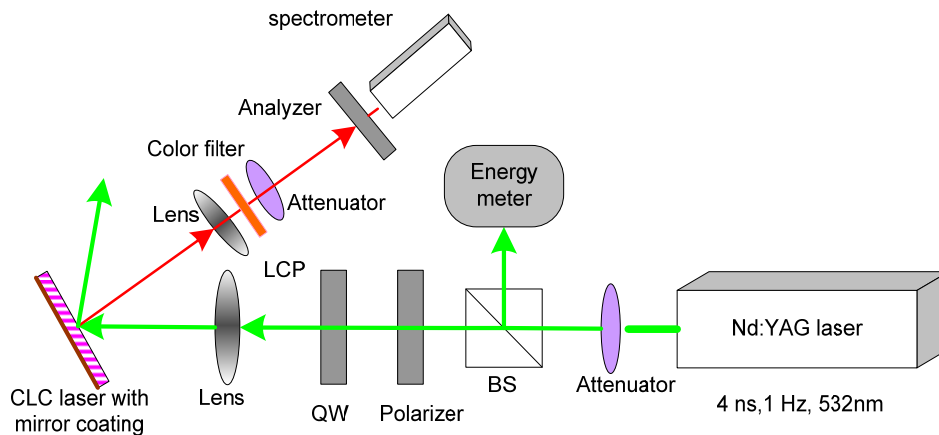
Fig. 3.18 Experimental setup at 30° oblique incidence. LCP: Left-handed circularly polarized light; QW: Quarter wave plate.

3.3.3 Enhanced linearly polarized laser emission

Figure 3.19 plots the transmission spectrum of normal dye-doped CLC lasers without mirror coating. Two samples, made of CLC mixture 1 (using BL006 host) and 2 (using ZLI-1694 host), are shown in blue and green curves, respectively. The data for CLC samples without DCM dopant give an 80 nm reflection band width for BL006 mixture and 40 nm for ZLI 1694 mixture (not shown here). The shorter wavelength edge of the reflection band is somewhat obscured depending on different dye concentrations. As an example, the lasing spectrum from mirror reflective CLC laser using BL006 mixture is plotted as well. The lasing wavelength is 601 nm for the BL006 CLC laser and 610 nm for the ZLI-1694 CLC laser. The FWHM of laser line is around 0.8 nm.
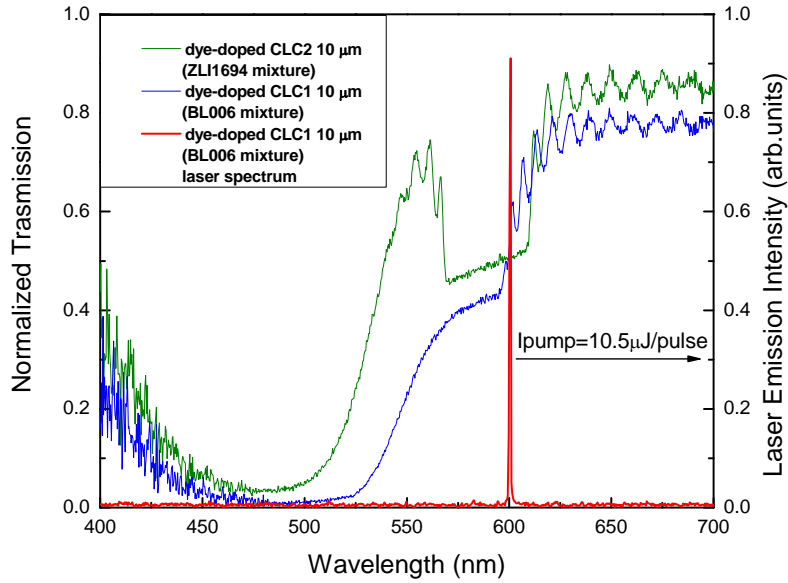
Fig. 3.19 Reflection spectra of a 10-μm-thick dye-doped CLC sample 1 (BL006 +27.3% MLC6248 + 1.5% DCM), a 10-μm-thick CLC sample 2 (ZLI1694+22.9% MLC6248+1% DCM), and lasing spectrum from mirror reflective CLC laser using mixture 1.

Using the setup in Fig. 3.18, we measured the laser emission from the dye-doped BL006 CLC sample in a 10 μm cell with mirror coating on one substrate. Figures 3.20(a)-(b) depict the laser output power change along different analyzer direction at pumping energy of 30 μJ/pulse and 10 μJ/pulse. The blue line shows the experimental results and the red line shows the simulation results, calculated according to Malus's Law [43] as Eq. (3-3) shows:

$$I_{output} = \cos^2(\phi) \tag{3-3}$$

Here I_{output} is the output power after the analyzer and ϕ is the relative angle between the linearly polarization direction and the analyzer. Results here indicate that when rotating the analyzer before the detector, we observed the laser emission power changes as square of cosine at both low and high pumping energies.
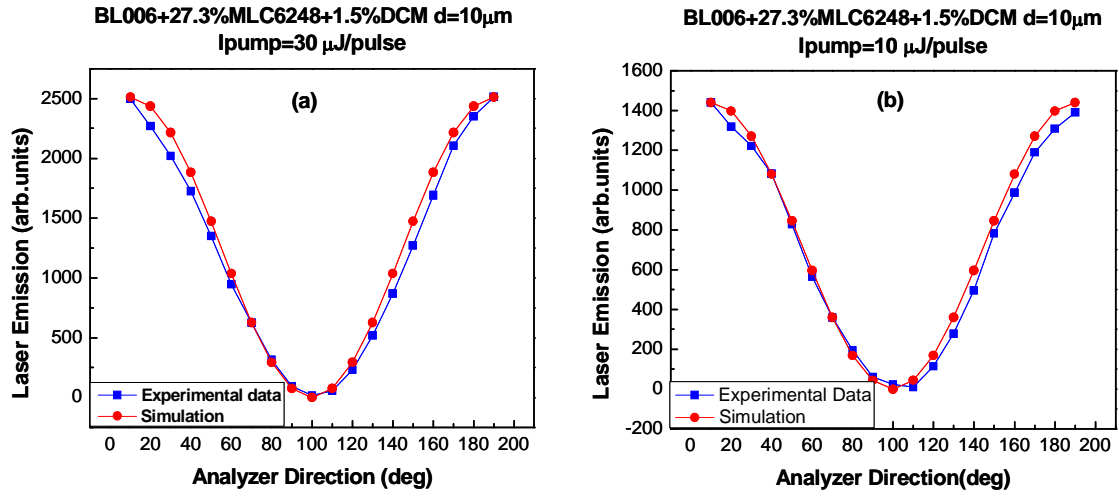
Fig. 3.20 Linearly polarized laser output power change with the analyzer direction. (a): pump energy at 30 µJ/pulse and (b): pump energy at 10 µJ/pulse.

To evaluate the purity of the linearly polarized light, we define the linearity β as:

$$\beta = \frac{I_{\max} - I_{\min}}{I_{\max} + I_{\min}} \tag{3-4}$$

where $I_{\max}$ and $I_{\min}$ represent the maximum and minimum light intensity when rotating the analyzer. A perfect linearly polarized light gives β= 1. Under this definition, our measured data show a linearity β=0.986 at both high and low pump, indicating a very pure linearly polarized laser light.

In comparison, we also measured the output power from a normal CLC sample and the CLC sample with mirror coating. Figure 3.21 shows the pump energy dependent laser emission with red line representing the CLC laser with mirror coating and blue line representing the normal CLC laser. The threshold energy was measured to be 0.7 µJ/pulse and 1.2 µJ/pulse, respectively. It is found that the mirror reflective CLC has a stronger laser emission than the normal one under the same setup configuration. Although the normal CLC

laser emits photons from both sides rather than single side as the mirror reflective CLC laser does, the average enhancement ratio (the output ratio between these two lasers) reaches ~5.6X, much higher than twice. That means the mirror reflective CLC laser has much higher efficiency, which is attributed to the double pump during the path of laser generation. In our experiment, the pump beam is around ~200 μm in diameter. Hence for the 10 μm cell gap, the pump beam can be almost completely reflected back to the original pumping area even at an oblique incidence.
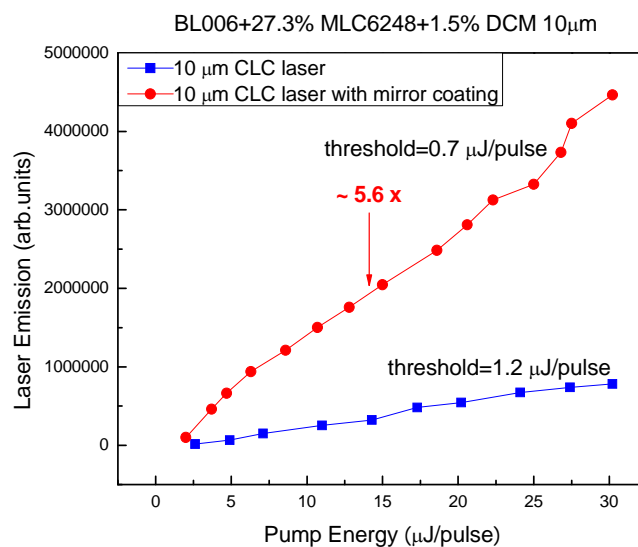
Fig. 3.21 Pumping energy dependent laser emission from a 10-μm normal CLC laser and a mirror reflective CLC laser.
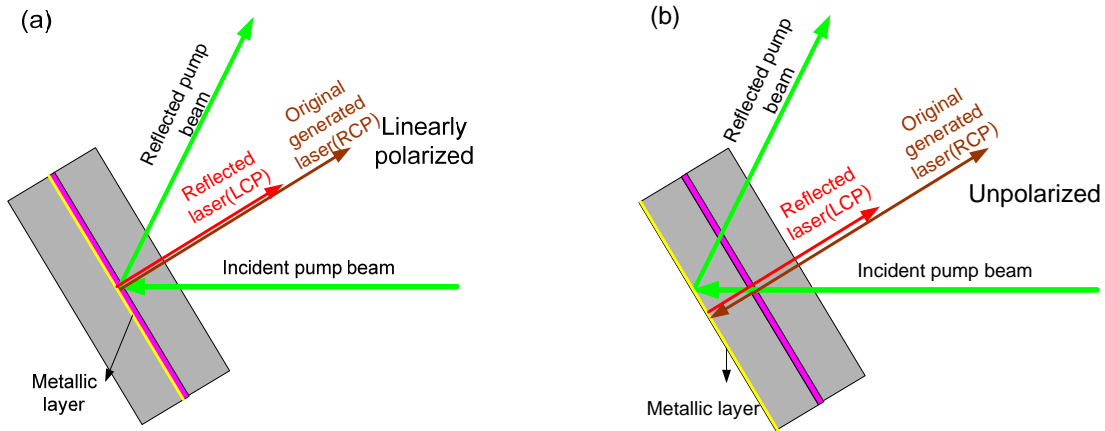
Fig. 3.22 CLC laser at oblique incident pump with metallic mirror at (a) inner surface of the cell; and (b) at outer surface of the cell

We have demonstrated that the mirror reflective CLC laser generates very pure linearly polarized laser light and, furthermore, such a reflective structure substantially enhances the laser output compared to the normal CLC laser. In the meantime, we also found that the orientation of the linearly polarized laser light exactly followed the rotation of the whole cell. This fact implies the linear polarization direction is associated with the LC cell's rubbing direction. Though the cholesteric liquid crystal has a symmetric structure, the rubbing direction determines the boundary conditions, which accounts for the reference axis of the linear polarization direction.

3.4.4 Theory of linearly polarized direction

Assuming wave propagates along +z axis, the electric field along x and y can be expressed as Eqs. (3-5)-(3-6) [43]:

$$\vec{E}_x = E_{x0} \cos(kz - \omega t) \tag{3-5}$$

$$\vec{E}_y = E_{y0} \cos(kz - \omega t + \delta) \tag{3-6}$$

where δ is the phase difference between $\vec{E}_y$ and $\vec{E}_x$ component. For $\delta > 0$, $\vec{E}_y$ lags behind $\vec{E}_x$ by δ. Based on this convention, left-handed circularly polarized light (LCP) and right-handed circularly polarized light (RCP) can be denoted by Jones vector as $\frac{1}{\sqrt{2}}\begin{bmatrix} 1 \\ -i \end{bmatrix}$ and $\frac{1}{\sqrt{2}}\begin{bmatrix} 1 \\ i \end{bmatrix}$, respectively [44].

For a right-handed cholesteric liquid crystal, the original laser emitted from both sides is right-handed circularly polarized. Upon reflection at the mirror surface, the reflected laser beam gains a π phase change and thus becomes left-handed circularly polarized. Consequently, these two orthogonal laser beams would combine together based on coherent superposition, where LCP and RCP experience a different phase delay. The linear superposition of the two beams can be expressed as Eq. (3-7):

$$
\begin{aligned}
& \frac{1}{\sqrt{2}}\begin{bmatrix} 1 \\ i \end{bmatrix} + \frac{1}{\sqrt{2}}\begin{bmatrix} 1 \\ -i \end{bmatrix}e^{i\delta} \\
&= \frac{1}{\sqrt{2}}\begin{bmatrix} (1+\cos\delta)+i\sin\delta \\ \sin\delta + i(1-\cos\delta) \end{bmatrix} \\
&= \frac{1}{\sqrt{2}}\begin{bmatrix} (1+\cos\delta)+i\sin\delta \\ \sin\delta + i(1-\cos\delta) \end{bmatrix} \times \begin{bmatrix} (1+\cos\delta)-i\sin\delta \\ (1+\cos\delta)-i\sin\delta \end{bmatrix} \\
&= \sqrt{2}\begin{bmatrix} 1+\cos\delta \\ \sin\delta \end{bmatrix} \\
&\propto \begin{bmatrix} \cos(\delta/2) \\ \sin(\delta/2) \end{bmatrix}
\end{aligned}
\tag{3-7}
$$

where $\delta = 2\pi OPD/\lambda$ is the phase delay between LCP and RCP, and *OPD* represents the optical path difference. When the two circularly polarized beams combine together including a phase delay between them, it gives out a linearly polarized light oriented along the $\delta/2$ direction.

Because of periodic index modulation, the cholesteric liquid crystal builds up a good Bragg reflection (with reflectivity higher than ~98%) as long as the number of pitches is above 15 [42]. RCP and LCP are two orthogonal eigen-modes. Given a right-handed CLC, within the reflection band, RCP experiences high reflectivity while LCP directly transmits through. Therefore, we can infer that RCP sees the refractive index modulation as n_e-n_o-n_e-$n_{o...}$ when propagating through the medium while LCP sees an isotropic medium with refractive index n_o. On the other hand, the original laser generated from different layers of CLC is assumed to be completely in phase because the time duration for the laser passing through the distance of a cell gap (only few microns) is so much smaller than the pulse duration (ns) of the pumping beam. Furthermore, each periodic medium (i.e. each pitch) produces a 2π reflective phase shift. Thus, the reflection after multiple pitches is constructive with zero phase shift. Consequently the accumulation of phase delay δ over the periodic medium can be described as:

$$\delta = \frac{2\pi}{\lambda_0} OPD = \frac{2\pi}{\lambda_0} \cdot \frac{\Delta n_{eff} d}{2} \tag{3-8}$$

Let λ_0, d and $\Delta n_{eff} = \Delta n \cdot c$ wt% be the lasing wavelength, cell gap, and the effective birefringence of the cholesteric mixture, respectively. Δn and c wt% are the birefringence and weight concentration of the nematic liquid crystal.

From Eqs. (3-7)-(3-8), it is seen that a decrease in cell gap d causes a smaller phase delay and the decrease of the linear polarization angle ensues. In other words, when facing the laser propagation direction, we expect to observe the linearly polarized light rotating

clockwise.

3.3.5 Rotating the linearly polarized laser light direction

From Eq. (3-8), we know that the phase delay between two eigen modes, RCP and LCP are determined by lasing wavelength and effective birefringence, both of which are temperature sensitive. Therefore, we positioned the mirror reflective CLC laser (10 μm) on a temperature controller so that we observed the linear polarization rotated with the temperature change. Meanwhile, we used Eq. (3-8) to calculate the theoretical value of linear polarization rotation according to the exact effective birefringence at a specific lasing wavelength and temperature. Both measured data and theoretical calculation are listed in Table 1. The refractive index of BL006 at different temperatures and lasing wavelengths are extracted from the fitting curve, whose original data are measured using Abbe Refractometer (Atago DR-M4) and standard color filters [45].

Figure 3.23 describes both theoretical and measured data of linear polarization direction rotation with the increase of temperature. Here the direction angle is normalized to the end direction at 55 ^{o}C. The experimental results match very well with the theoretical calculation.
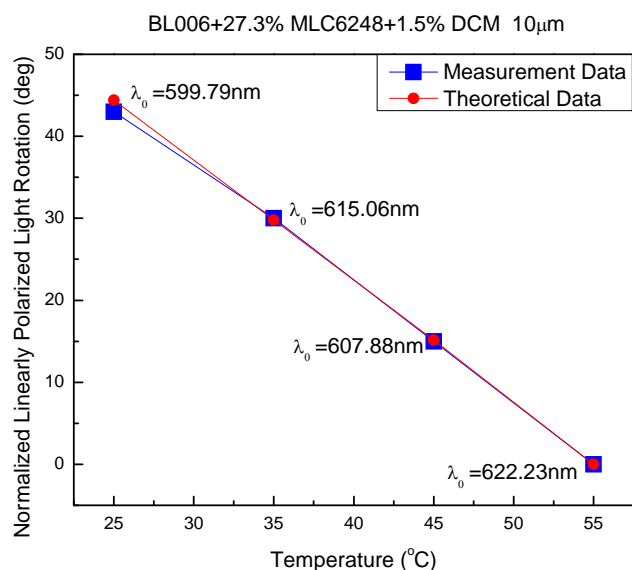
Fig. 3.23 Temperature dependent normalized linearly polarized light direction.

Table 3.1 Calculated and measured linear polarization direction rotation at different temperatures.

	25°C	35°C	45°C	55°C
λ_0(nm)	599.79	607.88	615.06	622.23
n_e	1.8067	1.7943	1.7813	1.7682
n_o	1.5275	1.5249	1.5225	1.5208
Δn	0.2792	0.2694	0.2588	0.2474
$\Delta n\_eff = \Delta n \cdot c$ %	0.2030	0.1959	0.1882	0.1799
$\delta = \dfrac{2\pi}{\lambda_0} \cdot \dfrac{\Delta nd}{2}$ (rad)	10.63	10.12	9.61	9.08
$\theta_{calculated} = \delta/2$ (deg)	44.4	29.8	15.1	0
$\theta_{measured}$ (deg)	43.0	30.0	15.0	0

Results presented above demonstrate that linear polarization direction can be tuned by controlling the temperature. However, as reported in Ref. [46], lasing wavelength shifts discontinuously with temperature, and thus a discontinuous tuning of polarization direction.

In order to fine tune the direction in a continuous manner, we made a wedged cell with cell gap varied around ~8-15 μm. Because the cell gap increases gradually in a row within a wedged cell, polarization direction can be controlled continuously.
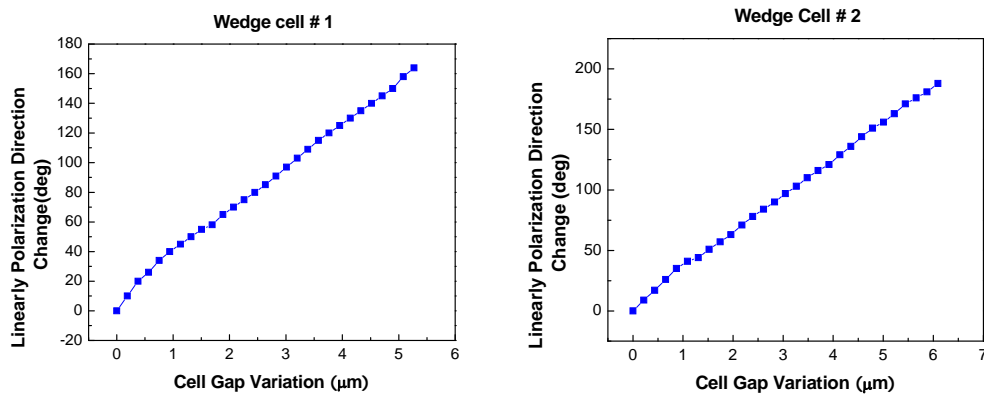
Fig. 3.24 Cell gap variation dependent linear polarized light rotation for wedge cell #1(left) and wedge cell #2 (right) by mixture 1 (BL006 + 27.3%MLC6248 + 1.5%DCM).
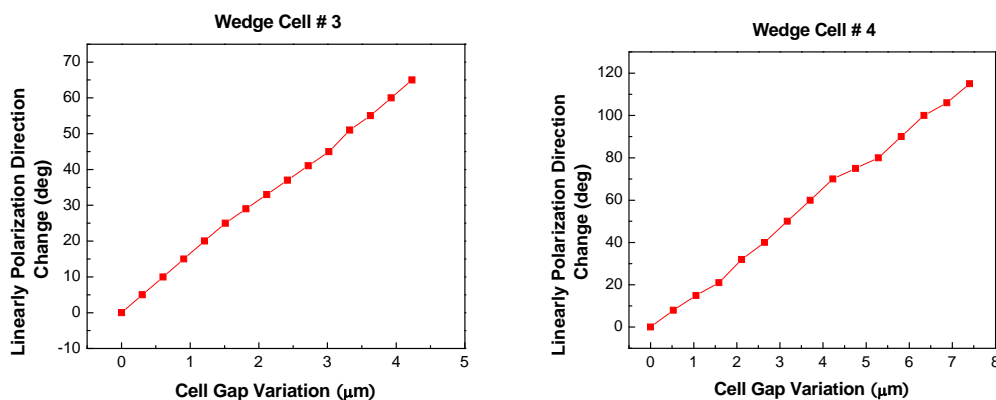
Fig. 3.25 Cell gap variation dependent linear polarized light rotation for wedge cell #3(left) and wedge cell #4 (right) by mixture 2 (ZLI1694 + 22.9%MLC6248 + 1 %DCM).

Using the CLC mixture 1 (BL006+27.3%MLC6248+1.5%DCM), we made two different wedged CLC lasers with a relatively large birefringence. Using CLC mixture 2 (ZLI6248 +22.9%MLC6248+1%DCM) we made the other two wedged CLC lasers with birefringence almost half of the first one. Subsequently CLC laser is scanning-pumped across

46

the fringes. At different scanning positions, linear polarization direction is measured to rotate linearly with the cell gap variation, as shown in Fig. 3.24 (wedged cells #1 and #2, from CLC mixture 1) and Fig. 3.25 (wedged cells #3 and #4, from CLC mixture 2).

Table 3.2   Calculated and measured linear polarization rotation period for mixture 1 (BL006+27.3%MLC6248+1.5%DCM) and mixture 2 (ZLI-6248+22.9%MLC6248+1%DCM). Pcalculated and pmeasured are calculated rotation period and measured rotation period. N is the number of fringes and d is the cell gap variation over the measured range. λVIS is chosen as 550 nm, the center of visible light.

	BL006+27.3%MLC6248 +1.5% DCM		ZLI1694+ 22.9%MLC6248 + 1.5% DCM	
$\langle n \rangle$	1.67		1.56	
Δn	0.28		0.13	
$\Delta \lambda$ (nm)	80		40	
$\Delta n\_eff = \Delta n \cdot c\%$	0.204		0.102	
$P_{calculated} = \dfrac{2 \cdot \lambda_0}{\Delta n\_eff}$ (µm)	5.8		11.9	
	Wedge #1	Wedge #2	Wedge #3	Wedge #4
N (# of fringes)	32	37	24	42
$d = \dfrac{\lambda_{VIS}}{2} * \dfrac{N}{\langle n \rangle}$ (µm)	5.27	6.09	4.23	7.4
$\Delta \theta$ (deg)	164	188	65	115
$p_{measured} = \dfrac{d * 180^o}{\Delta \theta}$ (µm)	5.78	5.83	11.72	11.59

According to the rotation angle over the measured cell gap variation, the rotation period, which means the thickness variation over which the linearly polarized light will rotate 180°, can be obtained. In these figures, polarization direction angle is normalized to the starting point on the thinner side of the wedged cell. Due to the birefringence difference, the

47

wedged cells #3 and #4 exhibit almost twice of rotation period as the wedged cells #1 and #2. Detailed calculation results are listed in Table 2. The theoretically calculated rotation period $P_{calculated}$ matches well with the experimental rotation period $p_{measured}$, where the error is within 1-2 fringes.

3.4   Emission enhancement by an external metallic reflector
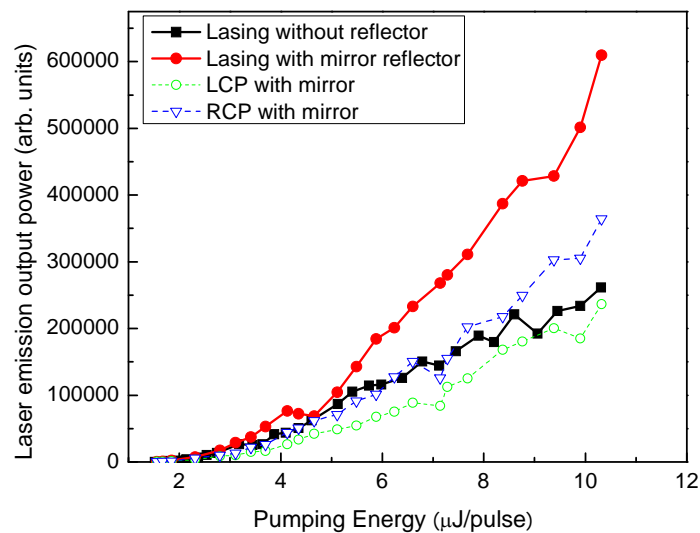
Fig. 3.26 Pump energy dependent laser output power of a CLC laser with/without a metallic mirror reflector attached outside the active cell.

For a comparison, we show here the results of a CLC laser when attached by a mirror reflector outside the active cell. The active cell has a mixture composed of BL006, 36% of right-handed chiral dopant CB15 (from Merck), and 2% of DCM showing a reflection band from 555-635 nm. The passive reflector is composed of BL006 and 34% of CB 15, showing a reflection band from 600-680 nm. The results in Fig. 3.26 show the laser emission is nearly doubled with 60% of RCP component and 40% of LCP component. Upon the reflection, the reflected light gains π phase change but combines with the intrinsic RCP emission based on

48

incoherent superposition, giving rise to a nearly-unpolarized emission.

3.5 Conclusions

In this chapter we demonstrated single reflector approach for laser emission enhancement and output polarization manipulation of the CLC lasers.

A passive CLC external reflector will not only enhance the output laser light dramatically but also reduce the beam divergence. The passive CLC reflector is a polarization-conserved reflector, giving rise to a virtually doubled feedback and a second stimulated amplification. Therefore, the laser emission is redirected to one direction and dramatically enhanced with circular polarization dominating the output. The beam divergence is greatly reduced as well, thanks to the increased cavity length from micrometer to millimeter due to inserted glass substrates.

The CLC laser with an in-cell metallic mirror works only at reflective scheme. The enhanced output is a result of double pump of the active area. The reflected laser light by the in-cell metallic mirror is converted into circular polarization in opposite handedness because of the introduced π phase change. Thus the output is highly purified linear polarized light owing to coherent superposition. In contrast, the external metallic mirror will only generate nearly-unpolarized output with doubled output power owing to the incoherent superposition. Furthermore, we also demonstrated temperature and thickness dependent rotation of the linear polarization.

3.6   References

1. N. V. Kukhtarev, "Cholesteric liquid crystal laser with distributed feedback," Sov. J. Quantum Electron. 8, 774 (1978).

2. I. P. II' Chishin, E. A. Tikhonov, V. G. Tishchenko, and M. T. Shpak, "Generation of a tunable radiation by impurity cholesteric liquid crystal," JETP Lett. 32, 24 (1980).

3. J. P. Dowling, M. Scalora, M. J. Bloemer, and C. M. Bowden, "The photonic band edge laser: A new approach to gain enhancement," J. Appl. Phys. 75, 1896 (1994).

4. V. I. Kopp, B. Fan, H. K. M. Vithana, A. Z. Genack, "Low-threshold lasing at the edge of a photonic stop band in cholesteric liquid crystals," Opt. Lett. 23, 1707 (1998).

5. A. Munoz F., P. Palffy-Muhoray, and B. Taheri, "Ultraviolet lasing in cholesteric liquid crystals," Opt. Lett. 26, 804 (2001).

6. S. Y. Lin, J. G. Fleming, and I. Ei-Kady, "Experimental observation of photonic-crystal emission near a photonic band edge," Appl. Phys. Lett. **83**, 593 (2003).

7. A. Chanishvili, G. Chilaya, and G. Petriashivili, "Laser emission from a dye-doped cholesteric liquid crystal pumped by another cholesteric liquid crystal laser," Appl. Phys. Lett. 85, 3378 (2004).

8. K. Shirota, H. B. Sun, S. Kawata, "Two-photon lasing of dye-doped photonic crystal laser," App. Phys. Lett. 84, 1632 (2004).

9. M. Ozaki, M. Kasano, D. Ganzke, W. Haase, and K. Yoshina, "Mirrorless lasing in a dye-doped ferroelectric liquid crystal," Adv. Mater. 14, 306 (2002).

10. M. Ozaki, M. Kasano, T. Kitasho, D. Ganzke, W. Haase, and K. Yoshino, "Electro-

tunable liquid-crystal laser," Adv. Mater. 15, 974 (2003).

11. W. Cao, A. Munoz, P. Palffy-Muhoray, and B. Taheri, "Lasing in a three-dimensional photonic crystal of the liquid crystal blue phase," Nat. Mater. 1, 111 (2002).

12. S. Yokoyama, S. Mashiko, H. Kikuchi, K. Uchida, T. Nagamura, "Laser Emission from a Polymer-Stabilized Liquid-Crystalline Blue Phase," Adv. Mater. 18, 48 (2005).

13. H. Finkelmann, S. T. Kim, A. Munoz, P. Palffy-Muhoray, and B. Taheri, "Tunable mirrorless lasing in cholesteric liquid crystalline elastomers," Adv. Mater. 13, 1069 (2001).

14. P. V. Shibaev, V. Kopp, A. Genack, and E. Hanelt, "Lasing from chiral photonic band gap materials based on cholesteric glasses," Liq. Cryst. 30, 1391 (2003).

15. P. V. Shibaev, V. Kopp, A. Z. Genack, "Photonic materials based on mixtures of cholesteric liquid crystals with polymers," J. Phys. Chem. B 107, 6961 (2003).

16. V. Hsiao, C. Lu, G. He, M. Pan, A. Cartwright, P. Prasad, R. Jakubiak, R. Vaia, and T. Bunning, "High contrast switching of distributed-feedback lasing in dye-doped H-PDLC transmission grating structures," Opt. Express 13, 3787 (2005).

17. T. Matsui, R. Ozaki, K. Funamoto, M. Ozaki, and K. Yoshino, "Flexible mirrorless laser based on a free-standing film of photo polymerized cholesteric liquid crystal," Appl. Phys. Lett. 81, 3741 (2002).

18. Seiichi Furumi, Shiyoshi Yokoyama, Akira Otomo and Shinro Mashiko, "Study on laser action from UV-curable chiral nematic liquid crystals," Thin Solid Films, 438, 423(2003).

19. T. Ohta, M. H. Song, Y. Tsunoda, T. Nagata, K. C. Shin, F. Araoka, Y. Takanishi, K.

Ishkawa, J. Watanabe, S. Nishimura, T. Toyooka, and H. Takezoe, "Monodomain film formation and lasing in dye-doped polymer cholesteric liquid crystals," Jpn. J. Appl. Phys. 43, 6142 (2004).

20. T. Nagata, T. Ohta, M. H. Song, Y. Takanishi, K. Ishikawa, J. Watanabe, T. Toyooka, S. Nishimura, and H. Takezoe, "Anomalously directed amplified spontaneous emission from a wedge-shaped cell sandwiched by cholesteric liquid crystal films," Jpn. J. Appl. Phys. 43, L1220 (2004).

21. G. Strangi, V. Barna, R. Caputo, A. Luca, C. Versace, N. Scaramuzza, C. Umeto, R. Bartolina, and G. Price, "Color-tunable organic microcavity laser array using distributed feedback," Phys. Rev. Lett. 94, 063903 (2005).

22. Y. C. Yang, C. S. Kee, J. E. Kim, H. Y. Park, J. C. Lee, and Y. J. Jeon, "Photonic defect modes of cholesteric liquid crystals," Phys. Rev. E 60, 6852 (1999).

23. M. H. Song, B. Park, Y. Takanishi, K. Ishikawa, S. Nishimura, T. Toyooka, and H. Takezoe, "Lasing from thick anisotropic layer sandwiched between polymeric cholesteric liquid crystal films," Jpn. J. Appl. Phys. 44, 8165 (2005).

24. V. I. Kopp and A. Z. Genack, "Twist defect in chiral photonic structures," Phy. Rev. Lett. 89, 3901 (2002).

25. J. Schmidtke, W. Stille, and H. Finkelmann, "Defect mode emission of a dye doped cholesteric polymer network," Phys. Rev. Lett. 90, 083902 (2003)

26. Y. H. Huang, Y. Zhou, C. Doyle, and S. T. Wu, "Tuning the photonic band gap in cholesteric liquid crystals by temperature-dependent dopant solubility," Opt. Express 14,

1236 (2006).

27. S. Furumi, S. Yokoyama, A. Otomo, and S. Mashiko, "Electrical control of the structure and lasing in chiral photonic band-gap liquid crystals," Appl. Phys. Lett. 82, 16 (2003).

28. H. Yu, B. Tang, J. Li, and L. Li, "Electrically tunable lasers made from electro-optically active photonics band gap materials," Opt. Express 13, 7243 (2005).

29. M. F. Moreira and I. C. S. Carvalho, W. Cao, C. Bailey, B. Taheri, and P. Palffy-Muhoray, "Cholesteric liquid-crystal laser as an optic fiber-based temperature sensor", Appl. Phys. Lett. 85, 2691 (2004).

30. A. Chanishvili, G. Chilaya, G. Petriashvili, R. Barberi, R. Bartolino, G. Cipparrone, and A. Mazzulla, L. Oriol, "Phototunable lasing in dye-doped cholesteric liquid crystals," Appl. Phys. Lett. 83, 5353 (2003).

31. A. Y. G. Fuh, T. H. Lin, "Lasing in chiral photonic liquid crystals and associated frequency tuning," Opt. Express 12, 1857 (2004).

32. S. Furumi, S. Yokoyama, A. Otomo, S. Mashiko, "Phototunable photonic bandgap in a chiral liquid crystal laser device," Appl. Phys. Lett. 84, 2491 (2004).

33. A. Chanishvili, G. Chilaya, G. Petriashvili, R. Barberi, R. Bartolino, G. Cipparone, A. Mazzulla, L. Oriol, "Lasing in dye-doped cholesteric liquid crystals: Two New Tuning Strategies," Adv. Mat. 16, 791 (2004).

34. Peter Shibaev, R. Sanford, Daniel Chiappetta, Valery Milner, Azriel Genack and Alexei Bobrovsky, "Light controllable tuning and switching of lasing in chiral liquid crystals," Opt. Express, 13, 2358 (2005).

35. T. H. Lin, Y. J. Chen, C. H. Wu, and A. Y-G. Fuh, "Cholesteric liquid crystal laser with wide tuning capability," Appl. Phys, Lett. 86, 161120 (2005).

36. S. M. Morris, A. D. Ford, B. J. Broughton, M. N. Pivnenko, and H. J. Coles, "Liquid crystal lasers: coherent and incoherent microsources," Proc. SPIE, 5741, 118 (2005).

37. S. M. Morris, A. D. Ford, Mikhail N. Pivnenko, and H. J. Coles, "Structure-property relations of photonic band edge laser," Proc. SPIE 5289, 236 (2004).

38. S. M. Morris, A. D. ford, M. N. Pivnenko, and H. J. Coles, "Enhanced emission from liquid-crystal lasers," J. of Appl. Phys. 97, 023103 (2005).

39. F. Araoka, K.C. Shin, Y. Takanishi, K. Ishikawa, H. Takezio, Z. Zhu and T. M. Swager, "How doping a cholesteric liquid crystal with polymeric dye improves an order parameter and makes possible low threshold lasing," J. Appl. Phys. 94, 279 (2003).

40. K. Amemiya, T. Nagata, M. H. Song, Y. Takanishi, K. Ishikawa, S. Nishimura, T. Toyooka, and H. Takezoe, "Enhancement of laser emission intensity in dye-doped cholesteric liquid crystals with single-output window," Jpn. J. Appl. Phys. 44, 3748 (2005).

41. Y. Huang, Y. Zhou, Q. Hong, A. Rapaport, M. Bass, and S. T. Wu, "Incident angle and polarization effects on the dye-doped cholesteric liquid crystal laser," Opt. Commun. 261, 91(2006).

42. Q. Hong, T. X. Wu, and S. T. Wu, "Optical wave propagation in a cholesteric liquid crystal using the finite element method," Liq. Cryst. 30, 367 (2003).

43. E. Hecht, *Optics (2nd edition)*, Chapter 8, (Addison-Wesley, Massachusetts, 1987).

44. P. G. de Gennes and J. Prost, *The Physics of Liquid Crystals (2nd edition)*, (Oxford University Press, New York, 1993).

45. J. Li, G. Baird, Y. H. Lin, H. W. Ren, and S. T. Wu, "Refractive index matching between liquid crystals and photopolymers," J. SID. 13, 1017 (2005).

46. K. Funamoto, M. Ozaki, and K. Yoshino, "Discontinuous shift of lasing wavelength with temperature in cholesteric liquid crystal," Jpn. J. Appl. Phys. 42, L1523 (2003).

CHAPTER 4   EMISSION ENHANCEMENT OF CHOLESTERIC LIQUID CRYSTAL LASERS USING AN EXTERNAL RESONATOR

4.1   Introduction

Bragg reflection from cholesteric liquid crystals has been widely used not only for bistable reflective display applications, but also for circularly polarized reflectors and tunable lasers [1-3]. Especially for laser applications, two CLC reflectors can be used to form a circularly polarized resonator with the feedback for circularly polarized light only. The insertion of either an isotropic layer [4, 5], or an anisotropic layer [6-8] into the CLC resonator was investigated in order to lower the lasing threshold of a CLC laser. In some literatures, they are called *defect mode* lasing since a discontinuity or an interrupt of the helical twist is introduced. There are some papers that address the defect mode lasing in a CLC lasers. However by the time this work was done, the transmission spectrum of three cholesteric polymeric layers with different pitches was just calculated [9] and no further work in laser generation and output performance was carefully reported.

In this chapter, we use an external resonator which consists of two passive CLC reflectors to enhance the laser emission from a single dye-doped CLC cell. We not only demonstrate an enhanced emission from the active CLC cell sandwiched within a CLC resonator but also theoretically present the responsible physical mechanisms on the lasing mode and light amplification. Key parameters, such as the thickness of the active CLC middle layer and the amplification index constant are investigated to provide guidelines for device optimization. In addition, the effect of inserting glass substrates on the laser

performance is analyzed in detail.

4.2   Sample preparation and experiments

The active CLC sample was prepared by using a nematic LC host BL006 (Δn=0.286, n_e=1.826 @ λ=589 nm and T=20 $^{\circ}$C, from Merck) and 27.3% of right-handed chiral agent MLC6248 (HTP = 11.3 μm^{-1}, from Merck). The mixture was then doped with 1.5 wt% laser dye DCM (from Exciton) as the emissive medium. The passive CLC reflectors were prepared using BL006 and 25.3% of MLC6248. The mixture was filled into a 5-μm homogenous cell by capillary action under isotropic state. The inner surfaces of the cells were first coated with ITO (Indium-Tin-Oxide) layers and then polyimide alignment layers, which were rubbed in anti-parallel directions to produce a small (~3°) pretilt angle. The filled CLC cells were slowly cooled down to room temperature using a temperature controller in order to form a defect-free helical structure. In this work, the 5-μm active CLC cell was sandwiched between two 5-μm CLC reflectors in optical contact to form a 3-cell CLC laser assembly, as Fig. 4.1 shows. The cells were stacked together tightly using a demountable holder which has a screw in each of the four corners for controlling the uniformity. No special process for monitoring the parallelism was performed during cell assembly. In our experiment, it is not difficult to find the emission point with a dramatically enhanced output; the whole assembly is not as sensitive to parallelism as the structure which has an anisotropic emissive layer in the middle (e.g., the dye-doped nematic liquid crystal). This is because the middle CLC layer lases itself and the feedback comes from both the CLC layer in the middle and the passive reflectors.
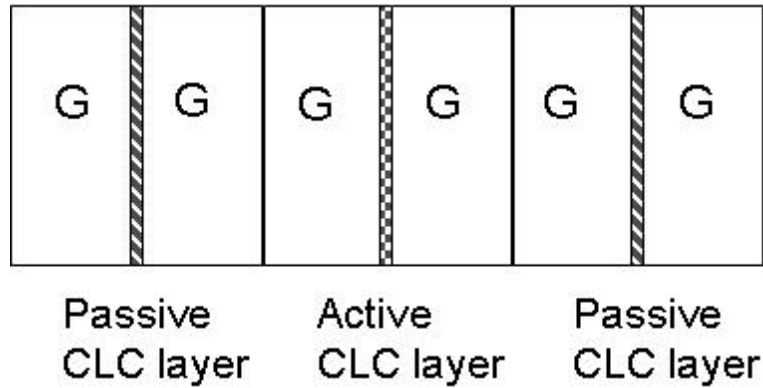
Fig. 4.1 The structure of a 3-CLC cell laser assembly. G represents the glass substrate. In experiment $d_{active\ CLC} = d_{passive\ CLC} = 5$ μm; $d_{glass\ substrate} = 1.1$ mm.

The experimental setup was the same as the one shown in Fig. 4.2 at normal incidence. Since the passive CLC reflecting layer transmits the pump laser (532 nm), such a configuration will reduce the surface reflection and, moreover, the laser emission after multiple reflections inside the CLC resonator can still be aligned into one spot with a relatively small divergence. On the other hand, the oblique pump results in multiple reflections of the pumping beam (532 nm) inside the CLC resonator due to the glass surfaces. Each reflection path penetrates the gain medium once and generates a small laser beam because the external CLC resonator provides the feedback. Therefore multiple CLC laser beams will be observed in a row with gradually decreased power. This will definitely decrease the output power compared to the case of single gain point under excitation. Figure 4.3 shows how it works and this phenomenon was indeed observed in our experiment.

active layer
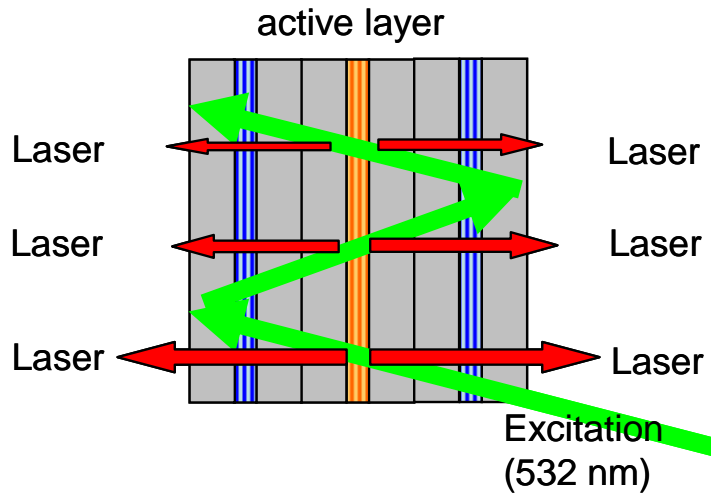
Fig. 4.3 Sketch of multiple laser spots generated from a CLC laser within a CLC resonator when pumped at oblique incidence.

4.3   Experimental results

Figure 4.4 depicts the normalized transmittance of the active CLC cell (thin solid line) and the passive CLC reflector (dotted line), from which the reflection band can be clearly characterized. With DCM doped, the short wavelength band edge of the active CLC cell is completely obscured by the absorption of the laser dye. The reflection band of the 5-µm CLC reflector is chosen to cover the lasing wavelength and its measured reflectivity at $\lambda=600$ nm is ~97%. As an example, the lasing spectrum at 33.4 µJ/pulse pump energy is also plotted (thick solid line) in the same figure to allow an easy justification for lasing action at the photonic band edge.
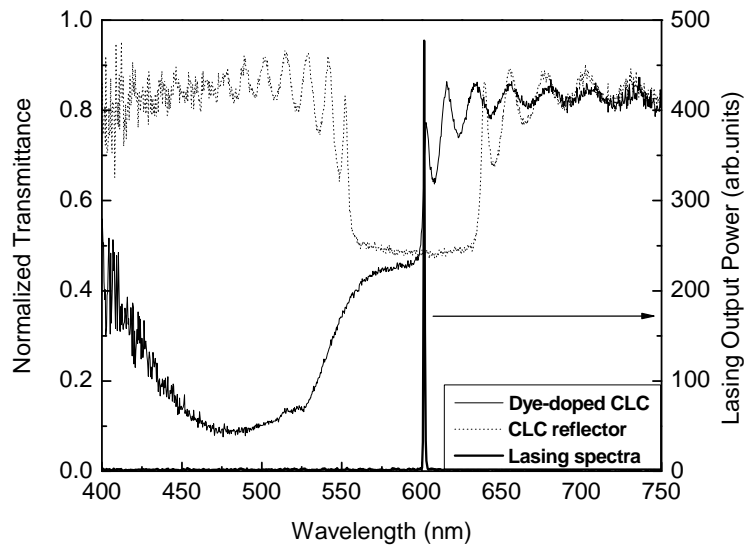
Fig. 4.4 Measured normalized transmittance of the dye-doped CLC cell (thin solid line), the measured normalized transmittance of passive CLC reflector (thin dotted line), and the emission spectra of CLC laser assembly pumped at 33.4 μJ/pulse (thick solid line).

Laser output power at different pump energy for the 5-μm CLC laser within a CLC resonator was measured. Results are plotted in Fig. 4.5 as marked by triangles. To compare the enhancement factor, the laser output power of a single 5-μm CLC cell (squares), as well as the 5-μm CLC laser with one CLC reflector (circles) was measured. From Fig. 4.5, the single 5-μm dye-doped CLC cell generates a weak laser emission because of its thin CLC emissive layer and short feedback length. With the help of a CLC reflector incorporated in good contact at one end, the laser emission from one direction is reflected back into the cavity. Because the circular polarization state of the reflected beam is preserved by the "polarization-conserved CLC reflector" and is further amplified by the cavity, the output emission is dramatically enhanced. Under this circumstance, the output is still right-handed circularly polarized, the same as its original polarization state. The observed laser emission is ~80X

stronger as compared to the emission from the single active CLC alone. Furthermore, we found that when the active CLC cell is confined between two CLC reflectors, the output emission is further enhanced by ~9.4X as detected from one end of the laser cavity. Because of the structure symmetry, the laser output has equal power coming from both ends. The lasing wavelength is located at λ = 602 nm, exactly at the long wavelength band edge of the middle CLC lasing cell and it is elliptically polarized. Meanwhile, as the right-handed cholesteric reflector is incorporated to the single CLC laser from one side to two sides, the lasing threshold decreases from 22 µJ/pulse to 10 µJ/pulse, and finally down to 2.1 µJ/pulse. The reduction is about one order of magnitude.
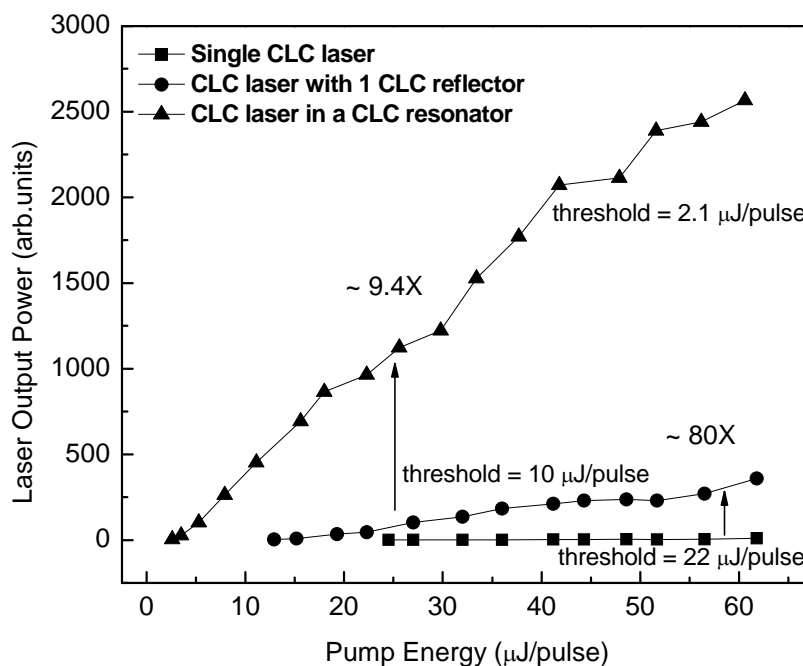
Fig. 4.5 Pump energy dependent laser output power of a single 5-µm active CLC cell (squares), a 5-µm active CLC cell with a 5-µm passive reflector enhanced (circles), and a 5-µm active CLC cell within a CLC circularly polarized resonator (triangles).

4.4   Theoretical analysis of a resonator enhanced CLC laser

4.2.1   Simulation results of the passive CLC assembly

To understand how the external resonator enhances the band edge lasing of the middle

CLC cell, we calculate the transmittance and the coherent amplification of light for different

polarizations using improved 4×4 transfer matrix and scattering matrix. In this method, the

4×4 matrix for each slice is diagonalized and thus the equations become very concise.

Detailed derivations can be found in Appendix and Ref. 10, 11. The employed method

rigorously takes into account the boundary conditions and multiple interface reflections of the

LC medium.
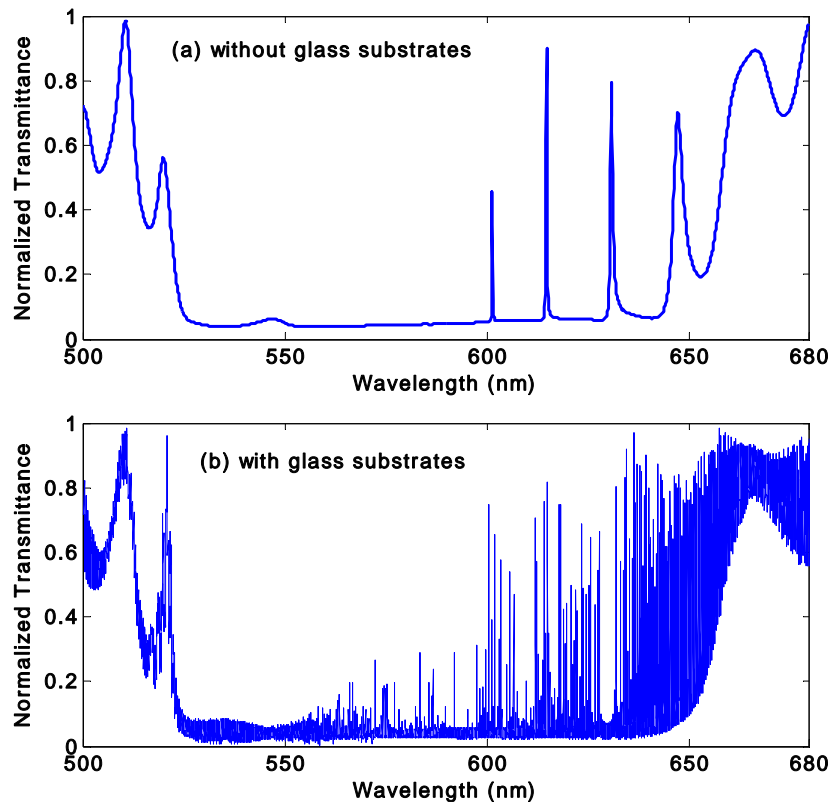
Fig. 4.6 Simulated normalized transmittance of the passive 3-CLC assembly: (a) with no glass substrates present for each cell, immersed in air; (b) with glass substrates for each cell, immersed in air.

Figure 4.6 is a plot of normalized transmittance of a passive 3-CLC assembly without doping DCM laser dye. In order to see the characteristic spectral lines introduced by Fabry-Perot (FP) effect from the resonator, we first calculate the transmittance of three CLC layers directly attached to each other, assuming that glass substrates are absent. Results are shown in Fig. 4.6(a). Afterwards, the transmittance of 3 real CLC cells (with glass substrates) is calculated as Fig. 4.6(b) shows. The thickness of each glass substrate is 1.1 mm. Some basic parameters used for simulation are listed as follows: refractive index of air n_{air} = 1, and LC n_o = 1.50, n_e = 1.70; the active CLC middle layer is right-handed with pitch length p_1 = 0.35 μm and cell gap d_1 = 5 μm; the two CLC reflectors are also right-handed with pitch length p_2 = 0.375 μm and cell gap d_2 = 2.25 μm in order to reach ~96.5% reflectivity. The incident light is right-handed circularly polarized (RCP). Doping 25%-27% of the chiral material into nematic LC host causes a decrease in birefringence of the whole CLC mixture to ~ 0.2. Although the LC refractive indices and the birefringence used for simulations are somewhat different from those of BL006, the simulation result of a single CLC layer does give a reflection band from 525 to 600 nm for the middle CLC layer and 560-640 nm for the passive CLC reflectors. These simulated results agree with experimental data reasonably well.

From Fig. 4.6(a), when the right-handed CLC reflectors are present at both ends, the resonator produces several transmission peaks in the 600-640 nm range. In other words, the resonance modes only exist within the reflection band of the passive reflectors (~560-640 nm) which does no overlap with that of the middle CLC (~525-600 nm). The mode spacing corresponds to a Fabry-Perot whose cavity length is equal to the total thickness of the three

CLC layers (d = 9.5 μm, n = 1.6). However, within the overlapping reflection band of the active CLC middle layer and the passive CLC reflectors (ranged 560-600 nm), the transmission peaks are completely suppressed except the one at the band edge (600 nm). More simulation results (not shown here) indicate that there always appears a transmission peak near the band edge even if the band edge does not coincide with the FP transmission peak introduced by the CLC resonator. This means the photonic band edge mode of the active CLC can be well preserved and, more importantly, be further strengthened by the external resonator.

As Fig. 4.6(b) shows, with glass substrates present the increased FP length brings in a lot of oscillations, the extra possible resonance modes. They function as high frequency modulation superimposed onto the original characteristic spectral lines. Yet the envelope of these oscillations can still be distinguished to match the characteristic spectral lines assuming that the spectrum step for calculation is small enough.

These oscillations are not randomly distributed; instead they ensue from the several embedded FP cavities built up with CLC layers and the glass substrates. Figure 4.7 shows a detailed outlook of these oscillation modes within 614.2-614.8 nm range as an example, where one of the characteristic spectral lines of the 3-CLC layer assembly locates (see from Fig. 4.6(a)).
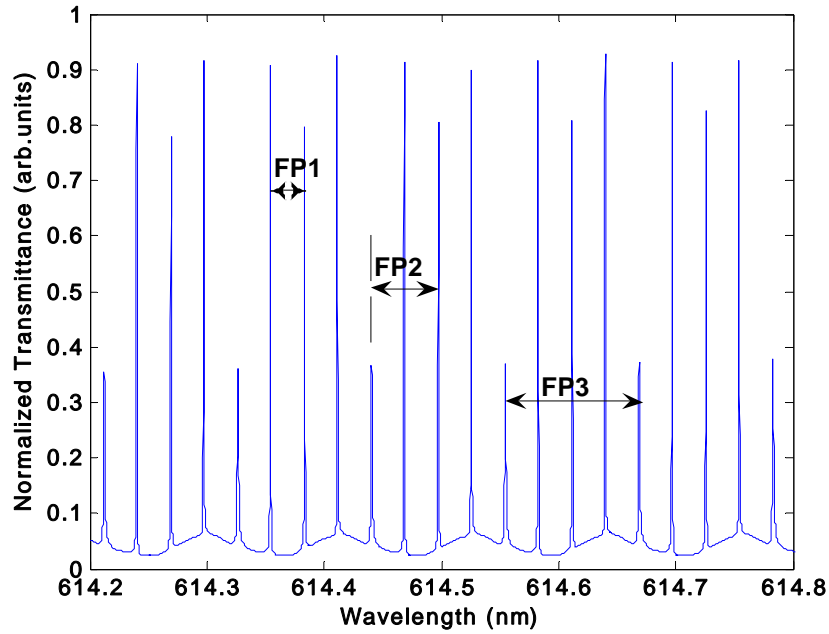
Fig. 4.7 Detailed view of simulated normalized transmittance of the passive 3-CLC assembly with glass substrates (n=1.5) in detail.

For a typical FP, the free spectral range $\Delta\lambda_l$ can be calculated according to the equation $\Delta\lambda_l = \dfrac{\lambda_l{}^2}{2nd}$ [12], where λ_l is the wavelength of interest, n is the refractive index, and d is the gap of the FP cavity. From Fig. 4.7, we found different free spectral ranges superimposed on each other. There are basically three FP cavities contributing to these oscillation peaks: 1) FP1, formed by the two passive CLC layers ($d= \sim 4.4$ mm), corresponding to $\Delta\lambda_l = 0.028$ nm. This is the most dominant factor in the spectrum. 2) FP2, formed by one passive CLC layer and the active CLC layer ($d = \sim 2.2$ mm), corresponding to $\Delta\lambda_l = 0.056$ nm. The wavelength λ_l (=614 nm) we investigate here is actually beyond the reflection band of the active CLC in the middle (525-600 nm), whereas due to Bragg reflection the side oscillation near its band edge causes ~3.3% reflectivity for RCP at 614 nm.

65

www.manaraa.com

This is why the active and the passive CLC layers still form a FP even the wavelength is outside the reflection band of one of the two CLC layers. As a result, it superimposes the lower frequency oscillations onto the transmission spectrum from FP1. 3) FP3, formed between the air-glass interface and its neighboring passive CLC layer (d= ~ 1.1 mm). This corresponds to $\Delta\lambda_l$ = 0.112 nm. The total effect of 3 embedded FPs is that the transmission peaks with a higher frequency oscillation as from FP1 are modulated by the lower frequency oscillations as from FP2 and FP3.

In theory, the reflectivity of a 2.25-μm CLC reflector should already reach 96.5% for the RCP incidence at its reflection band center (λ~600 nm) although the Bragg reflection is not completely established. In reality, our CLC reflector is 5-μm thick but its reflectivity at 600 nm was measured to be ~97% because of the imperfect helical distribution of LC directors. Besides, the possible air gap between the CLC cells in experiment may further decrease the reflectivity. In our simulation the effect of ITO layer was not taken into consideration because a typical ITO layer with index ~1.7 and thickness ~100 nm will only decrease the reflectivity of our CLC reflector (at 600 nm) by ~0.5%, which will not significantly affect the results. Simulation also reveals that to further increase the cell gap of the CLC reflector to 8 μm does not generate any stronger laser emission because the optimal output for FP not only requires a high reflectivity but also an indispensably small transmittance so as not to block all the output. Experimental measurement of transmittance does not exhibit these narrow transmission peaks clearly other than some undulations because the resolution of the spectrometer (~1 nm) is much larger than the band width of the

transmission peaks (~ 0.2 nm @ λ=601 nm).

4.2.2 Simulation results of the active CLC assembly

To simulate the light amplification behavior inside the dye-doped CLC layer, the refractive index of the active CLC is modified to calculate the normalized transmittance of 3 CLC cells assembly. According to the plane wave definition $\vec{E} = \vec{E}_0 \exp[-i(\omega t - kz)]$ (with $\vec{E}_0$, ω, k and z representing the amplitude, frequency, propagation constant, and distance, respectively), a negative imaginary part is added to the refractive index of each sliced CLC layer as $n_o = n_o - n''i$ and $n_e = n_e - n''i$ ($n'' > 0$). In calculations, this imaginary part functions equivalently as a gain parameter of the gain medium inside the LC. Thus, the onset of laser oscillation is indicated by the divergence of the transmittance and the light amplification is represented by a normalized transmittance larger than unity. The complex relationship between the amplification index constant n'' and what follows the real fluorescent material parameters, together with the output intensity are out of our current research scope. For simplicity, we can choose n'' to be a frequency independent constant. Simulation under such an assumption was validated in some other literatures [13-15]. The amplification index constant n'' should not be too large to ensure the convergence of the program. In our simulation, we set $n'' = 0.0001$.

Without glass substrates present, simulation results with RCP and LCP incidence are shown in Figs. 4.8(a) and (b), respectively, where the light amplification at the band edge wavelength (~ 601 nm) can be observed for both RCP and LCP. This is attributed to the high

reflectivity of RCP from the right-handed CLC and the low reflectivity of LCP from the interface reflection of the air and the CLC layer. As a consequence, the light near the band edge can be effectively amplified by the external resonator for both orthogonal polarizations. The final output beam is elliptically polarized owing to the superposition of both amplified RCP and LCP beams.
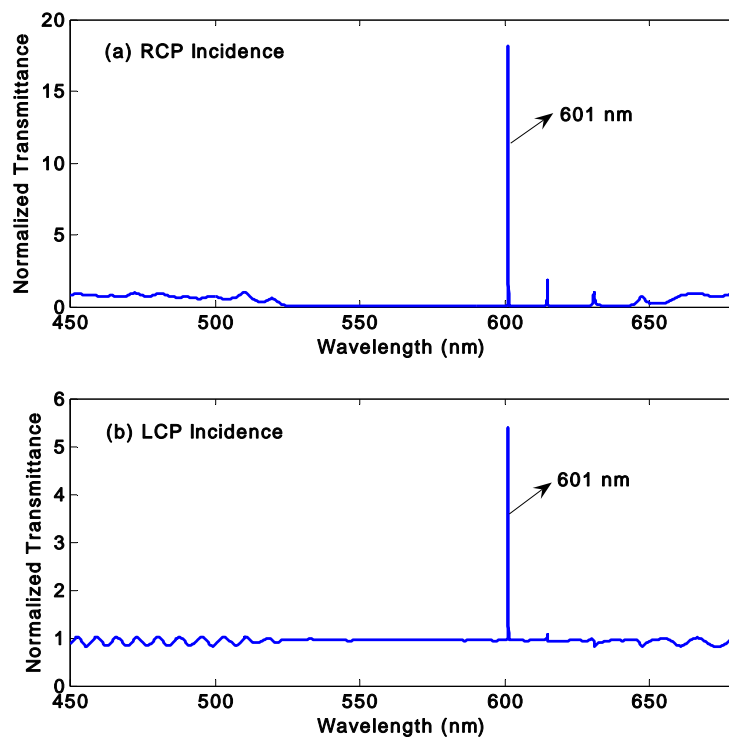
Fig. 4.8 Simulated normalized transmittance with amplifying medium in the middle CLC cell without glass substrates: (a) RCP as incidence; (b) LCP as incidence. Peak wavelength is at 601 nm.

With glass substrates present, the light also gets amplified at the band edge (~ 601 nm) for both RCP and LCP incidence as shown in Figs. 4.9(a) and (b), which resembles the phenomena in the case without glass substrates. The peak power at the amplified mode reaches almost the same value as that from Fig. 4.8. In addition, a preliminary measurement

68

on the beam divergence half angle has shown a remarkable decrease from ~ 4.5 deg (single CLC cell) to ~0.5 deg (3-CLC cells assembly). Together with Fig. 4.6(b), we note that the effects caused by glass substrates are summarized as follows: 1) a lot of oscillations are superimposed onto the characteristic spectral lines whereas the main features still remain. Therefore, introducing the substrates will not obviously pull the amplified mode away; 2) ideally, introducing the glass substrates into the CLC assembly will not noticeably decrease the peak power of the dominant amplified mode because the refractive index of glass is close to the average refractive index of CLC. However, the air gaps between the CLC cells in experiment may slightly deteriorate the lasing output power; and 3) the increased cavity length to *mm* scale dramatically decreases the beam divergence. Compared to the CLC cells assembly, such a structure can be realized using three stacked cholesteric polymer films (one active film between two passive films) as well. The major advantage of such a configuration is that the glass substrates can be completely removed and the device can be very thin. However, to fabricate such cholesteric polymer films a UV curing process is commonly practiced so that the dye bleaching problem during UV exposure is a concern. Moreover, the employed LC polymer usually has a smaller birefringence (e.g., $\Delta n \sim 0.1$ for the Merck chiral monomers RMM154 and RMM153) than BL006 ($\Delta n \sim 0.286$). As a result, the overall lasing efficiency would be lower and beam divergence larger than the corresponding three CLC cells assembly. This is indeed observed in our experiment.
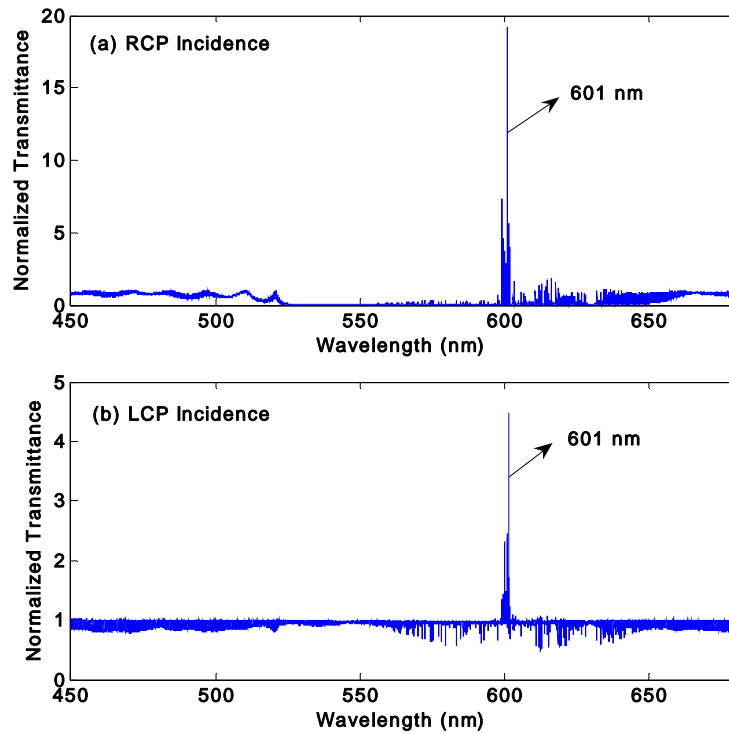
Fig. 4.9 Simulated normalized transmittance with amplifying medium in the middle CLC cell with glass substrates: (a) RCP as incidence; (b) LCP as incidence. Peak wavelength is at 601 nm.
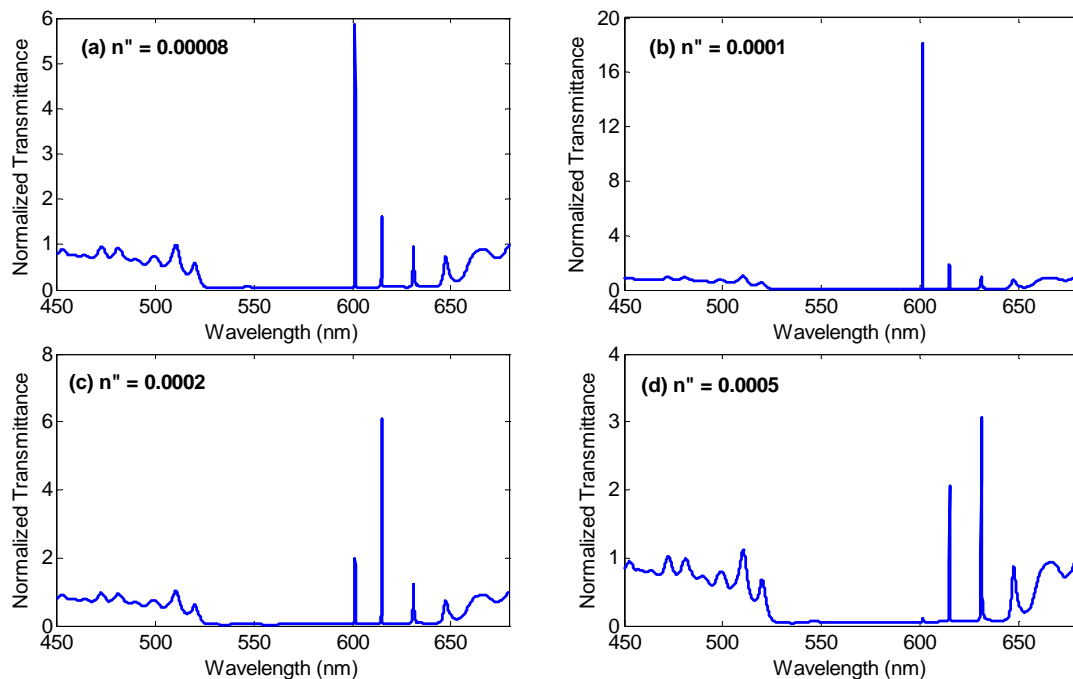
Fig. 4.10   Amplification index constant n" dependent light amplification performance: (a)n"=0.00008 ; (b)n"= 0.0001 ; (c)n"=0.0002 ;(d)n"=0.0005 ; The incidence is RCP.

In order to find out the optimal parameters for the CLC resonator and the active CLC cell, we investigate the amplification performance as a function of the amplification index constant n'' and the thickness of the active CLC cell d_1 using RCP as the incidence. Figures 4.10(a)-(d) give the results of light amplification as n'' gradually increases. As shown in Figs. 4.10(a) and (b), at smaller n'' the incident RCP light gets amplified at the band edge wavelength of the active CLC cell (the mode at 600 nm). As n'' increases, the amplification gets stronger. However, further increasing n'' does not give rise to a stronger emission; on the contrary, it weakens the amplification performance accompanied by a mode shift. As Figs. 10(c) and (d) show, the mode closer to the band edge of the CLC reflector (the mode at 640 nm) becomes more predominant as n'' increases. This implies that within the reflection band of the resonator the PBE mode (at 600 nm) of the active CLC is easier to be amplified than the band edge mode (at 640 nm) of the passive reflector. This trend is in accordance with the amplification behavior of the resonance modes in a typical FP, assuming a wavelength independent gain. The calculation of a simple FP with a complex refractive index for the medium between two end mirrors shows that the mode near the reflection band center is amplified at a smaller n'' value while the one near the band edge is amplified at a larger n'' value. However, in practice the PBE mode (600 nm) appears first and this mode will suppress the other possible laser modes. Therefore, in experiment only the mode at 600 nm can be readily observed other than the modes from FP effect of the resonator. On the other hand, the fluorescence peak of the emissive medium DCM is around 590-600 nm. For the laser modes beyond this range, the fluorescent intensity drops quickly, which also contributes to the

dominant band edge mode.
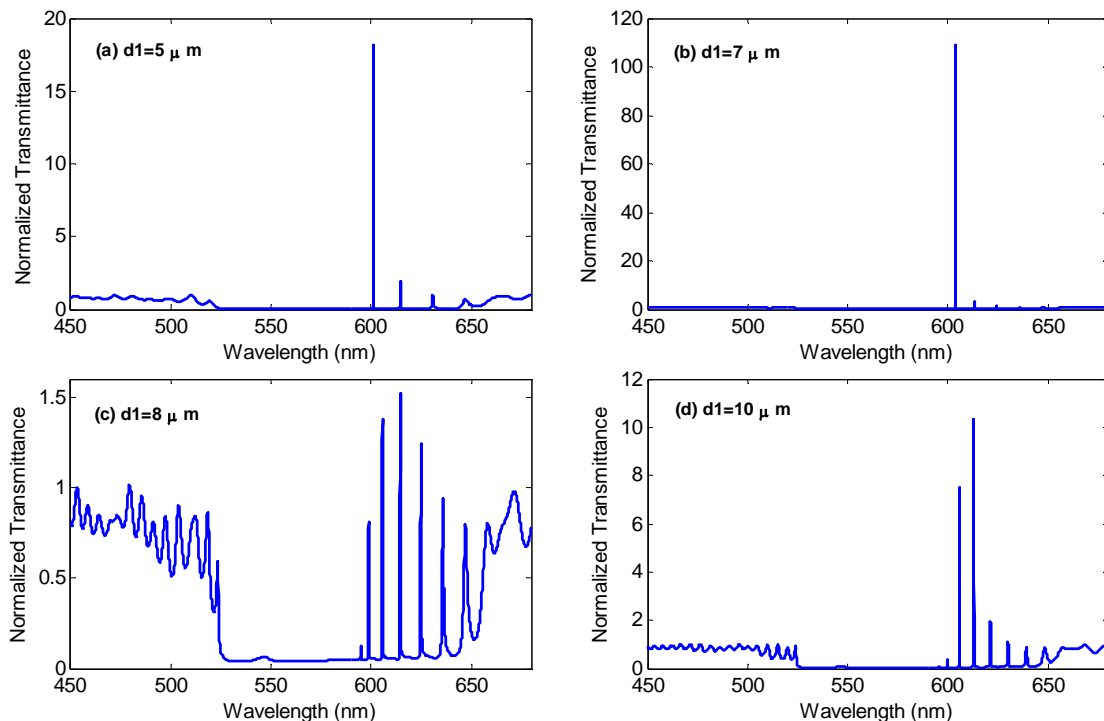
Fig. 4.11   Thickness of the active CLC middle cell d_1 dependent light amplification
performance: (a) d_1=5 μm; (b) d_1=7 μm; (c) d_1=8 μm; (d) d_1=10 μm. The incidence is RCP.

By varying the thickness of the active CLC cell in the middle, the tendency is similar

to the behavior exhibited in Figs. 4.11(a)-(d). Here n'' is again fixed at 0.0001. From Figs.

4.11(a) and (b), as the thickness of the active CLC layer is increased from 5 to 7 μm, the RCP

incident light is amplified at the band edge of the active CLC cell and the lasing strength is

boosted by ~6X. While beyond a certain value, the dominant amplified mode shifts towards

the band edge of the CLC reflector and the peak power decreases. This critical thickness,

above which the mode shift starts to occur, is of course relying on the setting value of n''.

The n'' in our current calculations is not directly correlated to the dye's absorption,

fluorescence, and the population inversion, nevertheless the tendency found here is again

confirmed by the fact that we did not experimentally obtain any stronger emission from the 8-μm or thicker active CLC laser in the resonator. Increasing the thickness of the active CLC cell is equivalent to increasing the n'' value except a longer feedback length, since the gain is increased for both cases. Thus, a similar tendency is observed here as that manifested in Fig. 4.10.

In general, the optimal output should be obtained at a relatively thin emissive CLC cell (< 8 μm) and the cell gap of CLC reflector used for the external resonator should not be too thick (< 5 μm) in order to allow ~3-4% transmittance. Our investigation on the system parameters aims to provide some guidelines for designing the photonic band edge CLC lasers with an external resonator supported. These critical values of the key parameters are based on the current materials and concentrations that we employed. Although the simulations of the n'' and d_1 dependencies are only based on three CLC layers without glass substrates, the physical mechanism and the tendency discussed here still hold for the real CLC cells without losing generality.

Our current device configuration of symmetric CLC Fabry-Perot external cavity can be easily extended to asymmetric case where the two CLC reflectors having different cell gaps to achieve a different reflectivity. Laser emission will be accordingly redirected to mainly emit from a single direction rather than both, which will be more attractive for practical applications.

4.5   Conclusions

In this chapter, we demonstrated a CLC circularly polarized resonator enhanced CLC

laser. Compared to the single reflector enhancement approach in Chapter 2, this approach shows a much higher enhancement ratio, which generates the highest lasing efficiency ~10% that we have obtained so far. The beam divergence is reduced by one order of magnitude due to the increased cavity length and the inserted glass substrates. The enhancement phenomenon is based on the Fabry-Perot supported photonic band edge mode. The integrated DFB and FP feedback gives the CLC laser a much higher lasing efficiency and the approach is general to different materials, i.e., be easily extended to CLC polymer film lasers. The theoretical analysis based on 4×4 transfer matrix and scattering matrix confirms the conservation and amplification of the PBE mode of the middle CLC layer. Design rules are given to guide how to achieve the optimal output.

4.6   References

1. P. Kipfer, R. Klappert, H. P. Herzig, J. Grupp, and R. Dandliker, "Improved red color with cholesteric liquid crystal in Bragg reflection mode," Opt. Eng. 41, 638 (2002).

2. J. C. Lee and S. D. Jacobs, "Design and construction of 1064-nm liquid-crystal laser cavity end mirrors," J. Appl. Phys. 68, 6523 (1990).

3. Y. Tanaka, H. Takano, and T. Kurokawa, "Circular polarization resonator based on cholesteric liquid crytal," Jpn. J. Appl. Phys. 43, 1062 (2004).

4. Y. C. Yang, C. S. Kee, J. E. Kim, H. Y. Park, J. C. Lee, and Y. J. Jeon, "Photonic defect modes of cholesteric liquid crystals," Phys. Rev. E 60, 6852 (1999).

5. S. M. Jeong, N. Y. Ha, Y. Takanishi, K. Ishikawa, H. Takezoe, S. Nishimura, and G. Suzaki, "Defect mode lasing from a double-layered dye-doped polymeric cholesteric liquid crystal films with a thin rubbed defect layer, " Appl. Phys. Letts. 90, 261108 (2007).

6. M. H. Song, K. C. Shin, B. Park, Y. Takanishi, K. Ishikawa, J. Watanabe, S. Nishimura, T. Toyooka, Z. Zhu, T. M. Swager, and H. Takezoe, "Polarization characteristics of phase retardation defect mode lasing in polymeric cholesteric liquid crystals," Sci. Technol. Adv. Mater. 5, 437 (2004).

7. M. H. Song, B. Park, K. C. Shin, T. Ohta, Y. Tsunoda, H. Hoshi, Y. Takanishi, K. Ishikawa, J. Watanabe, S. Nishimura, T. Toyooka, Z. Zhu, T. M. Swager, and H. Takezoe, "Effect of phase retardation on defect-mode lasing in polymeric cholesteric liquid crystals," Adv. Mater., 16, 779 (2004).

8. M. H. Song, B. Park, Y. Takanishi, K. Ishikawa, S. Nishimura, T. Toyooka, and H. Takezoe, "Lasing from thick anisotropic layer sandwiched between polymeric cholesteric liquid crystal films," Jpn. J. Appl. Phys. 44, 8165 (2005).

9. R. Ozaki, T. Sanda, H. Yoshida, Y. Matsuhisa, M. Ozaki, and K. Yoshino, "Defect mode in cholesteric liquid crystal consisting of two helicoidal periodicities," Jpn. J. Appl. Phys. 45, 493 (2006).

10. Z. Ge, T. X. Wu, X. Zhu, and S. T. Wu, "Reflective liquid crystal displays with asymmetric incidence and exit angles," J. Opt. Soc. Am. A 22, 966 (2005).

11. Y. Huang, T. X. Wu, and S. T. Wu, "Simulations of liquid-crystal Fabry-Perot etalons by an improved 4×4 matrix method," J. Appl. Phys. 93, 2490 (2003).

12. E. Hecht, Optics (2nd edition) (Addison-Wesley, Massachusetts, 1987).

13. A. D'Orazio, V. D. Palo, M. D. Sario, V. Petruzzelli, and F. Prudenzano, "Finite difference time domain modeling of light amplification in active photonic band gap structures," Progress in Electromagnetics Research, PIER, 39, 299 (2003).

14. O. N. Kozina and L. A. Melnikov, "Laser action in 1D photonic crystal structures with active layers," Proceedings of the Third Moscow International Symposium on Magnetism, 45 (2005).

15. O. N. Kozina and L. A. Melnikov, "Gain properties of one-dimensional photonic crystals with finite number of active layers," Proc. of SPIE, 5067, 194 (2003).

CHAPTER 5   CHOLESTERIC LIQUID CRYSTAL POLYMER FILM
LASERS

5.1   Introduction

Liquid crystal polymers (LCPs) are a unique class of wholly aromatic polyester polymers that provide high performance properties. In particular, they are highly inert chemically and highly resistant to fire. The polymerizable functional groups in the molecular structure offer the possibility for crosslinking and forming a long chain network while maintaining the order. The solid state polymer film possessing a cholesteric planar structure can be used as a reflecting layer, exhibiting similar optical properties as cholesteric liquid crystals. It has been used as end mirrors or circular polarized resonators for laser applications [1-3].

Recently, the tendency towards miniaturization and portability in the emerging CLC-based mirrorless lasers brings forward new research interests in cholesteric polymer lasers. By using solid state polymeric cholesteric liquid crystal film with a fixed cholesteric order, more stable lasing can be achieved because lasing condition is often suffered from distortions of cholesteric order, mainly due to the heat dissipated during the lasing process. Once polymerized, it can survive high temperature up to 150 ^{o}C without losing its order. Furthermore, polymeric films can be peeled off from the glass substrate so that they become free standing polymer films with sufficient mechanical strength and elastic flexibility. As a result, they have been widely used in CLC lasers especially when a defect mode lasing is needed due to a twist discontinuity or chirality discontinuity.

Some efforts have been focused on the lasing action in dye-doped cholesteric free standing polymer films [4-6], cholesteric elastomer films [7], cholesteric oligomer derivatives [8], and spatially tunable lasing films [9]. On the other hand, defect mode lasing was demonstrated using cholesteric polymeric films based on either a twist jump [10], or a helix discontinuity [11-14]. More recently, CLC polymer films have been used to polarize and enhance the electro-luminescence from OLED based on photon recycling [15].

There are several factors that limit the output power from the CLC polymer lasers, such as dye-bleaching during the UV polymerization process and deformation of the ordered cholesteric structure due to insufficient surface anchoring energy. In order to increase the output power and, in the meantime, lower the threshold, different approaches have been proposed, such as adding external reflectors [2-3, 16-17] or stacking multiple active polymer films [18]. All the approaches of emission enhancement discussed in Chap. 3 and Chap. 4 apply to CLC polymer film lasers without losing generality. As we mentioned in Sec. 3.2 and 3.4, adding a cholesteric passive reflecting layer helps to enhance the laser output based on a further coherent amplification while the enhancement from a metallic mirror essentially results from the second pump of the active layer.

In this chapter, we combine these two effects together for enhancing the output from a CLC polymer film laser by sandwiching the dye-doped CLC polymer film between a mirror and a CLC reflecting film. Unlike the single reflecting layer enhancement approaches, such a structure creates an incomplete resonant cavity because the metal layer and the cholesteric reflecting layer select a different polarization for reflection. Hence the output power is

dramatically improved. More importantly, the output beam is circularly polarized, but opposite to the handedness of the cholesteric helix. Based on light recycling effect, the original impure circularly polarized laser (from a single active CLC polymer film) can be recycled and maximally purified by the two reflecting layers. The responsible physical mechanisms are discussed in detail. In addition, the different lasing performance from different sides of the dye-doped CLC polymer film is investigated and the underlying mechanism is analyzed. This work cannot be realized using CLC cell stack because of indirect contact between each layer. Such an approach not only improves the output power but also opens a way for polarization manipulation and control in CLC polymer- based laser devices.

5.2 Sample preparation and experimental layout
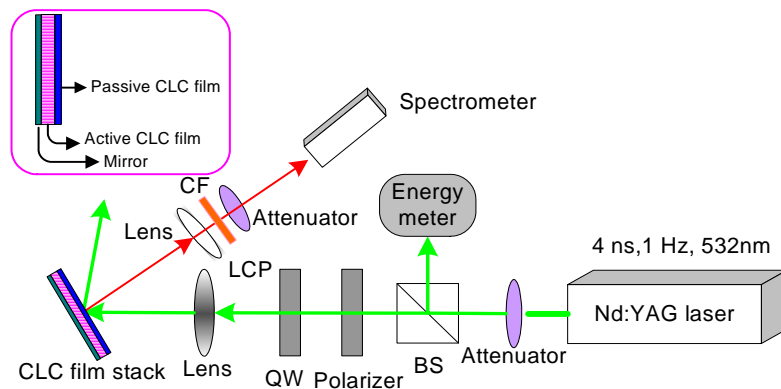
Fig. 5.1 Experimental setup: BS: Beam splitter; QW: Quarter-wave plate; CF: Color filter; LCP: left-handed circularly polarized light.

Figure 5.1 shows the experimental setup at 20° oblique incidence. The setup is basically the same as the one used in Sec. 3.4. Under the pump, the sample stack was placed in series as mirror-active CLC film-passive CLC film with the passive CLC film facing the

pump.

The mixture was prepared by mixing 44% of a chiral reactive mesogen RMM154, 44% of a reactive mesogen RM82 and 12% of a right-handed chiral agent CB15 (all from Merck). To make the active CLC lasing film, the laser dye DCM was doped into the mixture at 1.7 wt% concentration. For the passive reflective film the CB15 concentration was slightly lowered in order to shift the reflection band to cover the lasing wavelength. After the mixture was thoroughly stirred for several hours it was filled into an empty cell in an isotropic state through capillary action. The inner surfaces of the cell were first coated with indium-tin-oxide (ITO) electrodes and then polyimide alignment layers. In reality, these ITO layers were not needed because no voltage was applied to the cell. Both substrates were rubbed in anti-parallel directions to produce a small (~3°) pretilt angle. The sample was slowly cooled down to ~55 °C so that less defect was formed in its cholesteric planar structure. Subsequently the sample was exposed under a UV light for ~45 min while keeping the temperature at 55 °C. The upper surface of the polymer film, which is facing the UV lamp during exposure, is called *top side* in this work. In contrast the lower surface of the polymer film, which is further away from the UV lamp but closer to the heating stage, is called *bottom side*. We differentiate these two sides because they exhibit a dramatic difference in the lasing performance when different sides face the pumping laser.

The thickness of the active CLC polymer film is 15 μm and the passive CLC polymer film is 8 μm. To fabricate the stacked CLC polymer laser, we first peeled off the 15 μm dye-doped CLC film from the substrates and put it in optical contact on a substrate which was

coated with a thin aluminum layer. Afterwards the 8 μm CLC film was peeled off from the substrates and attached in optical contact with the 15 μm film. Any air gap between the polymer films will deteriorate the lasing power. In order to achieve a stronger laser output, when assembling the film stack, the top side of the active CLC film should face the passive CLC film and the pump beam because of the different lasing capabilities between the top side and the bottom side. The device structure is illustrated in the upper-left corner of Fig. 5.1.

5.3   Enhanced laser emission in opposite handed polarization

First, we characterized the reflection band of both active and passive films. We measured the reflection band using a white light source (DH-2000, Instec, UV-VIS-NIR) and a spectrometer (the same one shown in Fig. 5.1) at normal incidence. Results are shown in Fig. 5.2, where the top side reflection bands of the 15 μm active film and the 8 μm passive film are shown in red and blue curves, respectively. Lasing spectrum centered at λ=613 nm with 53 μJ/pulse pumping energy is also included in the figure as the green curve shows. From Fig. 5.2, laser action takes place at the long wavelength band edge of the active film and, in the meantime, within the reflection band of the passive film. The thicker film (15 μm) has a lower reflectivity because multi-domains and defect lines are formed during fabrication due to insufficient surface anchoring energy and lower order parameter of the LC polymer material.
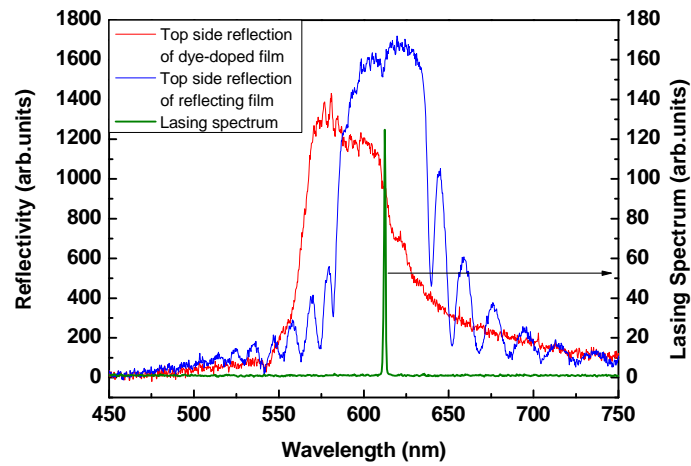
Fig. 5.2 Top side reflection bands of the 15 μm active film (red) and the 8 μm passive film (blue), and the lasing spectrum at 53 μJ/pulse pump (green).

Next, we measured the pump energy dependent lasing output power from our stacked CLC polymer laser, which consists of a mirror, an active CLC film (15 μm) and a passive CLC film (8 μm). Results are plotted in Fig. 5.3.
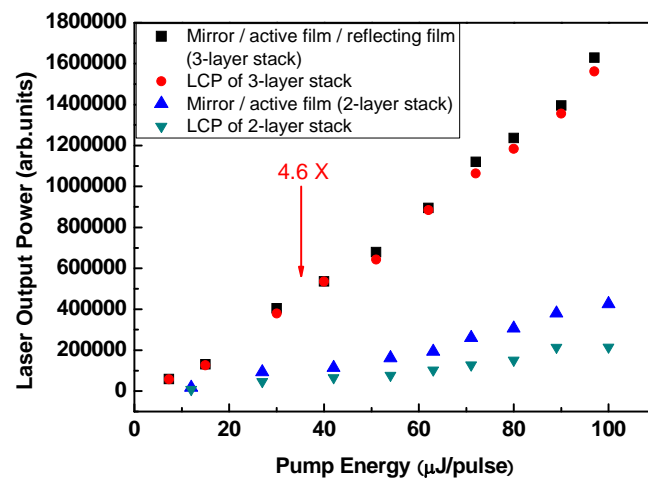
Fig. 5.3 The pump energy dependent laser output power of the total emission and LCP component from a {mirror/active CLC film/reflecting CLC film} laser and a {mirror/active CLC film} laser.

In Fig. 5.3, the total emission and the corresponding left-handed circularly polarized (LCP) component of this 3-layer CLC laser (mirror/active CLC film/passive CLC film) are shown in black and red, respectively. The LCP component occupies ~96% of the total emission. We then removed the passive CLC film from this film stack and measured the laser emission again at the same pumping spot. For this 2-layer CLC laser (mirror/active CLC film), the total emission and its LCP component are shown in blue and green, respectively. The LCP component occupies only ~52% of the total emission. Moreover, after removing the passive film the laser emission is ~4.6X weaker than that of the 3-layer CLC laser. The lasing threshold was measured to be 0.46 and 3.0 μJ/pulse for the 3-layer stacked CLC polymer laser and the 2-layer mirror reflected CLC polymer laser, respectively.

The results shown in Fig. 5.3 indicate that when the active layer is sandwiched between a mirror and a passive CLC reflector, we can obtain a dramatically enhanced LCP output whose polarization is opposite to the handedness of the cholesteric helix. This phenomenon is attributed to the further stimulated amplification of the reflected laser beam and light recycling effect. Intrinsically the single right-handed CLC film generates circularly polarized laser light in the same handedness as its helix. Hence for our 15 μm dye-doped CLC film, the laser emission is mostly right-handed circularly polarized (RCP). Here the lasing wavelength is designed to be within the reflection band of the passive CLC reflector. Therefore, when the laser light is reflected back by the passive CLC reflector, its original polarization state maintains, i.e. RCP in our case. Such RCP emission at the band edge wavelength will get further stimulated amplification when passing through the active CLC

layer due to its polarization-dependent DFB. On the other hand, the mirror reflection converts RCP into LCP which is highly transmitted by the passive CLC film and, in turn, contributes to the final enhanced LCP output. As a consequence, the originally generated laser light successively experiences the amplification process each time the RCP part propagates through the active layer, and then gets converted to LCP by the mirror. As this process continues, the output laser light is gradually enhanced and purified into an LCP.

Taking the surface reflection between the air and polymer films (estimated to be ~4%) into consideration, the measured 96% LCP output represents a highly purified polarized emission, almost reaching its ideal case of polarization recycling. The CLC polymer laser with mirror reflection only generates a linearly polarized emission so that ~52% of LCP component can be detected within the total output, as a result of coherent superposition of the original RCP and the reflected LCP.
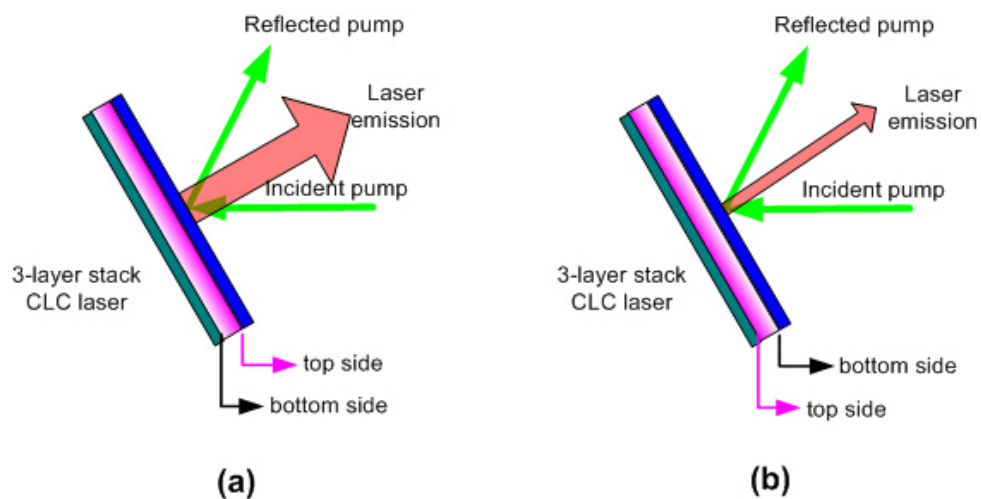
Fig. 5.4 Sample layout in the experimental setup: (a) top side of the active film is facing the pump beam and (b) bottom side of the active film is facing the pump beam. The 3-layer stack CLC laser: mirror (dark green) / active CLC film (magenta) / passive CLC film (blue).

Figures 5.4(a) and (b) show us the sample layout in the experiment, where the top side

(dark magenta) and the bottom side (light magenta) of the active film face towards the pumping beam, respectively. During the assembly of the 3-layer CLC polymer laser, we found that if the top side of the 15 μm active film was directly attached to the passive film (i.e., the top side is facing the pump source), the laser output was much stronger than when the bottom side was directly attached to the passive film. This is caused by the drastically different lasing performance of a single 15 μm active film between the top and bottom sides facing the pump.

In a similar layout as shown in Figs. 5.4(a) and (b) except without the mirror and the CLC reflecting film, the laser output was measured and results are shown in Fig. 5.5. The units on the ordinate scale are intentionally kept the same as that used in Fig. 5.3 to allow an easy comparison.
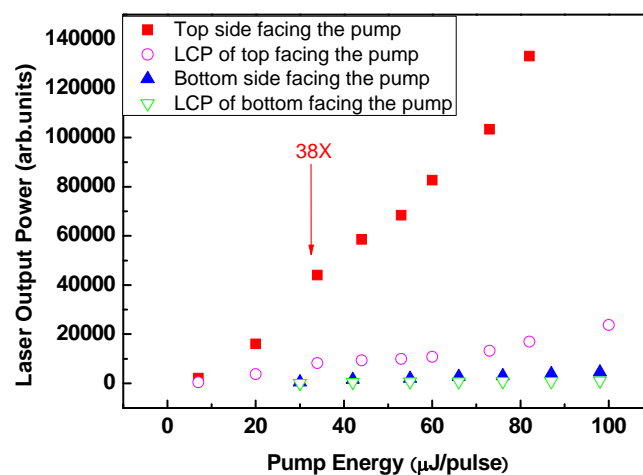
Fig. 5.5 The pump energy dependent laser output power from a single 15 μm active CLC film with the top side facing the pump source and the bottom side facing the pump source.

When the top side is facing the pump source (Fig. 5.4(a) layout with the active film

only), the total emission and LCP component are shown in red and pink, respectively. Correspondingly, when the bottom side is facing the pump (Fig. 5.4(b) layout with the active film only), the total emission and LCP component are shown in blue and green, respectively. Therefore the emission in the case of the top side facing the pump is, on average, ~38X stronger than that of the bottom side facing the pump. In addition, no matter whether the top or the bottom side is placed towards the pump, laser light is generated from both directions at almost equal power. The corresponding lasing thresholds for these two cases are 5.65 and 20 μJ/pulse, respectively. By measuring the LCP component, we found that there was ~13% LCP with the top side facing the pump and ~24% LCP with the bottom side facing the pump. The minority LCP component originates from the defects in the planar structure, which not only scatter the light but also deteriorate the output power and the purity of the polarizations.

Comparing the output power when the top side facing the pump (red squares) in Fig. 5.5 and that from a 2-layer mirror-reflected CLC polymer laser (blue triangles) in Fig. 5.3, we notice that the former one is ~2.3X stronger than the latter one. Because of the direct contact of the aluminum mirror and the active CLC film, the mirror will reflect back both the laser emission generated towards it and the pump beam. Under this circumstance, the active layer can be pumped once again however the bottom side of the active film generates a very weak laser emission when being pumped. As the result, the enhancement contribution due to re-pump of the active layer is unnoticeable.

In terms of the LCP component percentage, we can see that the 3-layer CLC polymer laser device performs a dramatic improvement in purifying the output polarization state from

87% of RCP output (13% of LCP as measured in Fig. 5.5) to 96% of LCP output, which is the maximum it can reach.

5.4   Photonic band deformation during polymerization

In order to understand why the top side and bottom side exhibit such a dramatic difference in the laser generation when they are pumped, we further investigate the reflection band of a CLC polymer film from both sides. Results are shown in Figs. 5.6(a) and 5.6(b).
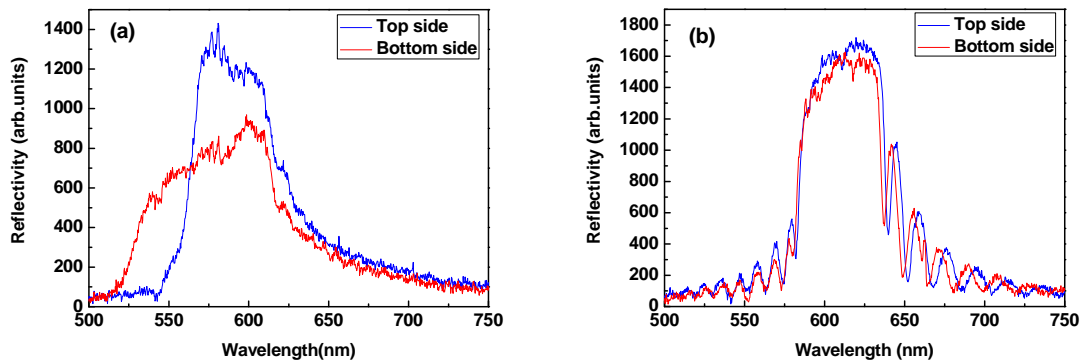
Fig. 5.6 The top side (blue) and bottom side (red) reflection bands of the CLC polymer film:
(a) the 15 μm dye-doped CLC polymer film (b) the 8 μm passive CLC polymer film.

Figure 5.6(a) describes the top and bottom side reflection bands of the 15 μm dye-doped CLC polymer film and Fig. 5.6(b) describes those of the 8 μm passive CLC polymer film. For the 15 μm dye-doped CLC film, after curing process the top side reflection band still maintains a relatively good shape and high reflectivity with a bandwidth of ~50 nm. However the bottom side reflection band shows an obviously broadened bandwidth to ~100 nm. Currently we believe this bandwidth broadening could be attributed to the gradient pitch formed inside the cholesteric structure from the top surface to the bottom surface. Because the employed laser dye has a strong absorption for the UV light, during exposure an UV

intensity gradient would be formed through the top surface to the bottom of the film. Near the top side the UV intensity is stronger and thus the polymerization reaction is faster. The quicker consumption of the polymer near the top region initiates the diffusion process due to the concentration difference. Therefore the top and bottom areas have different chiral concentrations and thus different pitches, leading to the observed bandwidth broadening. In addition, the ordered structures will be somewhat deteriorated during the monomer polymerization so that more defects are observed in the film after UV exposure. These defects will, in turn, lead to the decreased reflectivity within the reflection band. It is inferred that near the top side the cholesteric periodic structure is more ordered than that near the bottom side.

Under excitation, photons will be generated whereas the generation of laser light requires sufficient feedback with a reflectivity high enough to overcome the cavity loss. Accordingly, when the top side is pumped, the generated photons near the top surface experience a better periodic structure and thus a better feedback. Moreover, at this time, the area near the top side is more strongly pumped than the bottom area due to the absorption of DCM. However, in the case of bottom side facing the pump, the photons generated in the stronger pump area cannot get sufficient distributed feedback. This gives rise to the difference in lasing output power between the two sides.

Unlike the broadened reflection band in dye-doped CLC polymer film, the 8 μm CLC polymer film shows almost the same band shape between the top and bottom sides. There is a very small blue shift and slight reflectivity decrease observed in the reflection band of the

bottom side. This is due to the slightly different measurement positions on the film, where the reflection band is not perfectly uniform over the whole cell. Nevertheless the reflection band shape and reflectivity are not changed noticeably because no laser dye is present, and hence no obvious UV intensity gradient and pitch gradient are formed throughout the film. As a polarization recycling layer and polarization dependent reflector, the passive film shows a higher reflectivity than the 15 μm dye-doped CLC film does, providing good polarization conversion efficiency.

5.5   Conclusions

In this chapter, we demonstrated cholesteric polymeric film lasers. The CLC polymer lasers are flexible, rollable, free standing and easily deformed to any shape with its order preserved. By sandwiching the dye-doped CLC film within a mirror reflecting layer and a cholesteric reflecting layer, the laser emission is dramatically enhanced and with its circular polarization state opposite to the intrinsic helix based on light recycling effect. Moreover, we observed reflection band deterioration and broadening from different sides of the film, as a consequence of gradient curing intensity throughout the film thickness and the resulting gradient pitch.

5.6   References

1. Y. Tanaka, H. Takano, and T. Kurokawa, "Circular polarization resonator based on cholesteric liquid crystal," Jpn. J. Appl. Phys. 43, 1062 (2004).

2. K. Amemiya, T. Nagata, M. H. Song, Y. Takanishi, K. Ishikawa, S. Nishimura, T. Toyooka, and H. Takezoe, "Enhancement of laser emission in dye-doped cholesteric liquid crystals with single-output window," Jpn. J. Appl. Phys. 44, 3748 (2005).

3. K. Amemiya, M. H. Song, Y. Takanishi, K. Ishikawa, S. Nishimura, T. Toyooka, and H. Takezoe, "Lowering the lasing threshold by introducing cholesteric liquid crystal films to dye-doped cholesteric liquid crystal cell surfaces," Jpn. J. Appl. Phys. 44, 7966 (2005).

4. J. Schmidtke, W. Stille, and H. Finkelmann, and S. T. Kim, "Laser emission in a dye doped cholesteric polymer network," Adv. Mater. 14, 746 (2002).

5. T. Matsui, R. Ozaki, K. Funamoto, M. Ozaki, and K. Yoshino, "Flexible mirrorless laser based on a free-standing film of photopolymerized cholesteric liquid crystal," Appl. Phys. Lett. 81, 3741 (2002).

6. T. Ohta, M. H. Song, Y. Tsunoda, T. Nagata, K. C. Shin, F. Araoka, Y. Takanishi, K. Ishkawa, J. Watanabe, S. Nishimura, T. Toyooka, and H. Takezoe, "Monodomain film formation and lasing in dye-doped polymer cholesteric liquid crystals," Jpn. J. Appl. Phys. 43, 6142 (2004).

7. H. Finkelmann, S. T. Kim, A. Munoz, P. Palffy-Muhoray, and B. Taheri, "Tunable mirrorless lasing in cholesteric liquid crystalline elastomers," Adv. Mater. 13, 1069 (2001).

8. K. Amemiya, K. C. Shin, Y. Takanishi, K. Ishikawa, R. Azumi, and H. Takezoe, "Lasing in cholesteric liquid crystals doped with oligothiophene derivatives," Jpn. J. Appl. Phys. 43, 6084 (2004).

9. Y. Huang, L. P. Chen, C. Doyle, Y. Zhou, and S. T. Wu, "Spatially tunable laser emission in dye-doped cholesteric polymer films," Appl. Phys. Lett. 89, 111106 (2006).

10. M. Ozaki, R. Ozaki, T. Matsui, and K. Yoshino, "Twist-defect-mode lasing in photopolymerized cholesteric liquid crystal," Jpn. J. Appl. Phys. 42, L472 (2003).

11. J. Schmidtke, W. Stille, and H. Finkelmann, "Defect mode emission of a dye doped cholesteric polymer network," Phys, Rev. Lett. 90, 083902 (2003).

12. M. H. Song, B. Park, Y. Takanishi, K. Ishikawa, S. Nishimura, T. Toyooka, and H. Takezoe, "Lasing from thick anisotropic layer sandwiched between polymeric cholesteric liquid crystal films," Jpn. J. Appl. Phys. 44, 8165(2005).

13. Y. Takanishi, N. Tomoe, N. Y. HA, T. Toyooka, S. Nishimura, K. Ishikawa, and H. Takezoe, "Defect-mode lasing from a three layered helical cholesteric liquid crystal structure," Jpn. J. Appl. Phys. 46, 3510 (2006).

14. S. M. Jeong, N. Y. Ha, Y. Takanishi, K. Ishikawa, and H. Takezoe, "Defect mode lasing from a double-layered dye-doped polymeric cholesteric liquid crystal films with a thin rubbed defect layer," Appl. Phys. Lett. 90, 261108 (2007).

15. S. M. Jeong, Y. Ohtsuka, N. Y. Ha, Y. Takanishi, K. Ishikawa, and H. Takezoe, "Highly circurlary polarized electroluminescence form organic light-emitting diodes with wide-band reflective polymeric cholesteric liquid crystal films," Appl. Phys. Lett. 90, 211106

(2007).

16. Y. Zhou, Y. Huang, and S. T. Wu, "Enhancing cholesteric liquid crystal laser performance using a cholesteric reflector," Opt. Express 14, 4479 (2006).

17. Y. Zhou, Y. Huang, T. H. Lin, L. P. Chen, Q. Hong, and S. T. Wu, "Directional controllable linearly polarized laser from a dye-doped cholesteric liquid crystal," Opt. Express 14, 5571 (2006).

18. Y. Huang, T. H. Lin, Y. Zhou, and S. T. Wu, "Enhancing the laser power by stacking multiple dye-doped chiral polymer films," Opt. Express 14, 11299 (2006).

CHAPTER 6   CHOLESTERIC LIQUID CRYSTAL and POLYMER BASED BROAD BAND CIRCULAR POLARIZERS

6.1   Introduction

Circular polarizers are critical components for optical communications, optical remote sensors, as well as liquid crystal displays (LCDs) [1-3]. For reflective and transflective LCDs, the single circular polarizer is employed on the top of the LC layers because it functions as a pair of crossed polarizers favorable for achieving high contrast ratio [1]. While for transmissive and projection LCDs, the circular polarizer in conjunction with a quarter-wave plate can be used for converting the unpolarized light from the backlight lamp into a linearly polarized light without much backlight energy lost [4]. Typically two methods have been employed for making a circular polarizer: 1) to laminate a linear polarizer with a quarter wave film [5, 6] and 2) to utilize the Bragg reflection of a cholesteric liquid crystal (CLC) film [8, 12-21]. In the first approach, if an absorption-type linear polarizer is employed, more than 50% of the incident light is absorbed. Therefore, a non-absorptive polarizer, such as the polarizing beam splitter (PBS) is highly desirable.

The principle of backlight recycling based on a reflective polarizer can be described as follows: the back reflector, the light source, and the reflective polarizer are placed in series. Assuming that the polarizer (exp, a PBS) transmits p-wave but reflects s-wave, the reflected p-wave is converted into s-wave by the reflector due to the induced π phase change. Then this s-wave will transmit through the polarizer without reflection. In this case, the backlight can be converted into s-wave without much loss. As a result, the optical efficiency from the

backlight unit of the LCD module would be doubled. This approach has been widely used in projection displays [7].

For large screen direct-view LCDs, the film-based polarization converter is more practical than PBS array due to its compactness. A polarization converter using CLC films with a reflector and a quarter-wave film has been proposed [8]. However, the bandwidth of a CLC film is determined by the LC birefringence (Δn) and the pitch length. To cover the entire visible spectral range (400-750 nm), a CLC film with $\Delta n > 0.7$ is required if a uniform pitch length is employed [9]. Although some super high birefringence liquid crystals do exist [10], their viscosity is high and chemical and photo stabilities are not sufficient for real applications.

Broadband reflective polarizer DEBEF (licensed by 3M Inc.) has been a successful example [11]. The device is based on multilayer structure with alternating isotropic layers and birefringent layers to allow one polarization state seeing the isotropic media and the other one experiencing a multilayer thin film structure (with index modulation n_e-n_o-n_e-n_o...). The broadband reflection for single polarization state requires over 1000 layers. The fabrication is hence challenging. Since it was invented, it has been the dominant technique in transmissive LCDs.

An alternative approach is to use a modest birefringence ($\Delta n \sim 0.2$) CLC which has a gradient pitch distribution along the helical axis [12-21]. Theoretical simulation shows that the gradient pitch in CLC leads to a much broader bandwidth [9]. It has attracted lot of research interests to realize it in real device. Here we will briefly discuss the prior art of

broadband reflective polarizers based on CLC with a gradient pitch.

The early work is dated back to 1995, when D. J. Broer (Philips Research Inc.) demonstrated the gradient pitch, for the first time, due to a photo-induced diffusion during a photo-polymerization reaction [12]. The material is a blend of cholesteric diacrylate monomer, which has two reactive sides per molecule, and nematic monoacrylate, which has only one reactive site. With the help of UV absorptive dye, a gradient of UV intensity can be achieved over the thickness of the sample. The polymerization rate will be the fastest at the top of the film (close to the lamp) resulting in a faster consumption of the most reactive monomer. The depletion of this monomer starts a diffusion process where the upper part of the layer is enriched with cholesteric material, and the lower part with nematic material. Such a cholesteric film reflector has a reflection band ~350 nm. It greatly improves the light yield by ~40%. The single film CLC broadband reflective polarizer with 15 μm thickness was realized, however it requires the addition of UV absorptive dye.

Unlike the linear variation of pitch mentioned above, the non-linear pitch distribution was realized in 1998 by L. Li et al [13, 14]. A blend of polysiloxane liquid crystal polymer (in cholesteric order), non-reactive nematic liquid crystal, and the photo initiator was used in a 20 μm cell. After annealed at 90 deg for several minutes and UV cured, a broadened reflection band over 750 nm (cover VIS) was achieved. Nematic LC was rich in the front surface (from which UV light is incident) where the UV intensity is stronger. The 800 nm wide reflection band with ~35% reflectivity and 30:1 contrast ratio in VIS was achieved.

Gradient pith was demonstrated in cholesteric liquid crystalline oligomers as well [15-

17]. The mixture consists of both non-chiral and chiral mesogen. Two mixtures are formulated with different reflection centers. In fabrication, each mixture is blade-coated on the glass substrate without alignment layer at 40 μm thick to form the semi-free films. Then two films are sandwiched together with 19 μm spacer disposed between the plates. In such a way the layers are in contact. At stable CLC phase temperature, a diffusion process between two compounds may occur and concentration gradient is formed, which is then frozen by quenching process. Cholesteric structure with gradient pitch distribution was consequently preserved by quickly turning into glassy state. No UV polymerization is needed and the broadband of 300 nm is achieved.

Another experimental route lies in a thermally-induced pitch variation simultaneously carried out with the UV-crosslinking reaction was employed to introduce gradient pitch in CLC [18]. 80% of RM9, a mixture of reactive monomer and side group LC polymer with siloxane backbone (Wacker Chemie Ltd), mixed with 20% of 5CB (nematic liquid crystal from Merck Inc.) was filled into a 20 μm homogeneous cell at 80 ^{o}C. Weak UV exposure (λ=365 nm @ 0.4mW/cm^{2}) was performed while ramping the temperature from 95°C to 62°C within 2 hours. Although the broadened reflection was observed, the bandwidth (Δλ~180 nm) and the reflectivity were quite insufficient.

In addition to CLC polymers and oligomer materials, polymer-stabilized cholesteric liquid crystal mixtures are also possible to produce gradient pitches [19]. The mixture consists of low molar mass liquid crystal BL090, cholesteric oligomer SB, and chiral reactive mesogen RMB in a concentration: 65% BL090 + {89%SB+11%RMB}. A similar fabrication

process as that in Refs. 15-17 was employed. Two mixtures with different pitch lengths were made into two polymer-stabilized cholesteric liquid crystal films by capillary filling into 12.5 μm cell and cured for 20 minutes by weak UV light (λ=365 nm @ 0.1mW/cm^2). Then a 12.5 μm sandwiched cell is made by two semi-films and a complementary UV-curing was followed. The complementary UV curing process polymerized and cross-linked the materials which had not reacted during the previous individual sequences. The time required for the two films to reach equilibrium gradient concentration is 1 day.

Doping much lower concentration of non-chiral reactive mesogen into cholesteric liquid crystals in a single film also results in broadened reflection band [20]. For example, ~91 wt% of cholesteric liquid crystal BL094 mixed with ~9 wt% of reactive mesogen RM257, and a small amount of photo initiator was introduced into an 8 μm thick homogeneous cell at 83 ^{o}C by capillary action. Weak UV illumination (λ=365 nm @ 0.1mW/cm2) was performed during 30 minutes. A 150 nm reflection band is formed after curing. It is believed to be owing to the highly attenuated UV intensity from up side to down side through the sample, as a result of absorption of liquid crystal material. However, such a low concentration of polymer does not support the free-standing film. More research work investigated the concentration effect in forming a broadened reflection band gap by doping 3 wt%-10wt% of monomer to create a polymeric network through the sample to stabilize the textures [21]. It appeared that network is denser on the surface strip close to the UV source. If UV gradient exists within the sample, there will be a gradient of consumption of the monomer. The consumption of the monomer is therefore higher in the areas closer to the UV lamp. The diffusion ensues for the

monomer from the areas with a lower irradiation to the area closer to the lamp with a higher irradiation. Thus the consumption of the monomer is greater. In 10 wt% monomer sample, the reflectivity of the front surface (closer to UV illuminant) is higher than that from the bottom surface. This is a result of denser polymer network near the front surface. A low intensity UV illumination is favorable for broadened band. Usually the broadening increases with the increasing concentration of the monomer. It is due to an inhomogeneous consumption of the chiral monomer within the sample.

In our research work, we use either cholesteric liquid crystalline monomer, or a mixture of cholesteric liquid crystal and cholesteric monomer in a concentration high enough to form a single free-standing film. Our goal is to achieve circular polarizers with a reflection band broad enough to cover the whole visible spectral range while maintaining a single polymeric film. Although we also observed the inhomogeneous broadened reflection in cholesteric gel, it remains a gel structure without sufficient mechanical and elastic strength. Therefore it is beyond our research interests.

In this chapter, we demonstrated two devices to meet the challenges. Section 6.3 demonstrates a broadband circular polarizer using pure cholesteric liquid crystalline polymer by applying a new fabrication route [22]. Theoretically by applying the process repeatedly we can achieve the wide reflection band although every single layer exhibits a limited bandwidth of ~50 nm. The multiple-film stack becomes a single film after polymerization of the infiltrated materials.

In Section 6.4, we demonstrated a broadband circular polarizer using the mixture of

cholesteric liquid crystals and chiral monomers [23]. The chiral monomer is doped at a concentration of ~50% so that it stabilizes the cholesteric texture into a solid polymer film.

6.2   Experimental setup
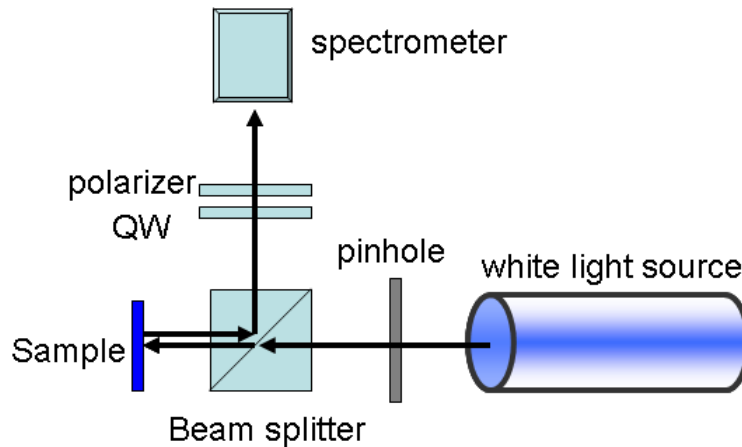
Fig. 6.1 Experimental setup for measuring the reflectivity and extinction ratio of the circular polarizer at normal incidence; QW: broadband quarter wave plate.

Figure 6.1 shows the setup of the reflectivity and extinction ratio measurement. The white light from the source is incident on the sample (shown as the dark blue plate) through a pinhole and then a beam splitter. The reflection from the normal direction is collected and redirected by the beam splitter into the fiber-based spectrometer (HR4000, Ocean Optics Inc. with resolution ~0.8 nm). In order to find the extinction ratio of the circularly polarized reflected light between two components in opposite handedness, we use a circularly polarized analyzer consisting of a broadband quarter-wave plate and a linear polarizer in front of the spectrometer. Since the quarter-wave plate converts the circularly polarized light into linearly polarized light, the intensity of the reflected light will reach maxima and minima while rotating the polarizer, respectively. Therefore, bright and dark states can be obtained by rotating the linear polarizer by 90° when the reflected light from the chiral polymer films

passes through the circular polarizer.

6.3   Broadband circular polarizer based on stacked CLC polymer films

In this work, we use pure chiral monomer material to fabricate the single polymeric film. Since the birefringence of the chiral monomer RMM154 and RMM153 (from Merck Inc.) is around ~0.1, the bandwidth in VIS is ~ 50 nm. The basic idea is to use the stack of multiple chiral films to cover the whole VIS spectral range. Thin cell were used to fabricate the single polymeric chiral film in order to reduce the defect lines. The single film will be then peeled off from the glass substrate and then rubbed homogeneously to serve as the substrate for making the next polymer film. The new infiltrated chiral monomer materials will be aligned by the top/bottom chiral films into planar structure and then be polymerized with the parent films into a single film.

6.3.1 Sample preparation

To fabricate chiral polymer films, the mixture was prepared by mixing the reactive mesogen RMM154 (chiral monomer), RM82 (non-chiral monomer), and chiral dopant CB15 at a ratio around 42.5%: 42.5%: 15%. We prepared three mixtures with slightly different chiral agent/monomer ratio in order to get three films with different pitch lengths, exhibiting a reflection peak in blue, green, and red spectral range, respectively. The mixtures were thoroughly mixed before they were capillary-filled into the empty 5 μm LC cells with an anti-parallel rubbing at the isotropic state. The samples were slowly cooled down to 55°C, at which temperature the sample was cured by UV light for ~ 1 hour. A further decrease of the

temperature will introduce more defects, which is not desired.

First we prepared two polymer films: one with a longer pitch (with a reflection peak in red spectral range) and the other with a shorter pitch (with a reflection peak in blue spectral range). The two cells were then opened and each polymer film stayed on one of the glass substrates. Next we rubbed the two semi-films to generate homogeneous surface anchoring. The two semi-films were assembled into a new cell with 5 μm mylar peripheral spacers. After that the mixture with a reflection peak in green was capillary-filled into the new cell at an isotropic state. After it was cooled down to 55°C, we cured it for ~ 1 hour. At this moment, the three cholesteric polymeric layers are turned to a single film. In this case, the top and bottom films function not only as the alignment layer but also as the reflecting layer. The broadened reflection is consequently created by multiple steps with each step adding additional reflection range.

6.3.2 Experimental Results

Figure 6.2 shows the transmission spectra of the three chiral polymer films we fabricated using the three mixtures with different pitch lengths. Each chiral polymer film has ~54 nm bandwidth. The films were confined in glass substrates. The ~20% transmission loss observed in Fig. 6.2 is due to the surface reflection of the employed ITO glass substrates. These substrates do not have any antireflection coatings. Thus, the chiral polymer films we fabricated are basically scattering free.
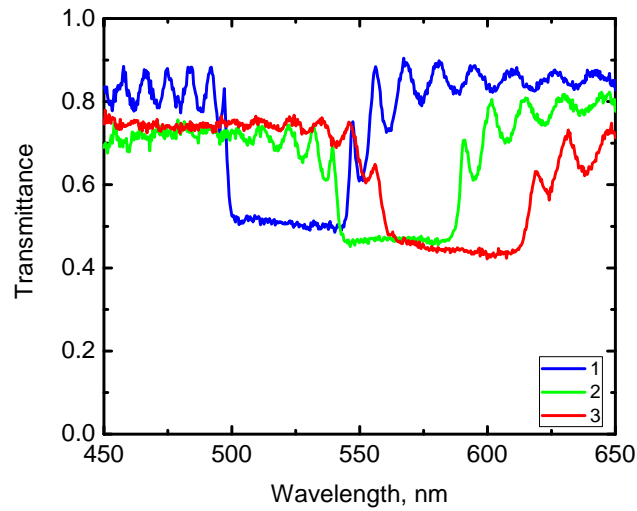
Fig. 6.2 Normalized transmittance of the chiral polymer films: red, green and blue lines represent the films with different pitches.

After the 3rd mixture is filled, the transmittance is shown in Fig. 6.3. We notice that the transmittance within and beyond the band gap is almost the same as the combination of the band gap from the single film, indicating that no additional optical loss is introduced.
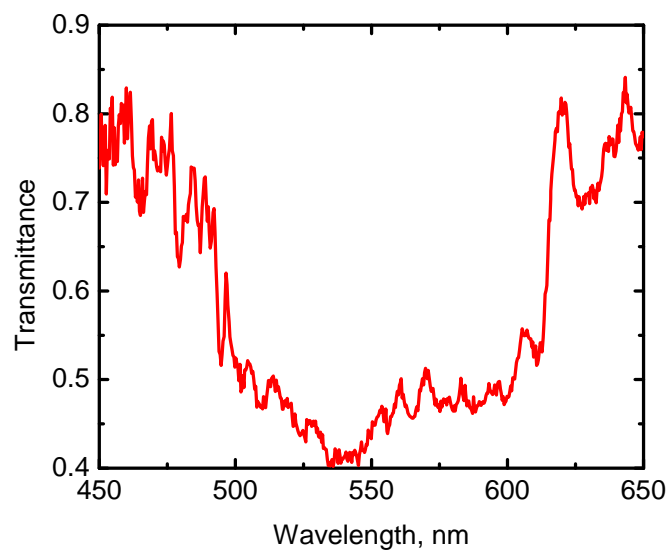
Fig. 6.3 Normalized transmittance of a circular polarizer with three stacked chiral polymer films.

102

Next, we used the setup of Fig. 6.1 to measure the extinction ratio of the broadband circular polarizer we demonstrated. Figure 6.4 shows the measured reflection spectrum of our broad band circular polarizer using the broad band circular polarizer composed of a broad band quarter wave plate and a linear sheet polarizer. Lines *1* and *2* represent the reflection spectrum of the polymer films when the circular analyzer exhibits the same or opposite handedness as that of the chiral polymer films, respectively. The measured extinction ratio of the circular polarizer made of three stacked chiral polymer films ranges from 8:1 to 30:1, depending on the wavelength. Two factors are contributing to the variation of the extinction ratio. Firstly, the circular polarizer employed does not have enough spectral range. A good dark state can only be obtained in a narrow spectral range. Secondly, the alignment performance for the cholesteric polymer film is not as good as the rubbed polyimide coated on the glass substrate. Hence, cholesteric planar structure of the middle layer will deteriorate and some defects are introduced. Although not perfect, it is still acceptable to be used in conjunction with a broadband quarter-wave film to convert an unpolarized white light into a linearly polarized light for LCD applications. In a typical LCD, two crossed linear polarizers are always needed in order to obtain a contrast ratio higher than 1000:1. Thus, with polarization conversion the optical efficiency of a LCD can almost be doubled if the circular polarizer made of stacked chiral polymer films can cover the whole visible range.
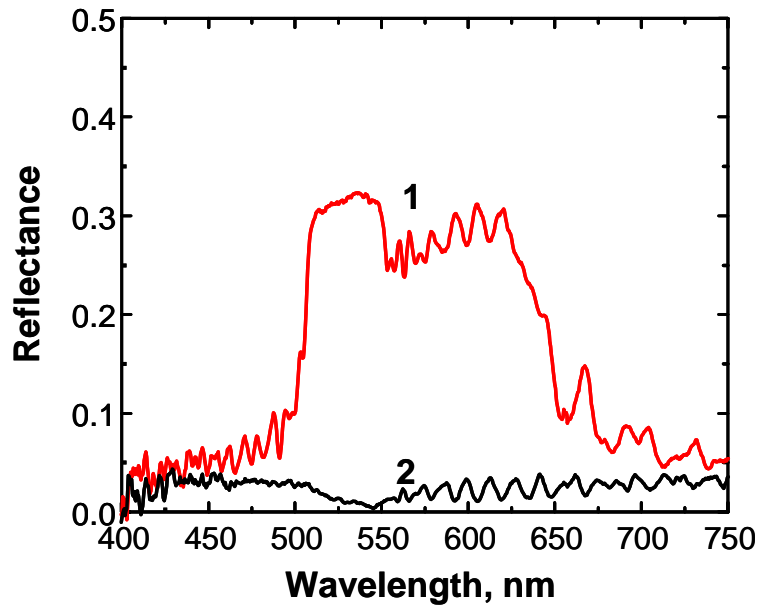
Fig. 6.4 Normalized reflection spectrum of the circular polarizer at normal incidence. Red and black lines represent the bright and dark states, respectively.

6.3.3 Simulations

By repeating the above fabrication method, it is possible to extend the reflection band of a single cholesteric polymer film to a much large spectral range. Hence the single film covering the whole wavelength range is possible to be achieved by multiple-step fabrication where the stepped pitch length is gradually created. In this section, we use 4×4 transfer matrix to simulate our experimental results. Furthermore, based on the current materials, we then theoretically design a broadband circular polarizer which covers the entire visible spectral range and specify the parameters of each layer.

According to our experimental results, the effective birefringence Δn, the average refractive index n_a, and the pitch length p (in nm) of cholesteric films 1-3 are calculated to be (0.146, 1.58, 371.66), (0.128, 1.575, 358.66), and (0.138, 1.565, 333.50), respectively. With these parameters, we simulated the transmittance spectra of films 1-3 using our improved 4×4

transfer matrix and scattering matrix [24, 25]. The simulation results are plotted in Fig. 6.5. The red, green, and blue lines in Fig. 6.5 represent the transmission spectra of films 1, 2, and 3, respectively.
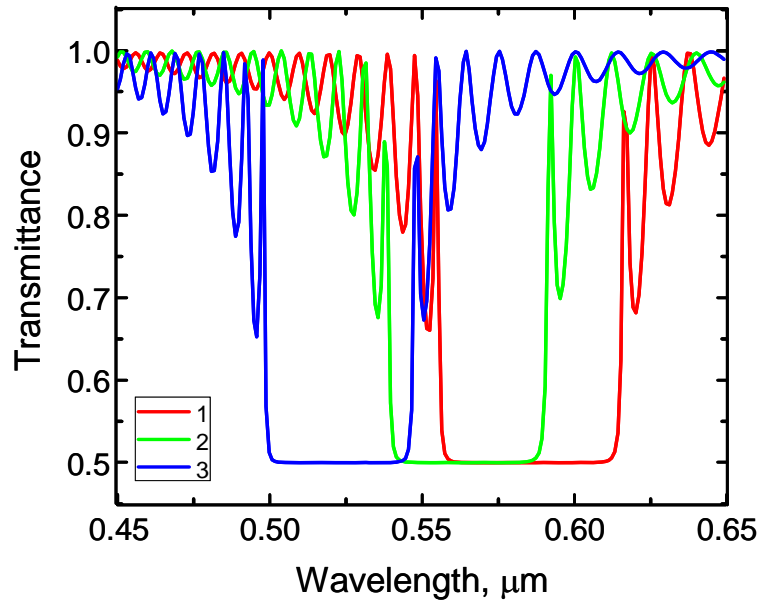
Fig. 6.5 Simulation results of the transmission spectra of each chiral polymer film.

Next, we simulated the transmission spectrum of the circular polarizer made of three stacked chiral polymer films using the above parameters. Results are shown in Fig. 6.6(a). In comparison with the experimental data shown in Fig. 6.6(b), we find that the simulation results are in good agreement with the experiments.

105
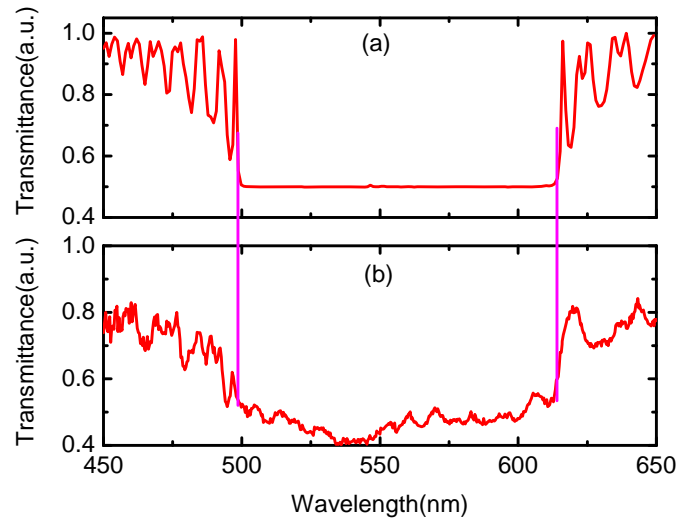
Fig. 6.6 Simulation (a) and experimental (b) results of the circular polarizer composed of 3 stacked chiral polymer films.

To enhance the optical efficiency of a LCD, a broadband circular polarizer covering the entire visible range is desired so as to avoid color shift at oblique incidence. Therefore, we designed a broadband circular polarizer by cholesteric polymer film with 8 layers with different pitch lengths. In our simulation, the birefringence of the monomer is assumed to be $\Delta n \sim 0.15$. The pitch lengths for the 8 films are $P_1 = 286$ nm, $P_2 = 308$ nm, $P_3 = 331$ nm, $P_4 = 358$ nm, $P_5 = 381$ nm, $P_6 = 413$ nm, $P_7 = 266$ nm, and $P_8 = 445$ nm, respectively. Figure 6.7 is a plot of the transmission spectrum of the simulated circular polarizer. The reflection bandwidth covers from 400 to 736 nm. If a high birefringence chiral polymer ($\Delta n \sim 0.35$) is applied, we only need three films with pitch lengths $P_1 = 266$ nm, $P_2 = 325$ nm, $P_3 = 400$ nm to achieve the same bandwidth. To reduce fabrication complexity, fewer films are highly desirable.
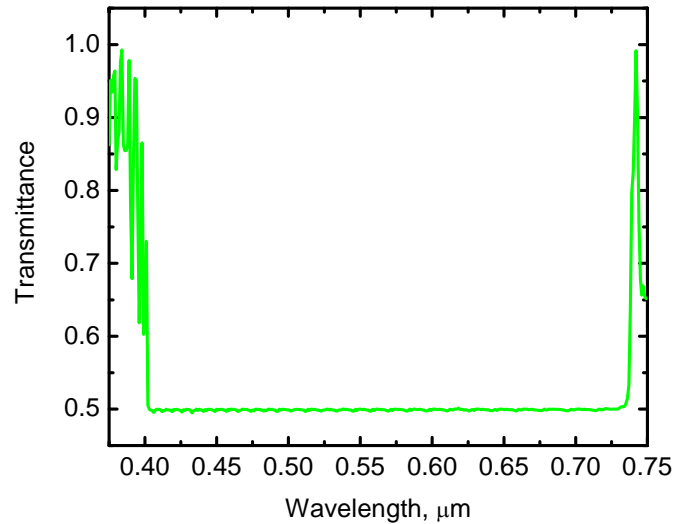
Fig. 6.7 Simulation result of a broadband circular polarizer by stacking 8 chiral polymer films together.

6.4   Broadband circular polarizer based on cholesteric LC and polymer composite films

Sec 6.3 describes the broadband circular polarizer based on pure CLC polymer films. The repetition of the process that CLC semi-films are made into the substrates and rubbed to provide anchoring, although it may not be strong for the next infiltrated CLC layer, will create a much broader reflection band. Usually the CLC monomer has very limited birefringence around 0.1-0.15, and thus the reflection band around 50 nm in VIS. Therefore the reflection band to start with is quite limited. In order to cover the whole VIS range, it requires 7-8 stacked film and the fabrication process becomes a challenge.

To overcome these challenges, we further developed the composite films made by cholesteric liquid crystal and cholesteric monomer instead of the pure cholesteric monomer. In this case, the addition part of liquid crystal helps increase of the birefringence of the single

107

film because the birefringence of nematic liquid crystal (0.2~0.3 for commercial high birefringence LC) is much larger than the LC monomer. Secondly, the composite film shows a cholesteric structure with cholesteric liquid crystals embedded in the CLC polymer network. When heated to a certain temperature, the cholesteric liquid crystal becomes less viscous and is still able to migrate and flow among the network. As a result, the diffusion is possible to be initiated.

6.4.1   Sample preparation

The materials that we used include high birefringence nematic liquid crystal BL036 ($\Delta n=0.267$, Merck), chiral agent CB15 (right-handed, Merck), chiral reactive mesogen RMM153 (right-handed, Merck) and reactive mesogen RM82 (Merck). 50% of cholesteric liquid crystals (composed of BL036 and CB15) and 50% of cholesteric monomer (composed of RMM153 and RM82) are mixed together, where the concentration of chiral and non-chiral materials is adjusted to achieve a certain reflection band at a desired wavelength range. We have formulated three mixtures: their selective reflection bands are 425-470 nm ($\Delta\lambda_I = 45$ nm), 670-735 nm ($\Delta\lambda_{II} = 65$ nm) and 520-575 nm ($\Delta\lambda_{III} = 55$ nm), respectively.

During fabrication, first we used the mixture I and mixture II to fabricate the top and bottom CLC films with a reflection band centered in blue and red spectral range, respectively. After thoroughly mixed, the mixture I and II was capillary-filled into an 8 μm cell at an isotropic state. The glass substrates were coated with indium-tin-oxide (ITO) layers and polyimide layers. The polyimide layers were rubbed in anti-parallel directions to produce ~3°

pretilt angle. A slow annealing process is necessary in order to reduce the defects in the CLC films. After 2 hours of UV curing at ~45 °C, the helical structure was fixed. Then we removed one of the glass substrates of each film so that a semi-film was obtained which would be used as the substrate for reassembling the new cell in the next step. Next we put two semi-films together with 8 μm mylar peripheral spacer in between. The mixture III was then filled into the new-assembled cell under an isotropic state and slowly cooled down to ~45 °C. For a comparison, Sample A and Sample B were made at different curing conditions. Sample A was cured for 2 hours immediately after it was cooled down to 45 °C while Sample B was cured for 2 hours 1 day right after it was cooled down to room temperature.

6.4.2 Experimental results

For the top and bottom semi-films, the reflection bands are shown in Fig. 6.8 with the orange curve representing film I and the blue curve representing film II. The CLC film I was made of the mixture I, which has a reflection band in blue region and the CLC film II was made of the mixture II, which has a reflection band in red region. The maximum transmittance does not reach 100% because of the surface reflection of the glass-air and the glass-ITO interfaces. There are slight defects introduced in the CLC-polymer composite films with increased scattering loss appeared as the shorter wavelength is approached.
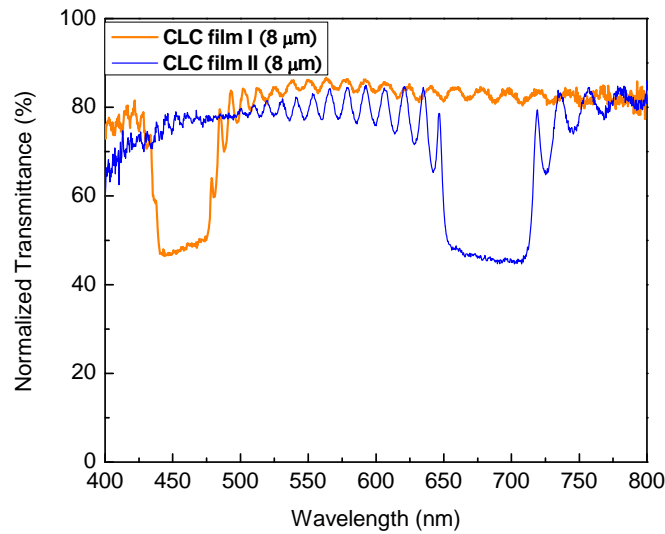
Fig. 6.8 Normalized transmittance of CLC film I (using mixture I with refection band in blue)
and CLC film II (using mixture II with refection band in red)

The reflection bands of Sample A and Sample B before and after the mixture III was
filled into the new-assembled cell were measured as Fig. 6.9 and Fig. 6.10 display,
respectively.

In Fig. 6.9, the blue curve corresponds to the transmittance of the new-assembled cell,
consisting of CLC semi-film I as the top substrate and CLC semi-film II as the bottom
substrate. The red curve corresponds to the transmittance after the mixture III was filled into
the assembled cell and cooled down. UV curing was performed immediately afterwards. Here
we observe three well-separated bands, corresponding to the reflection band of the top semi-
film, the bottom semi-film and the middle infiltrated CLC layer. The mismatch of the band
position in the blue region between the red curve and blue curve is due to the different
measurement positions on the cell since the reflection color is not completely uniform over

110

the cell for the top and the bottom semi-films.
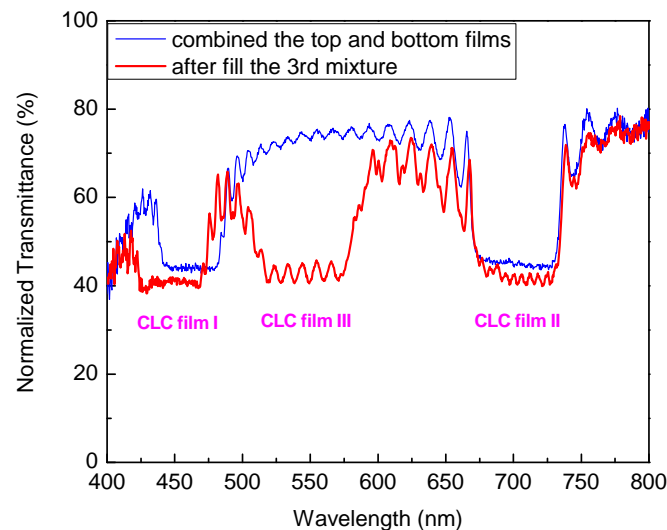
Fig. 6.9 Normalized transmittance of the Sample A (UV cured immediately after the mixture III was filled in and annealed) before and after the mixture III was filled into the assembled cell consisting of the top and bottom cholesteric semi-films.

In contrast, the Sample B, which was cured 1 day after the 3rd mixture was filled, shows a different phenomenon. In Fig. 6.10 the three bands (shown as the red spectrum) are not separated as it was observed in Fig. 6.9 but instead continuously flattened over 425-705 nm spectral range. This phenomenon is attributed to the diffusion process among the top, middle and bottom films. Although the top layer and the bottom layer were well cured, the CLC polymer network stabilized the helical structure where the embedded liquid crystals and chiral dopant can still migrate through the polymer networks. When the mixture III was filled in, a diffusion process took place among layers due to the difference in chiral concentration. Such a process is quite slow, which takes about 1 day to complete before it finally reaches the gradient balance. After final curing process, such a film stack becomes a solid single film and

the spectral characteristics will not change even it is heated up to 100 ^{o}C.
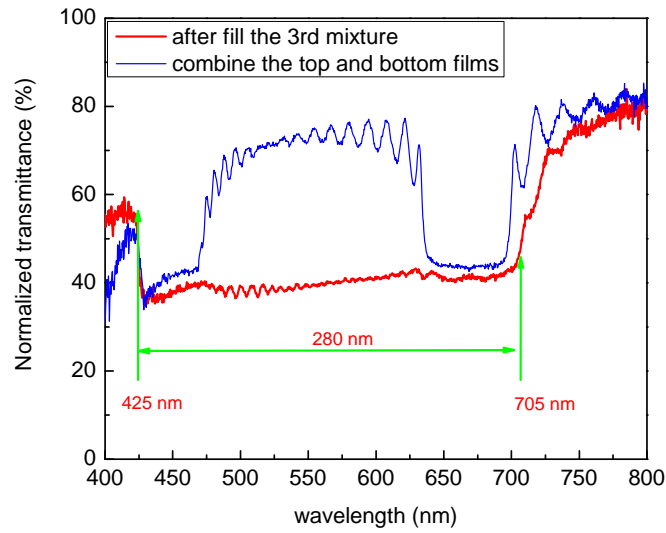
Fig. 6.10 Normalized transmittance of the Sample B (UV cured 1 day after the mixture III was filled in and annealed) before and after the mixture III was filled into the assembled cell consisting of the top and bottom cholesteric semi-films.
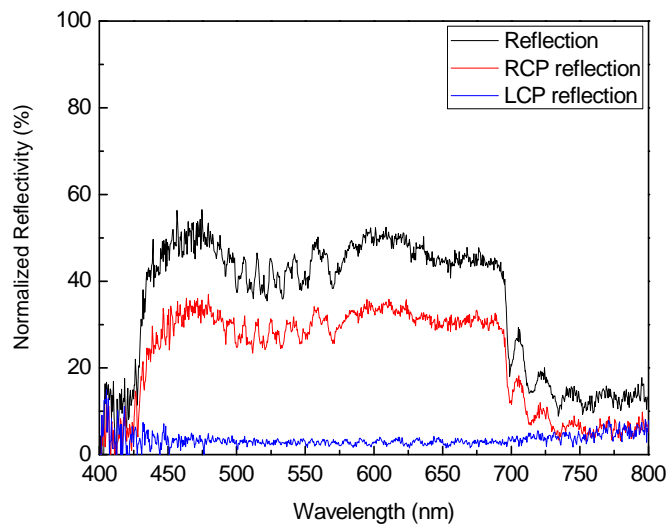
Fig. 6.11 Broadband reflection for right-handed (RCP) and left-handed (LCP) circular polarized components.

With a right-handed gradient pitched helical structure, such a film shows a broadband reflection for right-handed circularly polarized light. For practical use, the extinction ratio was measured in a reflective setup using a polarizer and a broadband quarter-wave plate in front of the spectrometer. Figure 6.11 shows the results where the black curve is the original reflection band, the red curve is the reflection band for right-handed circular polarized light (RCP), and the blue curve is the reflection band for left-handed circular polarized light (LCP). The extinction ratio is averaged to be ~11:1 from the red and blue curves within 450-675 nm range. Because the semi-films are thin and not solid enough, the capability of the semi-films to align the middle CLC mixture is slightly deteriorated and thus introduces defects and domains. These defects limit the extinction ratio but with the combination of a reflector and a quarter-wave plate, it is still acceptable for backlight recycling and enhancement applications because for high contrast purpose two crossed polarizers are always employed in displays.

6.5   Conclusions

In this chapter, we reviewed the different methods for achieving broadband reflection. Based on cholesteric liquid crystal and cholesteric liquid crystalline polymers, we demonstrated two different approaches. One circular polarizer is based on stacked chiral polymer films which are finally combined into a single film. The other approach is based on the diffusion of the unpolymerized liquid crystals between polymer networks. Both devices show a broad band reflection and good extinction ratio in a single film form. It will be very useful in backlight recycling of LCDs.

6.6   References

1.   S. T. Wu and D. K. Yang, Reflective Liquid Crystal Displays (Wiley, New York, 2001).

2.   M. Xu, F. Xu, and D. K. Yang, "Effects of cell structure on the reflection of cholesteric liquid crystal displays," J. Appl. Phys. 83, 1938 (1998).

3.   D. K. Yang , J. L. West, L. C. Chien, and J. W. Doane, "Control of reflectivity and bistability in displays using cholesteric liquid crystals," J. Appl. Phys. 76, 1331 (1994).

4.   S. V. Belayev, M. Schadt, M.I. Barnik, J. Funfchilling, N. V. Malimoneko and K. Schmitt, "Large aperture polarized light source and novel liquid crystal display operating modes," Jpn. J. Appl. Phys. 29, L634 (1990).

5.   S. Pancharatnam, "Achromatic combinations of birefringent plates," Proc. Ind. Acad. Sci. A41, 130 (1956).

6.   T. H. Yoon, G. D. Lee, and J. C. Kim, "Nontwist quarter-wave liquid-crystal cell for a high-contrast reflective display," Opt. Lett. 25, 1547 (2000).

7.   D. Armitage, I. Underwood, and S. T. Wu, Introduction to Microdisplays (Wiley, New York, 2006).

8.   D. Coates, M. J. Goulding, S. Greenfield, J. M. Hammer, S. A. Marden, and Q. L. Parri, "High performance wide-band reflective cholesteric polarizers," SID Tech. Digest Application Session, 27, 67 (1996).

9.   Q. Hong, T. X. Wu, and S. T. Wu, "Optical wave propagation in a cholesteric liquid crystal using the finite element method," Liq. Cryst. 30, 367 (2003).

10. S. Gauza, C. H. Wen, S. T. Wu, N. Janarthanan, and C. S. Hsu, "Super high birefringence

isothiocyanato biphenyl-bistolane liquid crystals," Jpn. J. Appl. Phys. 43, 7634 (2004).

11. M. F. Weber, C. A. Stover, L. R. Gilbert, T. J. Nevitt, and A. J. Ouderkirk, "Giant birefringent optics in multilayer polymer mirrors," Science, 287, 2451(2000).

12. D. J. Broer, J. Lub, and G. N. Mol, "Wide-band reflective polarizers from cholesteric polymer networks with a pitch gradient," Nature, 378, 467 (1995).

13. L. Li and S.M. Faris, "A single-layer super broadband reflective polarizer," SID'96 Digest, 111(1996).

14. L. Li, J. Li, B. Fan, Y. Jiang, and S.M. Faris, "Reflective cholesteric liquid crystal polarizer and their applications," Proc. of SPIE. 3560, 33 (1998).

15. M. Belalia, M. Mitov, C. Bourgerette, A. Krallafa, M. Belhakem, and D. Bormann, "Cholesteric liquid crystals with a helical pitch gradient: spatial distribution of the concentration of chiral groups by Raman mapping in relation with the optical response and the microstructure," Phys. Rev. E 74, 051704 (2006).

16. M. Mitov, A. Boudet, and P. Sopena, "From selective to wide-band light reflection: a simple thermal diffusion in a glassy cholesteric liquid crystal," Eur. Phys. J. B, 8, 327 (1999).

17. Y. J. Kwon, W. J. Lee, S. H. Paek, I. Kim, and K. Song, "Wide-band reflective polarizers from variable pitch cholesteric liquid crystal films," Mol. Cryst. Liq. Cryst. 377, 325 (2002).

18. A. Lavernhe, M. Mitov, C. Binet, and C. Bourgerette, "How to broaden the light reflection band in cholesteric liquid crystals? A new approach based on polymorphism,"

Liq. Cryst., 28, 803 (2001)

19. C. Binet, M. Mitov, and M. Mauzac, "Switchable broadband light reflection in polymer-stabilized cholesteric liquid crystals," J. Appl. Phys. 90, 1730 (2001).

20. Sabrina Relaix, Christian Bourgerette, and Michel Mitov, "Broadband reflective liquid crystalline gels due to the ultraviolet light screening made by the liquid crystal," Appl. Phys. Lett. 89, 251907(2006).

21. H. Guillard and P. Sixou, "Active broadband polymer stabilized liquid crystals," Liq. Cryst. 28, 933 (2001).

22. Y. Huang, Y. Zhou, and S. T. Wu, "Broadband circular polarizer using stacked chiral polymer films", Opt. Express, 15, 6414 (2007).

23. Y. Zhou, K. M. Chen, Y. Huang, and S.T. Wu, "Broadband circular polarizer based on cholesteric liquid crystal and cholesteric polymer composite films", IEEE/LEOS Annual Meeting Digest, (Orlando, FL) (2007).

24. Z. Ge, T. X. Wu, X. Zhu, and S. T. Wu, "Reflective liquid crystal displays with asymmetric incidence and exit angles," J. Opt. Soc. Am. A 22, 966 (2005).

25. Y. Huang, T. X. Wu, and S. T. Wu, "Simulations of liquid-crystal Fabry-Perot etalons by an improved 4 ×4 matrix method," J. Appl. Phys. 93, 2490 (2003).

CHAPTER 7   SUMMARY

As a promising photonic band gap medium, cholesteric liquid crystals and cholesteric polymers have initiated a new way in developing ultra-compact lasers and tunable photonic devices. Without a special selection of materials and a special design of the cavity, the optical efficiency is typically below 1%. In order to improve the laser's performance, for example, to enhance the output laser emission, reduce the beam divergence, and manipulate the output polarization state, we developed different approaches. On the other hand, we also developed novel single film broadband circular polarizers for display back light enhancement applications. The newness and major discoveries in this dissertation can be briefly summarized as follows:

(1)   Emission enhancement up to ~10X by adding a single external cholesteric liquid crystal reflector. The output enhancement is a result of virtually doubled gain length and feedback length.

(2)   Emission enhancement up to ~800X by using an external cholesteric resonator in a hybrid PBE-FP structure. The enhancement is mainly due to the feedback from both distributed feedback and external Fabry-Perot resonance. The best optical efficiency is achieved in this type of lasers as ~10%.

(3)   Laser beam divergence reduction around one order of magnitude of a CLC laser with an external CLC reflector or the external CLC resonator.

(4)   Emission enhancement and linear polarization output by in-cell metallic mirror reflector. The enhancement is mainly due to the double pump of the active area. The linearly

polarized output is due to the coherent superposition of two orthogonal polarization states. The linear polarization direction can be well controlled by the cell gap and the temperature.

(5)   Theoretical analysis on the potential resonant modes of a hybrid PBE-FP type CLC laser using 4×4 transfer matrix and scattering matrix. Light amplification is further theoretically investigated by introducing a complex refractive index of the gain medium. Physical mechanism of the laser enhancement by a CLC resonator and the optimal condition are investigated, which agrees reasonably well with our experimental results.

(6)   The ultra-compact cholesteric polymer film lasers are developed and laser output in opposite handedness to its intrinsic polarization are obtained due to light recycling effect.

(7)   Two different approaches for achieving broad band circular polarizers are developed. By stacking CLC polymer films with different pitches utilizing multiple fabrication steps, a much broadened circular polarizer (~120 nm using three films) can be achieved in VIS. By introducing diffusion process of the chiral materials among cholesteric LC-polymer composite film layers with different pitches, the circular polarizer coving ~280 nm in VIS can be obtained.

Our research work covers experimental demonstration as well as theoretical analysis of novel CLC devices to understand the underlying physics. This research is based on our specifically selected materials, hence different enhancement ratio might be found when applying a different material. Nevertheless the approaches proposed in this dissertation are general and the physics behind hold for all CLC laser devices. Based on our work, the output can be dramatically enhanced with beam quality greatly improved at the same time.

Therefore, our work has lot of impact in moving the CLC lasers toward a more practical stage. The unique advantages such as easy fabrication, compactness, miniaturization and tunability still maintain but a more compact pump source (exp. a diode-pump solid state laser) may work in the near future. The polarization manipulation has been realized so that CLC lasers are also applicable for flexible light sources where different polarization states are needed, exp biomedical detections. Polymer lasers are even more attractive as a flexible, rollable emissive layer or laser array with a few micrometers thick. Therefore we believe the compact CLC laser will be of great use in many applications. The circular polarizers with broadband reflection will also make a great impact in LCD backlight industry, which is a huge market in our daily life.

Our work is just a beginning of CLC related photonic devices. Further research efforts can be invested in developing highly efficient CLC lasers, electronically-tunable color filters, electronically-tunable lasers, micro-cavity polymer lasers, enhanced organic LED or LED sources and so on. We hope this work can more or less inspire more researchers to delve into this interesting area and stimulate more creative ideas in developing novel CLC and polymer based photonic devices.

APPENDIX   BACKWARD EIGENWAVE (BE) METHOD

A.1   Derivations

In this part, 4×4 matrix starting from Maxwell's equations through a different way from Berreman [1] and Wöhler [2] are derived based on backward eigenwave method [3, 4]. In this derivation, the 4×4 matrix for each slice is diagonalized and finally transferred to scattering matrix, thus the equation became extremely concise.

In the derivation for the general LCD devices with backward eigenwave method, we take the coordinate system shown in Fig. A.1.
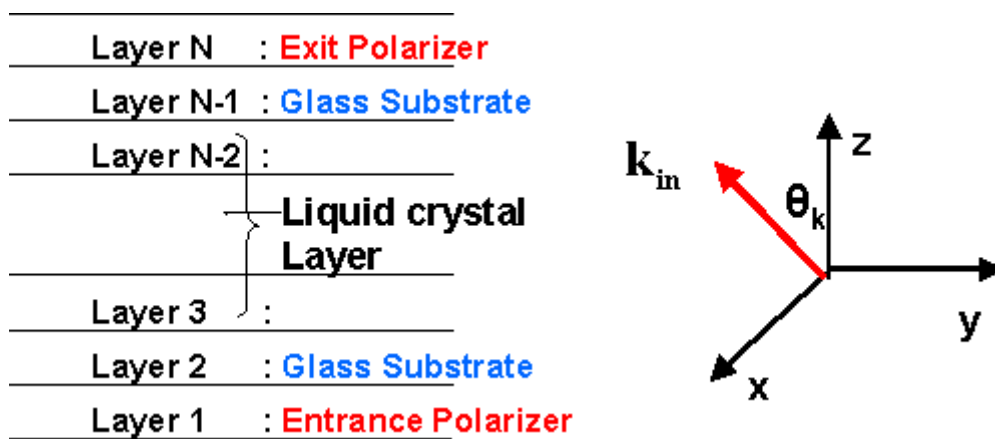
Fig. A.1. Coordinate system and LC device layout in the 4×4 matrix derivation.

We choose a coordinate system in which the wave vector k_{in} of the incident plane wave lies in the *x-z* plane. Here the +*z* axis points from the bottom glass substrate to the exit polarizer. The wave vector of the incident wave in this coordinate system is given by

$$k_{in} = k_0(\sin\theta_k, 0, \cos\theta_k) \qquad \text{(A-1)}$$

where $k_0 = \omega/c = 2\pi/\lambda$ is the wave number in free space, θ_k is elevation angle of the incident plane wave. The whole LCD system is divided into *N* layers in the *z* direction where

each layer is considered as a homogeneous one.

In a homogenous uniaxial medium layer with tilt angle θ and azimuthal angle ϕ, we can express the dielectric tensor as

$$\ddot{\varepsilon} = \begin{pmatrix} \varepsilon_{xx} & \varepsilon_{xy} & \varepsilon_{xz} \\ \varepsilon_{yx} & \varepsilon_{yy} & \varepsilon_{yz} \\ \varepsilon_{zx} & \varepsilon_{zy} & \varepsilon_{zz} \end{pmatrix} \qquad \text{(A-2)}$$

with

$$\varepsilon_{xx} = n_o^2 + (n_e^2 - n_o^2)\cos^2\theta\cos^2\phi, \qquad \text{(A-3a)}$$

$$\varepsilon_{xy} = \varepsilon_{yx} = (n_e^2 - n_o^2)\cos^2\theta\sin\phi\cos\phi, \qquad \text{(A-3b)}$$

$$\varepsilon_{xz} = \varepsilon_{zx} = (n_e^2 - n_o^2)\sin\theta\cos\theta\cos\phi, \qquad \text{(A-3c)}$$

$$\varepsilon_{yy} = n_o^2 + (n_e^2 - n_o^2)\cos^2\theta\sin^2\phi, \qquad \text{(A-3d)}$$

$$\varepsilon_{yz} = \varepsilon_{zy} = (n_e^2 - n_o^2)\sin\theta\cos\theta\sin\phi, \qquad \text{(A-3e)}$$

$$\varepsilon_{zz} = n_o^2 + (n_e^2 - n_o^2)\sin^2\theta, \qquad \text{(A-3f)}$$

where n_o and n_e are the ordinary and extraordinary refractive indices of each medium layer, respectively. For those absorption materials, such as polarizer, the refractive indices are complex values. With the dielectric tensor information, the matrix for each layer can be specified.

For simplicity, we normalize the magnetic field **H** as

$$\hat{\mathbf{H}} = \left(\frac{\mu_0}{\varepsilon_0}\right)^{1/2}\mathbf{H}. \qquad \text{(A-4)}$$

Maxwell equation can be expressed for **E** and $\hat{\mathbf{H}}$ in the following forms

$$\nabla \times \mathbf{E} = ik_0\hat{\mathbf{H}}, \qquad \text{(A-5a)}$$

122

$$\nabla \times \hat{\mathbf{H}} = -ik_0 \vec{\varepsilon} \mathbf{E} .\tag{A-5b}$$

With $\partial / \partial y = 0$ and $\partial / \partial x = ik_x$ we can expand Eqs. (A-5a) and (A-5b) to six equations as

$$-\frac{\partial E_y}{\partial z} = ik_0 \hat{H}_x \tag{A-6a}$$

$$-ik_x E_z + \frac{\partial E_x}{\partial z} = ik_0 \hat{H}_y \tag{A-6b}$$

$$ik_x E_y = ik_0 \hat{H}_z \tag{A-6c}$$

$$-\frac{\partial \hat{H}_y}{\partial z} = -ik_0 (\varepsilon_{xx} E_x + \varepsilon_{xy} E_y + \varepsilon_{xz} E_z) \tag{A-6d}$$

$$-ik_x \hat{H}_z + \frac{\partial \hat{H}_x}{\partial z} = -ik_0 (\varepsilon_{yx} E_x + \varepsilon_{yy} E_y + \varepsilon_{yz} E_z) \tag{A-6e}$$

$$ik_x \hat{H}_y = -ik_0 (\varepsilon_{zx} E_x + \varepsilon_{zy} E_y + \varepsilon_{zz} E_z) \tag{A-6f}$$

After eliminating the longitudinal components, these six equations can be written in a matrix representation as

$$\frac{\partial}{\partial z} \begin{pmatrix} E_x \\ E_y \\ \hat{H}_x \\ \hat{H}_y \end{pmatrix} = ik_0 \mathbf{Q} \begin{pmatrix} E_x \\ E_y \\ \hat{H}_x \\ \hat{H}_y \end{pmatrix}, \tag{A-7}$$

where

$$\mathbf{Q} = \begin{bmatrix} -\dfrac{\varepsilon_{zx}}{\varepsilon_{zz}} \sin \theta_k & -\dfrac{\varepsilon_{zy}}{\varepsilon_{zz}} \sin \theta_k & 0 & 1 - \dfrac{\sin^2 \theta_k}{\varepsilon_{zz}} \\ 0 & 0 & -1 & 0 \\ -\varepsilon_{yx} + \varepsilon_{yz} \dfrac{\varepsilon_{zx}}{\varepsilon_{zz}} & -\varepsilon_{yy} + \varepsilon_{yz} \dfrac{\varepsilon_{zy}}{\varepsilon_{zz}} + \sin^2 \theta_k & 0 & \dfrac{\varepsilon_{yz}}{\varepsilon_{zz}} \sin \theta_k \\ \varepsilon_{xx} - \varepsilon_{xz} \dfrac{\varepsilon_{zx}}{\varepsilon_{zz}} & \varepsilon_{xy} - \varepsilon_{xz} \dfrac{\varepsilon_{zy}}{\varepsilon_{zz}} & 0 & -\dfrac{\varepsilon_{xz}}{\varepsilon_{zz}} \sin \theta_k \end{bmatrix} . \tag{A-8}$$

From the theory of linear algebra, diagonalizing **Q** matrix to get its eigenvalues and eigenvectors can solve these coupled equations. This eigensystem can be solved by many

numerical software programs. By this method, we can express the diagonalized $\mathbf{Q}$ matrix as

$$\mathbf{Q} = \mathbf{T}\begin{bmatrix} q_1 & & & \\ & q_2 & & \\ & & q_3 & \\ & & & q_4 \end{bmatrix}\mathbf{T^{-1}}, \tag{A-9}$$

where q_1 to q_4 are the eigenvalues of $\mathbf{Q}$, and $\mathbf{T}$ is composed of the corresponding eigenvectors.

For simplicity, we intentionally adjust those q eigenvalues and eigenvector matrix T in a way

that q_1 and q_2 are positive and q_3, q_4 are negative.

With the diagonalized $\mathbf{Q}$ matrix, we can further conduct a variable transformation of

the tangential field components as

$$\begin{bmatrix} E_x \\ E_y \\ \hat{H}_x \\ \hat{H}_y \end{bmatrix} = T\begin{bmatrix} U_1 \\ U_2 \\ U_3 \\ U_4 \end{bmatrix} \tag{A-10}$$

where $\mathbf{T}$ is expanded as

$$T = \begin{bmatrix} T_{11} & T_{12} \\ T_{13} & T_{14} \end{bmatrix} \tag{A-11}$$

Substituting Eq. (A-10) into Eq. (A-7), we can obtain

$$\frac{\partial}{\partial z}\begin{bmatrix} U_1 \\ U_2 \\ U_3 \\ U_4 \end{bmatrix} = ik_0\begin{bmatrix} q_1 & & & \\ & q_2 & & \\ & & q_3 & \\ & & & q_4 \end{bmatrix}\begin{bmatrix} U_1 \\ U_2 \\ U_3 \\ U_4 \end{bmatrix}. \tag{A-12}$$

Equation (A-12) comprises of four uncoupled equations, in which U_1 and U_2 represent

the forward eigenwaves, while U_3 and U_4 represent the backward ones. According to Fig. A.1,

the solutions of Eq. (A-12) are

124

$$
\begin{bmatrix} U_1 \\ U_2 \\ U_3 \\ U_4 \end{bmatrix}_{n,d_n} = \mathbf{G}_n \begin{bmatrix} U_1 \\ U_2 \\ U_3 \\ U_4 \end{bmatrix}_{n,0} , \tag{A-13}
$$

where

$$
\mathbf{G}_n = \begin{bmatrix} \exp(\mathrm{i}k_{z1}d_n) & & & \\ & \exp(\mathrm{i}k_{z2}d_n) & & \\ & & \exp(\mathrm{i}k_{z3}d_n) & \\ & & & \exp(\mathrm{i}k_{z4}d_n) \end{bmatrix} , \tag{A-14}
$$

and

$$
k_{z1} = k_0 q_1 \tag{A-15a}
$$

$$
k_{z2} = k_0 q_2 \tag{A-15b}
$$

$$
k_{z3} = k_0 q_3 \tag{A-15c}
$$

$$
k_{z4} = k_0 q_4 \tag{A-15d}
$$

For the forward eigenwaves, we can correlate the U_1 and U_2 values on the top and bottom surfaces of nth layer as

$$
\begin{bmatrix} U_1 \\ U_2 \end{bmatrix}_{n,d_n} = \mathbf{F}_n \begin{bmatrix} U_1 \\ U_2 \end{bmatrix}_{n,0} , \tag{A-16}
$$

where

$$
\mathbf{F}_n = \begin{bmatrix} \exp(\mathrm{i}k_{z1}d_n) & 0 \\ 0 & \exp(\mathrm{i}k_{z2}d_n) \end{bmatrix} . \tag{A-17}
$$

Similar relation for the backward parts U_3 and U_4 can be expressed as

$$
\begin{bmatrix} U_3 \\ U_4 \end{bmatrix}_{n,d_n} = \mathbf{B}_n \begin{bmatrix} U_3 \\ U_4 \end{bmatrix}_{n,0} , \tag{A-18}
$$

with

$$\mathbf{B}_n = \begin{bmatrix} \exp(ik_{z3}d_n) & 0 \\ 0 & \exp(ik_{z4}d_n) \end{bmatrix}. \tag{A-19}$$

From Eqs. (A-10) and (A-11), the corresponding electric fields can be expressed by the forward (+) and backward (-) eigenwaves as

$$\begin{bmatrix} E_x \\ E_y \end{bmatrix} = \begin{bmatrix} E_x \\ E_y \end{bmatrix}^+ + \begin{bmatrix} E_x \\ E_y \end{bmatrix}^- = \mathbf{T}_{11} \begin{bmatrix} U_1 \\ U_2 \end{bmatrix} + \mathbf{T}_{12} \begin{bmatrix} U_3 \\ U_4 \end{bmatrix}. \tag{A-20}$$

According to the fact that in conventional liquid crystal displays, the backward eigenwaves are negligible, from Eq. (A-20) can be further expressed as

$$\begin{bmatrix} E_x \\ E_y \end{bmatrix} \approx \begin{bmatrix} E_x \\ E_y \end{bmatrix}^+ = \mathbf{T}_{11} \begin{bmatrix} U_1 \\ U_2 \end{bmatrix}, \tag{A-21}$$

Because the *x* and *y* field components are continuous on the interference of a layer, from Eqs. (A-16), (A-21) and Fig. A.1 electric fields between subsequent layers can be correlated as

$$\begin{bmatrix} E_x \\ E_y \end{bmatrix}_n^+ = \mathbf{J}_{e,n}^+ \begin{bmatrix} E_x \\ E_y \end{bmatrix}_{n+1}^+, \tag{A-22}$$

where

$$\mathbf{J}_{e,n}^+ = (\mathbf{T}_{11})_n \mathbf{F}_n (\mathbf{T}_{11})_n^{-1} \tag{A-23}$$

is the transforming matrix for forward tangential field components of subsequent layers. For the negligible backward field components, similar relation can be given as

$$\begin{bmatrix} E_x \\ E_y \end{bmatrix}^- = \mathbf{T}_{12} \begin{bmatrix} U_3 \\ U_4 \end{bmatrix}, \tag{A-24}$$

Along with Eq. (A-18), we can express the backward tangential field components between subsequent layers by

$$\begin{bmatrix} E_x \\ E_y \end{bmatrix}_{n+1}^- = (\mathbf{J}_{e,n}^-)^{-1} \begin{bmatrix} E_x \\ E_y \end{bmatrix}_n^-, \tag{A-25}$$

www.manaraa.com

where

$$(\mathbf{J}_{e,n}^{-})^{-1} = (\mathbf{T_{12}})_n (\mathbf{B}_n)^{-1} (\mathbf{T_{12}})_n^{-1}, \qquad\qquad (A\text{-}26)$$

is the transforming matrix.

A.2   References

1. D. W. Berreman, "Optics in stratified and anisotropic media: 4×4 matrix formulation," J. Opt. Soc. Am. 62, 502 (1972).

2. Hwohler, G. Hass, M. Fritsch, and D. A. Mlynski, "Faster 4×4 matrix method for uniaxial inhomogeneous media," J. Opt. Soc. Am. A. 5, 1554 (1988).

3. Z. Ge, T. X. Wu, X. Zhu, and S. T. Wu, "Reflective liquid crystal displays with asymmetric incidence and exit angles," J. Opt. Soc. Am. A 22, 966 (2005).

4. Y. Huang, T. X. Wu, and S. T. Wu, "Simulations of liquid-crystal Fabry-Perot etalons by an improved 4 ×4 matrix method," J. Appl. Phys. 93, 2490 (2003).

LIST OF PUBLICATIONS

Journal publications

1. Y. Huang, Y. Zhou, and S. T. Wu, "Broadband circular polarizer using stacked chiral polymer films", Opt. Express, 15, 6414-6419 (2007).

2. Y. Zhou, E-Eun Jang, Y. Huang, and Shin-Tson Wu, "Enhanced laser emission in opposite handedness using a cholesteric polymer film stack", Opt. Express, 15, 3470-3477 (2007).

3. Y. Matsuhisa, Y. Huang, Y. Zhou, S. T. Wu, R. Ozaki, Y. Takao, A. Fujii, and M. Ozaki, "Low threshold and high efficiency lasing upon band-edge excitation in a cholesteric liquid crystal", Appl. Phys. Lett. 90, 091114 (2007).

4. Y. Matsuhisa, Y. Huang, Y. Zhou, S. T. Wu, R. Ozaki, Y. Takao, A. Fujii, and M. Ozaki, "Cholesteric liquid crystal laser in a dielectric mirror cavity upon band-edge excitation", Opt. Express 15, 616-622 (2007).

5. Y. Zhou, Y. Huang, Z. Ge, L. P. Chen, Q. Hong, T. X. Wu, and S. T. Wu, "Enhanced photonic band edge laser emission in a cholesteric liquid crystal resonator", Phys. Rev. E 74, 061705 (2006).

6. Y. Huang, T. H. Lin, Y. Zhou, and S. T. Wu, "Enhancing the laser power by stacking multiple dye-doped chiral polymer films", Opt. Express 14, 11299-11303 (2006).

7. Y. Huang, L. P. Chen, C. Doyle, Y. Zhou, and S. T. Wu, "Spatially tunable laser emission in dye-doped cholesteric polymer films", Appl. Phys. Lett. 89, 111106 (2006).

8. Y. Zhou, Y. Huang, T. H. Lin, L. P. Chen, Q. Hong, and S. T. Wu, "Direction controllable

linearly polarized laser from a dye-doped cholesteric liquid crystal", Opt. Express 14, 5571-5580 (2006).

9.   T. H. Lin, Y. Huang, Y. Zhou, A. Y. G. Fuh, and S. T. Wu, "Photo-patterning micro-mirror devices using azo dye-doped cholesteric liquid crystals" Opt. Express 14, 4479-4485 (2006).

10. Y. Zhou, Y. Huang, and S.T. Wu, "Enhancing cholesteric liquid crystal laser performance using a cholesteric reflector", Opt. Express. 14, 3906-3916 (2006).

11. Y. Huang, Y. Zhou, C. Doyle, and S. T. Wu "Tuning photonic band gap in cholesteric liquid crystals by temperature-dependent dopant solubility" Opt. Express 14, 1236-1242 (2006).

12. Y. Huang, Y. Zhou, Q. Hong, A. Rapaport, M. Bass, and S.T. Wu, "Incident angle and polarization effects on the dye-doped cholesteric liquid crystal laser", Opt. Comm. 261, 91-96 (2006).

13. Y. Huang, Y. Zhou, and S. T. Wu, "Spatially tunable laser emission in dye-doped photonic liquid crystals", Appl. Phys. Lett., 88, 011107 (2006).

14. Y. Zhou, Y. Huang, A. Rapaport, M. Bass, S.T. Wu, "Experimental investigation of laser emission of dye-doped cholesteric liquid crystals with a cholesteric reflector", Mol. Cryst. Liq. Cryst., 454, 377-385 (2006).

15. Y. Huang, Y. Zhou, Q. Hong and S.T. Wu, "Lasing in dye-doped photonic liquid crystal devices", Mol. Cryst. Liq. Cryst., 453, 251-262 (2006).

16. Y. H. Lin, H. Ren, S. Gauza, Y. H. Wu, Y. Zhou, and S. T. Wu, "High contrast and fast

response polarization-independent reflective display using a dye-doped dual-frequency liquid crystal gel" , Mol. Cryst. Liq. Cryst. 453, 371-378 (2006).

17. Y. Zhou, Y. Huang, A. Rapaport, M. Bass, and S.T. Wu, "Doubling the optical efficiency of a chiral liquid crystal laser using a reflector", Appl. Phys. Lett., 87, 231107(2005).

18. Y. Zhou, G. J. Zeng, and F. H. Yu, "A particle swarm optimization-based approach for optical FIR filter design", Appl. Opt., 42, 1503-1507 (2003).

19 Y. Zhou, G. J. Zeng, F. H. Yu, and H. S. Kwok, "Study on optical FIR filter", Opt. Eng., 42, 2318-2323 (2003).

Conference proceedings

1. M. Ozaki, Y. Matsuhisa, H. Yoshida, A. Fujii, Y. Huang, Y. Zhou and S. T. Wu, "Enhanced band-edge and eefect-mode effects of laser action in chiral liquid crystals," 2007 IEEE/LEOS Summer Topical Meeting on Organic Photonic Media, Devices & Applications Digest, (Portland, Oregon, Jul., 2007).

2. Y. Zhou, K. M. Chen, Y. Huang, and S.T. Wu, "Broadband circular polarizer based on cholesteric liquid crystal and cholesteric polymer composite films", IEEE/LEOS Annual Meeting Digest, (2007 IEEE/LEOS Annual Meeting, Orlando, Oct., 2007).

3. Y. Zhou, Y. Huang, Z. Ge, and S. T. Wu, "Highly efficient photonic band-edge cholesteric liquid crystal lasers", Proc. SPIE 6487, 64870C (Photonic West 2007, San Jose, Jan., 2007).

4. Y. Huang, Y. Zhou, and S. T. Wu, "Random lasers from dye-doped chiral photonic crystal

films", Proc. SPIE 6480, 648006 (2007 Photonic West, San Jose, Jan., 2007).

5. Y. Zhou, Y. Huang, and S. T. Wu, "High Performance dye-doped cholesteric liquid crystal lasers", 2006 OSA Annual Meeting Digest, (2006 OSA Annual Meeting, Rochester, Oct., 2006).

6. Y. Zhou, Y. Huang, and S. T. Wu, "Nearly unpolarized and linearly polarized laser generation from dye-doped cholesteric liquid crystal laser using a mirror reflector", Proc. SPIE 6332, 633208 (2006 SPIE Annual Meeting, San Diego, Aug., 2006).

7. Y. Huang, Y. Zhou, and S. T. Wu, "Tunable photonic devices based on the temperature dependent photonic band gap in chiral nematic liquid crystals", Proc. SPIE 6332, 63320F (2006 SPIE Annual Meeting, San Diego, Aug., 2006).

8. Y. Zhou, Y. Huang, A. Rapaport, M. Bass, and S.T. Wu, "Doubling the output power of cholesteric liquid crystal lasers", Proc. SPIE, 6135, 613500 (2006 Photonics West, San Jose, Jan., 2006).

9. Y. Zhou, Y. Huang, A. Rapaport, M. Bass, and S.T. Wu, "Experimental investigation of laser emission properties of dye-doped cholesteric liquid crystals with a cholesteric liquid crystal reflector", The 11th International topical meeting on optics of liquid crystal, 91 (Clearwater, FL, Oct., 2005).

10. Y. Huang, Y. Zhou, Q. Hong, and S. T. Wu, "Incident angle and polarization effects on dye-doped cholesteric liquid crystal lasers", The 11th International topical meeting on optics of liquid crystal, 91 (Clearwater, FL, Oct., 2005).

11. Y. Zhou, G. Z. Wu, F. H. Yu, H. S. Kwok, "Optical FIR filter based on crystal

birefringence: Theory & Experimental investigation", Proc. SPIE, 4924, 145-152 (Shanghai, Oct., 2002).

12. J. Y. Xiong, Y. Zhou, G. Z. Wu, Z. F. Cen, F. H. Yu, "New analytical method for design of PIF used in color separation/combination optical engine for LCOS display", Proc. SPIE, 4929, 116-121 (Shanghai, Oct., 2002).

13. J. Y. Xiong, Y. Zhou, G. Z. Wu, Z. F. Cen, F. H. Yu, "Non-scanning selective-illumination optical sectioning microscope: Theory", Proc. SPIE, 4929, 105-115 (Shanghai, Oct., 2002).